International

WOCE

Newsletter

Number 24 October 1996

IN THIS ISSUE

Published by WOCE International Project Office at Southampton Oceanography Centre, UK

Plus ça Change

W. John Gould, Director, WOCE IPO, john.gould@soc.soton.ac.uk

The IPO is undergoing a change in staff. Andrea Frische our Newsletter Editor is expecting a baby in October and has now returned to Germany on maternity leave. From January onwards she plans to continue working part time for the IPO but based in Hamburg. She will take on responsibility for the co-ordination of planning of the 1998 WOCE Conference "Ocean Circulation and Climate". Andrea will gradually relinquish responsibility for the Newsletter to Roberta Boscolo who will join the IPO (initially) for 6 months starting in early October. Roberta has just completed a Masters degree in Oceanography and is working towards her PhD. I'm sure you'll wish to send best wishes to Andrea and her husband as they embark on this new phase of their lives.

Pacific Workshop

By all accounts the Pacific Workshop was a great success. Congratulations and thanks are due to Lynne Talley for the hard work she put in, to US WOCE for supporting the workshop and to the organising committee. There were about 150 people there and an "Old WOCE hand" reported that he knew only about 40% of them. That's a healthy sign since it indicates that the prospect of working with the WOCE data sets is attracting new people. We'll be assessing over the next few weeks what it was that people liked about the Pacific Workshop and if there are any lessons that we can learn that will help next year's South Atlantic and Southern Ocean Workshops to be as productive as possible. Our next Newsletter will have short papers based on some of the Pacific presentations.

In this issue you'll find announcements for the next two workshops so now is your chance to register.

Atlantic survey

While many WOCE observations have been made in the North Atlantic since 1990, it was decided to carry out a near-synoptic survey towards the end of WOCE. This 1996–97 survey is now under way. This autumn marks a decisive point with cruises in the subpolar gyre by Canada (Labrador Sea), and in the eastern basin by UK and USA. (Even as I write this, Penny Holliday from the IPO is on one of these cruises on RRS Discovery but is hove-to south of Iceland in F9 gales). Further cruises from Germany, UK, Spain, Portugal, USA, Canada and Russia are scheduled for 1997. See the DIU web page for further details.

Most significantly, by the end of the year the North Atlantic is going to be well-populated with profiling ALACE floats primarily from the USA and with MARVOR and RAFOS floats from the French/German/Spanish/UK Eurofloat and the French ARCANE projects.

Meetings

The WOCE SSG will be holding its 23rd meeting here in Southampton in mid October. Amongst other things we will be reviewing progress by the Synthesis and Modelling WG towards producing an implementation strategy for the WOCE AIMS phase, reviewing the Pacific workshop and starting discussions on the structure and objectives of the 1998 WOCE Conference "Ocean Circulation and Climate".

In the past two months there have been a number of WOCE-related meetings. In Reykjavik I co-convened a session at the annual meeting of the International Council for the Exploration of the Sea (ICES) where we sought to identify what lessons GLOBEC (the Global Ecosystem Dynamics Study) might learn from WOCE and JGOFS. While it is clear that WOCE results will underpin future deep ocean research in both physics and biology, the study of the marine ecosystem has a much greater complexity and needs to consider biologically productive shelf and slope areas which are outside the WOCE remit.

In the next Newsletter I will report on our SSG discussions and on the latest meeting of the WOCE Hydrographic Programme Planning Committee meeting in Woods Hole. One topic that will be discussed there will be the efforts needed to get the complete WHP data set into the WOCE system. All WOCE observations will be of use in defining spatial and temporal variability but we are already aware of some research groups that may need help with data processing and formatting.

Newsletter

We've had numerous compliments in recent months about the Newsletter and it has become a useful medium for spreading the word about WOCE results. We want to make sure that we are targeting the right people with our mailing of the Newsletter. Printing costs about $2.50 for the 40 pages (including 4 colour pages) so we don't want them to go to people who never look at them. So there is a card with this issue that we'd like you to return if you want to continue receiving the Newsletter. We'll put the new mailing list in place after number 25.

As a footnote – I hadn't intended that my question "How would you answer Henry Stommel?" in the last Newsletter should be a rhetorical one. So I would still like to have your input on how WOCE has changed our view of the ocean.

P.S. It's a boy! Paul arrived 20-X-96. All well.

A New Global Air-Sea Heat and Momentum Flux Climatology

Simon A. Josey, Elizabeth C. Kent, Daniel Oakley and Peter K. Taylor, James Rennell Division, Southampton Oceanography Centre, Empress Dock, Southampton, SO14 3ZH, UK, simon.a.josey@soc.soton.ac.uk

Reliable estimates of the air-sea fluxes of heat and momentum are vital to improve our understanding of the coupled ocean-atmosphere system. In this article, we present preliminary results from the analysis of a new global air-sea heat and momentum flux climatology currently being developed at the Southampton Oceanography Centre. In particular, we focus on the climatologically implied meridional heat transport in the Atlantic Ocean. Past climatological studies have been unable to obtain agreement between the implied transport and independent hydrographic estimates without imposing corrections on the various components of the heat budget throughout the basin (*e.g.* da Silva *et al*., 1994). We find that much of the discrepancy can be resolved by applying a relatively small reduction to the shortwave flux in the tropical North Atlantic alone and suggest that this may be justified given the effects of increased atmospheric aerosol loading in this region. In generating the climatology, estimates of the fluxes have been obtained from *in situ* reports within the COADS 1a (Comprehensive Ocean Atmosphere Dataset 1a), a global dataset containing of order 30 million surface observations from ships and buoys collected over the period 1980–93. The major difference between the new climatology and previous ones based on in situ data is that the reported meteorological variables used to calculate the fluxes have been corrected for various observational biases using additional information about measurement procedures which has been blended in from the WMO47 list of ships. By doing this we hope to reduce the errors in the derived flux fields although we have yet to quantify this in detail and do not discuss the impact of the corrections in this note. The flux estimates have been obtained using the bulk formulae of Smith (1988) for the latent and sensible heat, Clark *et al*. (1974) for the longwave and Reed (1977) for the shortwave. Observations made prior to 1980 are not included in our analysis. If there is significant interdecadal variability in the surface heat and momentum flux fields as several studies now suggest, it will be important to use a climatology based on recent observations when calculating quantities such as the climatological Ekman transport for use with the hydrographic data collected within WOCE. At this stage, we believe that there are two effects which we have not fully included in our calulations. The first of these concerns regional variations in the amount of aerosol loading in the atmosphere, the effects of which are not accounted for in the Reed (1977) formula. Gilman and Garrett (1994) have noted this problem in the context of a climatological study of the Mediterranean and discuss measurements made during GATE which suggest that aerosol loading over the tropical Atlantic can lead to a reduction of the surface shortwave by up to 25%. The second effect is an observational problem caused by accumulation of dirt on the wicks surrounding the wet bulb thermometers used to measure humidity at sea, which initial tests show can lead to an underestimate of the latent heat flux by up to 10%. In a first attempt at examining the likely impact of these effects, we have reduced the shortwave flux by 15% between the equator and 30°N, where the aerosol loading peaks, and increased the latent heat flux by 10% globally.

The climatological annual mean net heat flux field that we obtain with these additional modifications is shown in Fig. 1 (page 21). Heat gain is concentrated in the tropics, where shortwave heating dominates, while the major heat loss regions are over the western boundary currents, which are regions of strong latent and sensible heat loss, and the high latitudes. An initial assessment of the climatology has been carried out by calculating the implied heat transport in the Atlantic, using the estimate of 1.2 PW northward transport at 24°N by Hall and Bryden (1982) as a boundary condition, and comparing it with other hydrographic estimates, Fig. 2. We have considered three cases: (a) the unmodified fluxes (dashed line); (b) with the latent heat flux correction (dash-dot line) and (c) with the latent and shortwave flux corrections (solid line). It should be noted that comparisons of this kind are complicated by the fact that the climatologically derived transport is a long term mean whereas the hydrographic values are one time measurements which may be influenced by seasonal

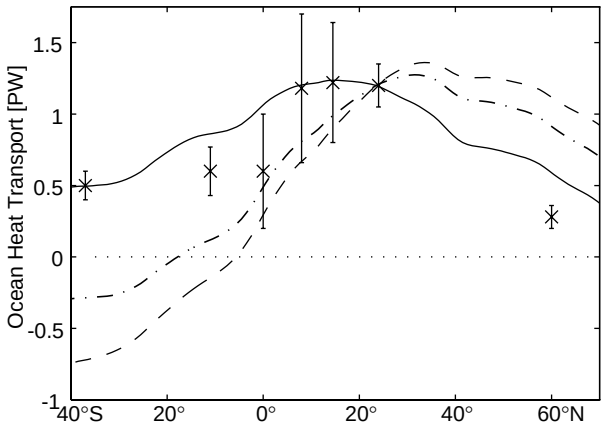

Figure 2. The climatologically implied meridional heat transport in the Atlantic. Dashed line: unmodified fluxes; dash-dot line: with latent heat flux correction; solid line: with latent and shortwave flux corrections. Crosses are hydrographic or inverse model estimates: 60°N (Bacon, 1996); 24°N (Hall and Bryden, 1982); 14.5 and 8°N (Klein et al., 1995); 0° (Wunsch, 1984); 11°S (Speer, pc); 37°S (Saunders and King, 1995). Note the latter is a zonal approximation of the dog-leg A11 section, similar agreement is found if the implied heat transport is calculated across the actual section.

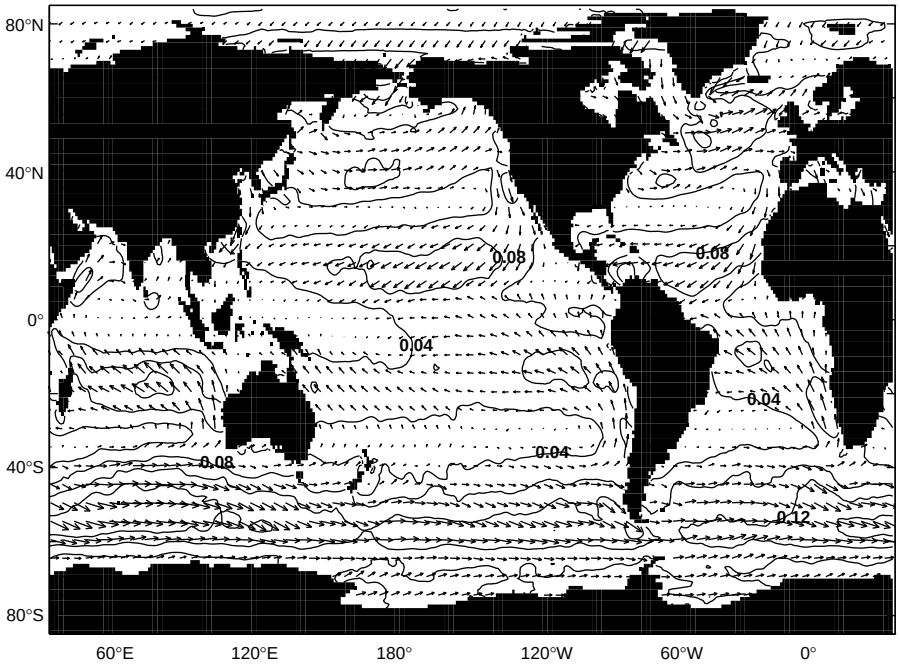

Figure 3. Climatological annual mean wind stress field (contour interval 0.04 N / m^2).

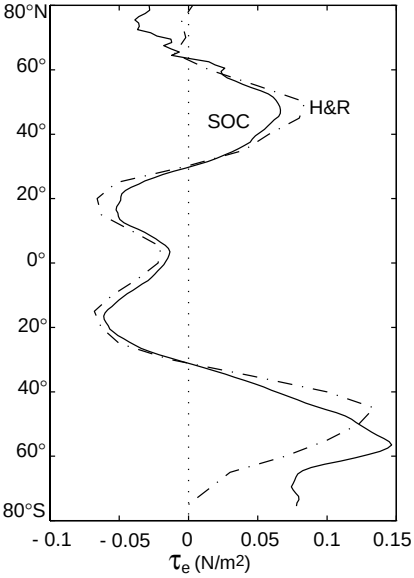

Figure 4. Meridional variation of the zonal mean of the eastward component of the wind stress. SOC = New climatology; H&R = Hellerman & Rosenstein climatology.

variations in the heat transport (Lamb and Bunker, 1982). Even with this caveat in mind it is clear that our unmodified heat flux field is not in balance with the hydrographic estimates of the heat transport in the Atlantic: the implied poleward transport remains untenably high at 70°N and there is too rapid a transition to southward transport in the South Atlantic. However, with the additional corrections discussed above the implied heat transport is in much better agreement with the hydrographic estimates, the major change being effected by the shortwave correction. We are of course aware that at this stage we have only included the aerosol correction in a very simple-minded way and the next stage of our analysis will be to include a detailed correction based on satellite retrieved values of the aerosol optical depth. Even so, the key point remains that we are able to obtain agreement largely on the basis of a regional correction to the shortwave with a physical basis as opposed to the basin-wide adjustments required by the inverse analyses carried out in past climatological studies. Consequently, the spatial variation of the net heat flux in our climatology will differ from that in past studies and this has potentially significant consequences for diagnostic studies such as those of water mass formation rates.

In addition to the heat flux we have also calculated the wind stress, for which the annual mean field is shown in Fig. 3. It suffers from less uncertainty than its heat flux counterpart as the drag coefficient relationship used to calculate the stress (Smith, 1980) has received recent support from the analysis of wind stress measurements made in the Southern Ocean by Yelland and Taylor (1996). Initial comparisons of the global mean eastward component of the wind stress with the Hellerman and Rosenstein (1983) climatology, see Fig. 4, indicates values which are up to 20% smaller in the latitude range 60°N–30°S, probably as a result of the lower drag coefficients employed. Note also that the zone of maximum wind stress in the Southern Ocean is displaced southwards by about 10° relative to that found by Hellerman and Rosenstein.

In conclusion, we stress that these are preliminary results and that much work remains to be done before completion of the climatology. It should be noted that the use of *in situ* reports alone has the disadvantage of poor sampling in regions such as the Southern Ocean and South Pacific and the challenge ahead will be to combine satellite and model estimates of the fluxes with the *in situ* values to improve the quality of the fields in such areas.

References

Bacon, S., 1996: Circulation and fluxes in the North Atlantic between Greenland and Ireland. J. Phys. Oceanogr., submitted.

Clark, N.E., L. Eber, R.M. Laurs, J.A. Renner, and J.F.T. Saur, 1974: Heat exchange between ocean and atmosphere in the eastern North Pacific for 1961–71. NOAA Tech. Rep. NMFS SSRF-682, U.S. Dept. of Commerce, Washington, D.C.

da Silva, A.M., C.C. Young, and S. Levitus, 1994: Atlas of surface marine data Vol. 1: Algorithms and procedures. NOAA Atlas series, , pp.74.

Gilman, C. and C. Garrett, 1994: Heat flux parameterizations for the Mediterranean Sea: The role of atmospheric aerosols and constraints from the water budget. J. Geophys. Res., 99(C3), 5119–5134.

Hall, M.M., and H.L. Bryden, 1982: Direct estimates and mechanisms of ocean heat transport. Deep-Sea Res., 29(3A), 339–359.

Hellerman, S., and M. Rosenstein, 1983: Normal monthly wind stress over the World Ocean with error estimates. J. Phys. Oceanogr., 13, 1093–1104.

Klein, B., R.L. Molinari, T.J. Müller, and G. Siedler, 1995: A transatlantic section at 14.5°N: Meridional volume and heat fluxes. J. Mar. Res., 53, 929–957.

Lamb, P.J., and A.F. Bunker, 1982: The annual march of the heat

budget of the North and Tropical Atlantic oceans. J. Phys. Oceanogr., 12, 1388–1410.
Reed, R. K., 1977: On estimating insolation over the ocean. J. Phys. Oceanogr., 7, 482–485.
Saunders, P.M., and B.A. King, 1995: Oceanic fluxes on the WOCE A11 section. J. Phys. Oceanogr., 25, 1942–1958.
Smith, S.D., 1980: Wind stress and heat flux over the ocean in gale force winds. J. Phys. Oceanogr., 10, 709–726.
Smith, S.D., 1988: Coefficients for sea surface wind stress, heat flux and wind profiles as a function of wind speed and temperature. J. Geophys. Res., 93, 15467–15474.
Wunsch, C., 1984: An eclectic Atlantic Ocean circulation model. Part I: The meridional flux of heat. J. Phys. Oceanogr., 14, 1712–1733.
Yelland, M.J., and P.K. Taylor, 1996: Wind stress measurements from the Open Ocean. J. Phys. Oceanogr., 26, 541–558.

Oceanic Estimates of Global Ocean Heat Transport

Alison M. Macdonald and Carl Wunsch, Massachusetts Institute of Technology, Cambridge, MA 02139-4307, USA, alison@plume.mit.edu

Because the oceanic heat budget is a major component of the climate system, its determination is a central WOCE goal. Existing estimates of oceanic heat fluxes occupy a wide range of values. Although there does appear to be some convergence in the more recent estimates (especially in the North Atlantic), not only the magnitude but also the sign of the heat flux remains in question at some latitudes over much of the globe. A major interpretive difficulty also exists in the common lack of error bars associated with published heat flux estimates. The intention of the present study is to compute estimates of zonally integrated meridional heat flux across all available latitudes based on a globally consistent mass-conserving circulation pattern and to provide estimates of the uncertainty in these values.

The circulation estimate described in Macdonald and Wunsch (1996) allows a calculation of the global oceanic heat budget. The transoceanic fluxes are shown in Table 1; these are compared to previous estimates (where the authors have produced useful error bars) in Fig. 1 (page 21). Our model provides estimates of the heat flux across three complete latitudinal circles: 47°N, 24°N and 30°S. At 30°S the estimated heat flux of -0.9 ±0.3 PW is dominated by a large (>1 PW) southward temperature flux in the Indian Ocean. This value is not significantly affected by the magnitude of the Pacific-Indian throughflow. At 47°N, the net northward heat flux of 0.6 ±0.3 PW is dominated by transport within the Atlantic basin. At 24°N, the model estimate of 1.5 ±0.3 PW is lower than, but consistent with, 2 ±0.3 PW suggested by Bryden et al. (1991). Most of the discrepancy between these values occurs in the Pacific and is due to differing Ekman transport estimates.

The heat flux estimates are robust, as they are insensitive to many of the choices that affect the mass transport estimates. They are, however, sensitive to the initial estimates of the Ekman transport (particularly at 10°N in the Pacific) and in some cases to estimates of western boundary current transport (*e.g.*, 11°N in the Atlantic). The model estimates of heat flux uncertainties are optimistic as they only represent the uncertainty in the absolute transport, which is due to the uncertainty in the reference level velocities. To account for the portion of the uncertainty that arises from the assumption that the data set represents a climatology, an additional 0.25 PW (Holfort, 1994) has been included in the quoted values of uncertainty (as a crude estimate). Error bars on the previously published values do not include this contribution.

Table 1. Estimates of heat (upper portion of the table) and temperature (lower portion of the table) fluxes across the model box boundaries. The sections are shown in Fig. 2. Positive values represent northward transport. The component due to Ekman flux is included. Temperature fluxes are given for non-mass conservation fluxes and are converted to equivalent heat fluxes using °C.

Section	Net Mass transport (10^9 kg/s)	Heat/Q transport (PW)
Atlantic 48°N	-1.0 ± 1.3	0.65 ± 0.25
Atlantic 36°N	-1.1 ± 1.1	1.01 ± 0.26
Atlantic 24°N	-1.0 ± 1.2	1.07 ± 0.26
Atlantic 11°N	-1.0 ± 1.9	1.39 ± 0.25
Atlantic 11°S	-1.1 ± 1.2	0.89 ± 0.25
Atlantic 23°S	-0.7 ± 1.1	0.33 ± 0.25
Atlantic 27°S	-0.7 ± 1.2	0.49 ± 0.25
Atlantic 57°S	0.0 ± 1.9	-0.03 ± 0.25
Pacific 47°N	0.6 ± 1.4	-0.08 ± 0.25
Pacific 24°N	0.6 ± 1.3	0.45 ± 0.26
Pacific 10°N	0.8 ± 1.7	0.44 ± 0.26
Mozambique Ch. 15°N	0.3 ± 1.6	0.03 ± 0.25
Mozambique Ch. 12°N	0.2 ± 1.4	0.01 ± 0.26
0°E south of 57°S	0.0 ± 1.0	0.03 ± 0.25
0°E north of 57°S	167.4 ± 5.2	1.85 ± 0.28
0°E to African Coast	142.7 ± 4.6	0.90 ± 0.31
Drake Passage	141.1 ± 3.4	1.40 ± 0.27
30°E	143.7 ± 4.7	1.16 ± 0.40
132°E	151.0 ± 7.9	1.73 ± 0.43
Pacific 28°S	9.5 ± 6.8	-0.04 ± 0.30
Pacific 43°S	9.4 ± 7.0	0.26 ± 0.28
Indian 18°S	-8.6 ± 6.5	-1.45 ± 0.30
Indian 32°S	-8.1 ± 6.6	-1.30 ± 0.28

Fig. 2 illustrates the pattern of oceanic heat divergence (the quantity of importance to atmospheric interaction) within the boxes. Although some of these values are not significantly different from zero, their pattern is recognizable. The expected net heat losses in the northern basins of the Atlantic and Pacific are apparent. Heat gain around the equatorial regions and loss throughout much of the Southern Ocean also is shown.

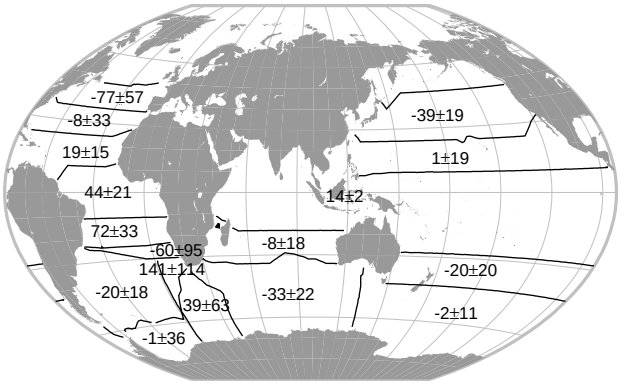

Figure 2. The estimated heat flux convergence and divergence. A convergence represents a net heat loss to the atmosphere. All values are in W/m^2.

The relative lack of direct estimates of the oceanic heat transport across latitudinal circles to compare to estimates of atmospheric heat transport in the global budget has been due to the paucity of data. As new WOCE sections become available, they will be included in the model. These data will fill in the broad regions of Fig. 1 where it has until now been impossible to make direct oceanic estimates of meridional heat flux. The new WOCE data also will allow direct estimates of zonal heat fluxes and divergences to be made.

References

Bryden, H.L., D.H. Roemmich, and J.A. Church, 1991: Ocean heat transport across 24°N in the Pacific. Deep-Sea Res., 38, 297–324.

Hall, M.M., and H.L. Bryden, 1982: Direct estimates and mechanisms of ocean heat transport. Deep-Sea Res., 29, 339–359.

Hastenrath, S., 1982: On meridional heat transports in the world ocean. J. Phys. Oceanogr., 12, 922–927.

Holfort, J., 1994: Grossräumige Zirkulation und meridionale Transporte im Südatlantik. Ph.D. thesis, 118 pp., Ber. Inst. Meeresk. Kiel (in German, English abstract).

Macdonald, A.M., 1993: Property fluxes at 30°S and their implications for the Pacific-Indian throughflow and the global heat budget. J. Geophys. Res., 98, 6851–6868.

Macdonald, A.M., and C. Wunsch, 1996: Indonesian throughflow influence on the global general circulation. US WOCE Report 1996, 23–25.

Rintoul, S.R., and C. Wunsch, 1991: Mass, heat, oxygen and nutrient fluxes and budgets in the North Atlantic Ocean. Deep-Sea Res., 38, Supplement 1A: 355–377.

Semtner, A.J., and R.M. Chervin, 1992: Ocean general circulation from a global eddy-resolving model. J. Geophys. Res., 97: 5493–5550.

Talley, L., 1984: Meridional heat transport in the Pacific Ocean. J. Phys. Oceanogr., 14, 231–241.

This article is a reprint from the US WOCE Report 1996.

Data Assimilation and Inverse Methods: A Summer School, 16–17 June 1997 at the College of Oceanic and Atmospheric Sciences, Oregon State University,Corvallis, Oregon

The College of Oceanic and Atmospheric Sciences at Oregon State University has, since 1988, offered an upper-level graduate course on data assimilation and inverse methods. The class notes have evolved into a monograph. They undergo continual update. The course is usually taught in about twenty-four 50-minute lectures and about eight 50-minute discussion sessions in the Winter Term (January–March), but in 1997 it will be offered by the OSU Summer School. The course will be presented in two weeks: 16–27 June, as twenty 60-minute classes meeting twice daily, and ten discussion sessions also meeting daily. Typeset notes will be distributed in class. Theoretical material will be supported, as in the regular course, with slide an video presentations of major applications in oceanography and meteorology. In addition to providing a lecture room, COAS will set up a laboratory housing 24 UNIX workstations reserved for this course. Supercomputer time will be available to ambitious and experienced students, using the COAS CM-5 Connection Machine and IBM SP-2.

A block of 24-single occupancy rooms with own or pair-shared bathrooms has been reserved in the College Inn, an upper-class residence hall next the OSU campus. It is likely that travel funds will be available for about 24 US-based graduate students, post-doctoral fellows or junior faculty members.

For further information, please e-mail Florence Beyer (fbeyer@oce.orst.edu).

An Investigation and Validation of a Global Ocean Model (OCCAM)

Peter M. Saunders and Andrew C. Coward, James Rennell Division, Southampton Oceanography Centre, UK, peter.saunders@soc.soton.ac.uk

The Model

A Bryan-Cox-Semtner numerical model of the global ocean has been coded for and run on a Cray-T3D with 256 parallel processors. The OCCAM (Ocean Circulation and Climate Advanced Model) Project is directed by Dr David Webb (SOC) who has led the development of the parallel code. The model has 36 levels in the vertical, 20 m at the surface increasing to 250 m at depth, a spatial resolution of 0.25° everywhere and a time step of 15 minutes. The model has realistic topography (consistent with its spatial resolution – though limited to 5500 m in depth), and has channel dynamics for the Bering Strait. Surface forcing is provided by wind stress vectors interpolated from an annual cycle of 12 monthly fields: these are derived from ECMWF data for the years 1986–1988. The initialisation of the potential temperature and salinity field was from the Levitus'94 mean climatology and surface values are relaxed to interpolated monthly values of Levitus'94 with a time constant of 30 days. A freshwater flux is applied to the surface salinity, rather than a salt flux: accordingly changes in the free surface height result.

Further details: the message passing routines amongst the processing elements, the rotated mapping of the Arctic to avoid the singularity of the pole and the use of a higher order upstream advection scheme, are described by Coward (1996).

At the time of writing the model has been run for 12 years but we have made use of an initial climatology constructed from 72 output dumps at 15 day intervals, and this is referred to as the 5–7 year climatology. For the WOCE Pacific Workshop (August 1996) we have concentrated exclusively on the Pacific region of the model and targeted zonal sections on which WOCE one-time observations were made. Some of our findings are reported here.

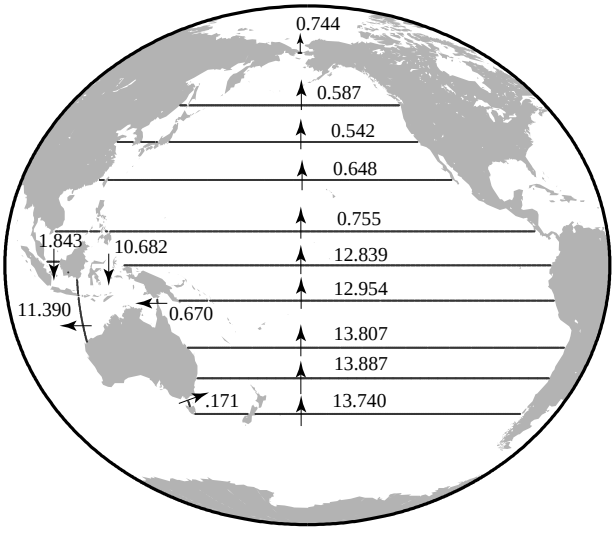

Figure 1. Volume flux in Sv from the OCCAM 5–7 year output. The first layer includes the free surface height contribution.

Volume fluxes

Volume and mass are interchangeable in the model and we shall employ the former with units of Sv (10^6 m^3 s^{-1} or 10^9 kgs^{-1}). Calculations of the volume fluxes on 12 WOCE sections are plotted in Fig. 1. The volume fluxes are of particular interest in the South Pacific because they reflect the exchange of water between the Pacific and Indian Oceans (the throughflow). The magnitude of the mean throughflow is seen to be ~13.2 Sv – measuring between Asia and Australia. The inflow at 43°S is ~13.9 Sv, the outflow through the Bering Strait at 65°N is ~0.75 Sv. Over the entire Pacific there is thus a very small imbalance ~0.05 Sv which corresponds to an excess of precipitation over evaporation of 1.2 cm/yr.

Estimates of the Indonesian throughflow vary widely (0 to 20 Sv) but we believe that only when the results from moored arrays of current meters deployed in the significant straits (principally the Makassar Strait according to OCCAM) will definitive values be established. A theoretical method for estimating the throughflow was proposed by Godfrey (1989) which he termed the Island Rule. An approximate expression for finding the circulating flux is to average the Sverdrup transport to the east of an Island (here Australia) reckoned from the nearest eastward land mass (here South America). We have found that averaging from the southern tip of Tasmania to the northern tip of Papua-New Guinea yields a value of 12.4 Sv northward, in the correct direction and very close in magnitude to the throughflow flux in OCCAM.

As seen from Fig. 1 the divergence of the volume flux is non-zero and dividing it by the area of the ocean surface between the sections yields values of precipitation minus evaporation. Fig. 2 shows this quantity expressed in cm/yr along with values (underlined) calculated from the tabulations of Baumgartner and Reichel (1975). According to OCCAM evaporation exceeds precipitation over the entire South Pacific and in the low and mid-latitude North Pacific. Elsewhere precipitation exceeds evaporation. The distribution is not only qualitatively reasonable but also quite accurately reflects the calculations of Baumgartner and Reichel. However over the Pacific as a whole the excess of precipitation (including runoff) over evaporation is 13 cm/yr, ten times the value for the OCCAM climatology.

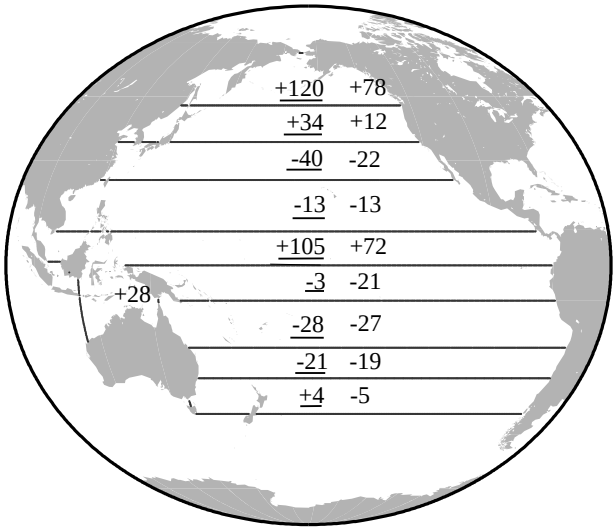

Figure 2. Volume flux divergence expressed as precipitation minus evaporation in cm/yr derived from Fig. 1. The underlined values are from Baumgartner and Reichel (1975).

Meridional heat fluxes

Table 1 presents estimates of the meridional heat fluxes on the WOCE sections. The heat flux calculation combines the mean north current with the the mean potential temperature: a second calculation in which the mean is found of the 72 individual current and temperature combinations has also been made (but is not shown). The difference represents the contribution by all transients, both seasonal and travelling eddies and model climate drift and is almost everywhere negligible, reaching a maximum of only .04 PW at the equator.

Table 1. OCCAM Heat Fluxes: 5-7 year averages

	Lat.	Ekvflux [Sv]	htflux [PW] total	over-turning	circu-lating
Scorpio+	43.5°S	7.6	0.26*	0.46*	-0.20
P6	32.5°S	1.5	0.28*	0.57*	-0.29
capricorn (P21)	23.5°S	-9.1	0.26*	0.38*	-0.12
P31+	10°S	-19.8	0.20*	0.10*	0.10
Equator	0		0.61*	0.30*	0.31
Throughflow	115°E		-0.75*	-0.80*	0.05
P4	9.5°N	26.5	0.39	0.55	-0.16
P3	24.25°N	9.6	0.38	0.10	0.28
P2	35.5°N	-4.9	0.30	-0.11	0.41
P1	47°N	-4.1	0.08	-0.04	-0.12

*significant contributions arise from the net flux (13–14 Sv).

Table 1 shows a decomposition between the overturning (thermohaline) and horizontal circulating mode. The latter are independent of net volume fluxes but the former are not. Indeed because of the large volume fluxes which dominate the 'heat' flux values many authors prefer to combine the South Pacific with the corresponding latitude in the Indian Ocean since the net volume flux will then be small – as it is in the North Pacific. In the North Pacific the figures given can be interpreted at face value; thus the heat flux at 10°N and 24°N is about 0.4 PW which is two-thirds and one half of the values derived by Wijffels (1993) and Bryden *et al*. (1991) respectively. The northern sections at 35°N and 47°N yield 0.3 and 0.1 PW northwards both having the opposite sign to the controversial small southward results of Roemmich and McCallister (1989).

Throughout the Pacific heat flux divergence can be calculated and interpreted as air-sea exchange. This ignores model drift terms which at the corresponding stage of the FRAM integration were found small but not negligible. The results are presented in Fig. 3 and show extremely small heat fluxes for the entire South Pacific. These results imply that in the mean the model remains very close to climatological values. There are numerous air-sea exchange climatologies with which comparisons can be made, we have chosen a recent one by Large and Doney (1996) and from their maps have attempted ROUGH estimates of band averages (underlined). Although the latter values have large uncertainties the conclusion can be drawn that in the North Pacific the OCCAM virtual exchanges are smaller than the air-sea exchange estimates. This is consistent with the smaller meridional estimates in the model compared with the observationalists estimates.

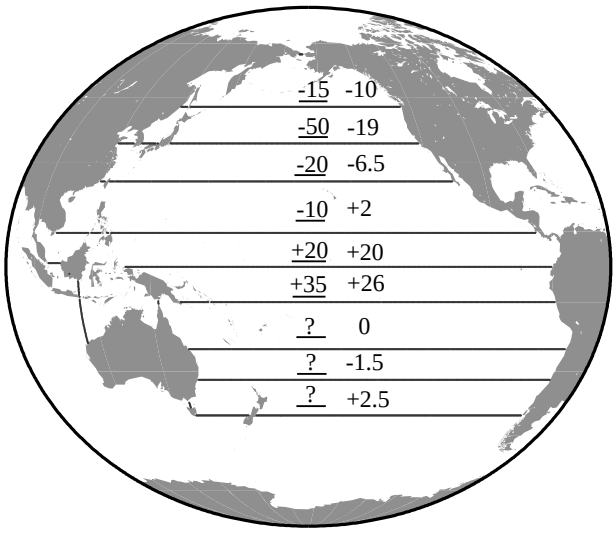

Figure 3. Heat flux divergence in W / m^2 from OCCAM 5–7 yr output (plus is ocean gain). Underlined values are from Large and Doney (1996).

Meridional cold water fluxes

In the South Pacific two observational estimates have been made of the cold bottom water invading the region from the Antarctic. These are in the Samoa Passage at 10°S and east of the Kermadec-Tonga Ridge at 32°S.

Samoa Passage

At 10°S the principal channel for water below 4000 m depth is the Samoa Passage (170°W). By hydrographic survey Roemmich *et al.* (1996) have determined that additional flows occur to the west on Robbie Ridge (175°W), and east of the Manihiki Plateau (160°W). Rudnick (pers. comm.) reported flux measurements from an array of current meters in the Samoa passage but at the other two locations only estimates from the hydrography are available. Fig. 4b (page 22) shows the northward currents derived from OCCAM in the region revealing the three cores of flow – in the expected locations. Fig 4a (page 22) shows the currents derived from the Levitus climatology and an assumed deep reference level. It is difficult to see any connection between the initial and the 5–7 year states of the model. Table 2 shows the agreement of the flux estimates – observations and model which is remarkably good.

Table 2. Abyssal Transport (Sv) through the Samoa Passage and adjacent regions (10°S)

Location	Robbie Ridge	Samoa Passage	Manihiki Plateau
Longitude	175°W	170°W	160°W
Roemmich *et al.* (ref. 1.2°C)	1.1	7.8	2.8
Rudnick (>4Km)		6.0 ±1.5	
OCCAM (>4Km)	1.3	5.9	1.8

WOCE P6

At 32°S a massive array consisting of 20 moorings and 60 current meters was deployed over a distance of 1000 km. Although the records are freely available no definitive flux estimate has been published. Whitworth (pers. comm.) states that the transport below 2000 m for all the records has a two year mean of 13.3 Sv: our estimate (from current meters) for transport colder than 1.5°C (near 3000 m) is 14.8 Sv. Over the same longitude range the OCCAM flux for water colder than 1.5°C is only 8.0 Sv, only 55% of the observed value. The flux accumulated across the entire section in the model amounts to only 10.8 Sv so that little in the interior augments the deep western boundary current flux.

The cold flux is determined in OCCAM by determining the transport below the time mean depth of the selected isotherm. From the covariance of flow and temperature at this mean depth the time-dependent contribution can be found. The cold flux is found negatively correlated with the depth of the isotherm but the contribution is alas only ~0.1 Sv and does not explain the discrepancy. Rather there are various indications that the bottom flow in the 5–7 year climatology has not yet reached an equilibrium condition – that is the deep model layers are filling with and emptying of cold water.

Other conclusions

We have examined far more of the output than is described here. Over large areas of the Pacific the interior flow is dominated by the Sverdrup balance which more or less correctly predicts the strength of the WBCs. In regions of significant topography, bottom pressure torqe terms are locally important, but when integrated basinwide they have small impact on the WBC strength. The inference is that much of the circulation is dominated by the stress (curl) with which the model is forced – and this includes the throughflow. We have found the study of the entire region, with which we were quite unfamiliar, a tremendous educational experience and predict that models such as OCCAM will have a training role for the oceanographers of the future.

References

Baumgartner, A., and E. Reichel, 1975: The World water balance. Elsevier, 179pp.

Bryden, H.L., D.H. Roemmich, and J.A. Church, 1991: Ocean heat transport across 24°N in the Pacific. Deep-Sea Res., 38(3), 297–324.

Coward, A.C., 1996: Current status of the OCCAM global ocean model. Sigma, 20, 4–6.

Godfrey, J.S., 1989: A Sverdrup model of the depth-integrated flow for the world ocean allowing for island circulations. Geophys. Astrophys. Fluid Dynamics, 45, 89–112.

Large, W.G., and S.C. Doney, 1996: Global surface forcing fluxes and parameters. U.S.WOCE Report 1996, 14-16. Texas A. & M., College Station, TX.

Roemmich, D., and T. McCallister, 1989: Large scale circulation of the North Pacific Ocean. Progress in Oceanogr., 22, 171–204.

Roemmich, D., S. Hautala, and D. Rudnick, 1996: Northward abyssal transport through the Samoan Passage and adjacent regions. J. Geophys. Res., in press.

Wijffels, S.E., 1993: Exchange between hemispheres and gyres: A direct approach to the mean circulation of the Equatorial Pacific. Ph.D Thesis. MIT/WHOI, WHOI-93-42.

Availability of OCCAM Model Output

The Ocean Circulation and Climate Advanced Modelling project (OCCAM) has successfully integrated its fully global, 1/4 degree resolution ocean model for 14 model years. Details of the model and example model output in the form of MPEG encoded animations are available via the WWW at:

http://www.soc.soton.ac.uk/JRD/OCCAM

Some analysis products may be made available via this service but space is limited. Instead, it is hoped to service requests for small to medium volumes of data via short-term postings in anonymous ftp space. Requests for large volumes of data will also be considered although preference will necessarily be given to requests leading to collaborative publications.

Requests for model output or further enquiries should be sent to the OCCAM project manager: Beverly de Cuevas (Beverly.Decuevas@soc.soton.ac.uk).

Heat Fluxes of the South Pacific Estimated Through Inverse Models

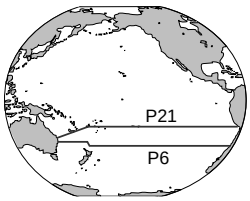

M.N. Tsimplis, S. Bacon and H.L. Bryden, James Rennell Division for Ocean Circulation, Southampton Oceanography Centre, UK, michael.tsimplis@soc.soton.ac.uk

WOCE zonal sections P6 (32˚S) and P21 (17˚S) across the South Pacific are combined through an inverse method in order to determine the circulation and estimate the heat fluxes. The hydrographic stations that make up the sections used in the present study are shown in Fig. 1. In order to reveal the consistent part of the circulation, an area enclosed by the two hydrographic sections and the coasts of Australia and South America is considered. Within this closed area the mass must be conserved and the mass fluxes between the two sections must be balanced.

The geostrophic shear across the pairs of stations is estimated from the temperature and salinity observations on the basis of some selected initial reference level. This provides a "starting" baroclinic velocity field. Following Banks *et al*. (1995) the starting reference level across the South West Pacific Basin was selected to coincide with the 1.5˚C and 1.2˚C potential temperature isotherms at P6 and P21 respectively. Choosing these potential temperature values effectively leads to a balance of the fluxes of the Deep Western Boundary Currents across the two sections. In the other parts after several tries with different values for the reference level a value of 3300 m was selected as the most suitable.

The water column was divided into 15 layers separated by appropriate isopycnal surfaces. The characteristics of the layers are shown in Table 1. Topographical constraints determine the water properties especially in the bottom layers. For example the distribution of temperature and salinity indicates that basins such as the New Caledonian Trough and the South Fiji Basin are filled with less dense water than the deep parts of the Tasman Sea, in the west and the South West Pacific Basin in the east. This is due to the fact that both these basins are closed to the south below 3500 m and therefore their deeper parts are filled with water from the north. In contrast the Tasman Sea which is closed at its northern boundary below 4000 m is filled with water that comes from the south. The deepest parts of the South West Pacific basin are filled with Lower Circumpolar Water and some traces of North Atlantic Deep water. This water is warmed up, by mixing, as it moves northwards from P6 to P21 and this is expressed in the reduction in size of the area of the deepest layers.

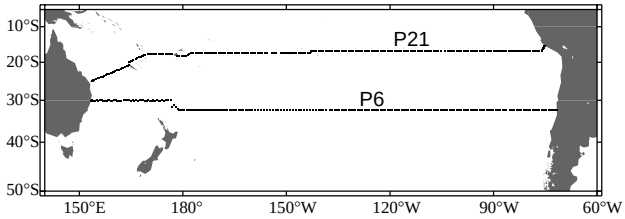

Figure 1. Location of WOCE sections P6 (May 1992) and P21 (May 1994).

The two sections and the isopycnals define closed boxes if there is no cross-isopycnal flux. An inverse problem (Wunsch, 1978) is then constructed as follows: In each box (defined in the vertical by the isopycnal layers) the baroclinic velocity field on the two sections should be corrected to conserve mass and salt. Moreover the correction should produce an overall geostrophic velocity field that balances the Ekman fluxes as calculated from the Hellerman and Rosenstein (1983) climatology.

The deepest parts of some of the basins are closed, therefore the corrections should result into zero total flux across these areas. As the Indonesian Throughflow is estimated to be between 0 and 20 Sv, there is a significant uncertainty regarding the net mass flux across the two sections. Experiments with several values of net mass flux representing the throughflow showed that our methodology is not able to discriminate against any of the values nor to indicate a preferred value.

Table 1. Mean depths and mean thickness of layers. The density surfaces used as separation boundaries are expressed in sigma 0, sigma 2, and sigma 4.

Layer		Density of upper surface	Mean Depth (m)		Mean Thickness (m)	
			P6	P21	P6	P21
	1	Surface	106	155	213	311
	2	26.130	282	357	138	100
s_0	3	26.635	476	475	248	137
	4	26.966	764	627	334	166
	5	27.154	1075	884	288	351
	6	36.500	1360	1234	298	369
	7	36.700	1715	1655	428	490
s_2	8	36.850	2055	2014	267	255
	9	36.900	2459	2409	555	556
	10	36.960	2931	2941	420	523
	11	45.800	3191	3337	289	386
	12	45.820	3449	3597	343	426
s_4	13	45.850	3871	3913	719	717
	14	45.930	4370	4394	475	400
	15	45.960	5005	4907	1053	726

The dataset consists of measurements taken within three months for each section with a difference of two years between the two sections. Therefore the model may have to accommodate interannual variability and transient localised features of the circulation. It is routine procedure to truncate the solution and assume that the highest degrees do not correspond to part of the (assumed) steady large scale circulation. The variability introduced by the truncation can be seen in Fig. 2 where the integrated zonal circulation

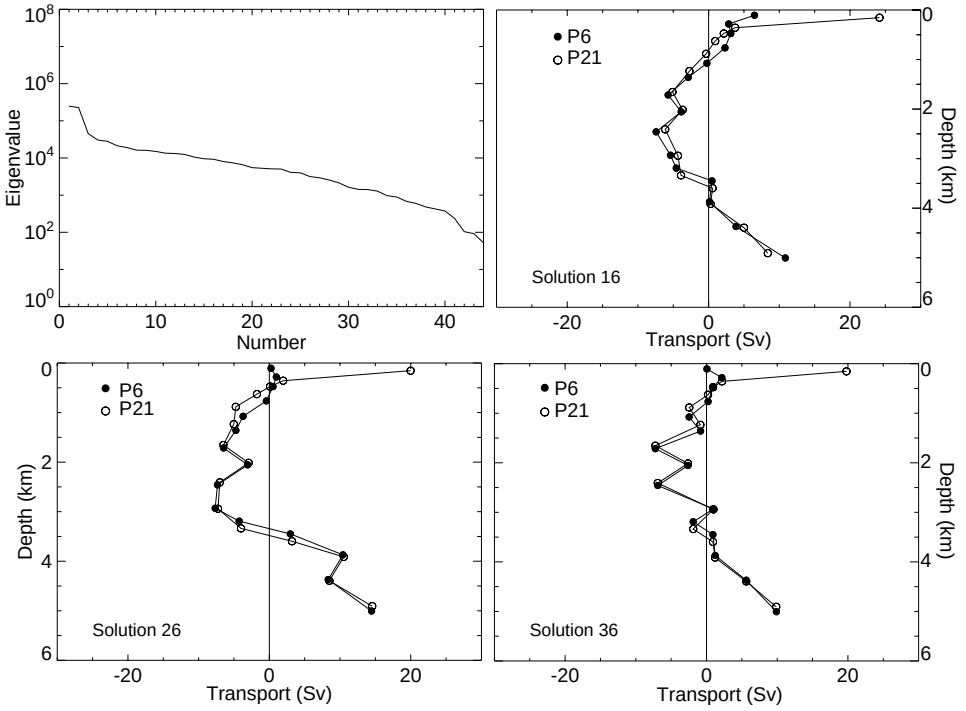

Figure 2. The eigenvalues of the standard model (top left). The zonally integrated transport for the two sections for three solution degrees. The Indonesian Throughflow is assumed zero.

that corresponds to zero net flux for three solution degrees is shown. The northward flow of the deepest waters, the southward moving middle layers and the northward moving top layers are all in reasonable agreement with the study of Wunsch *et al*. (1983) based on the Scorpio sections across 28˚S and 43˚S, done in 1967.

From the volume fluxes of the model and the temperature distribution, heat fluxes can be estimated. These are variable depending on the constrains of the model and the selected solution degree. The characteristics of nine models are described in Table 2. In Fig. 3 the resulting heat fluxes for some of the models are shown for all solution degrees. As different constrains apply to each of the model the rank of the model varies.

To calculate the values of Fig. 3 the climatological annual mean Ekman heat fluxes have been added to the model results. Model 2, in which vertical velocities are included, and model 4 in which the salt conservation is also applied at the top layer provide significantly different answers from the rest of the solutions. It should be noted that the lower degree solutions do not satisfy all the constrains. In the present case all the solutions corresponding to degrees less than 20 did not provide mass flux balance at the first layer consistent with the climatological mean. Therefore the selection of a "preferred" solution for the models should be after the sharp decrease of the flux curves that occurs between degrees 15 and 21 (29 for the model involving vertical velocities). Nevertheless it is clear that the selection of the solution degree, or equivalently the modification of the Ekman flux estimate, is in general more important than the selection of the model. Our best estimates resulting from the standard model and the

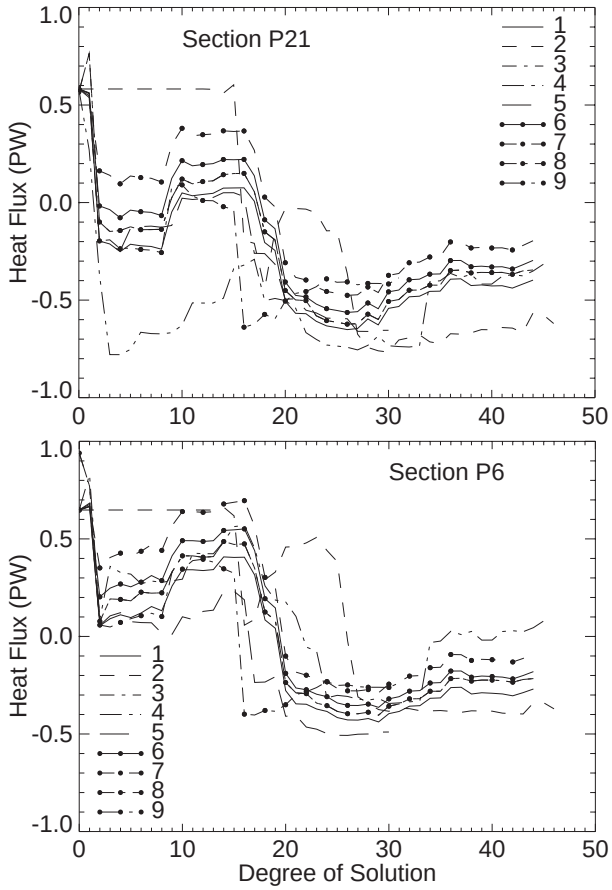

Figure 3. The net heat fluxes across the two sections calculated for 9 models assuming that the Ekman transports are equal to the annual means by Hellerman and Rosenstein (1983), 19.8 Sv at P21 and 0.06 Sv at P6.

scattering of the values is 0.36 ± 0.20 PW southwards for P21 and 0.26 ± 0.3 PW southwards for P6.

The above values strongly depend on the assumed Ekman flux. There is a substantial seasonal variation in Ekman transport between 7.1 Sv northwards and 6.2 Sv southwards at P6 and 25 to 15 Sv northwards at P21. If, for example, the values for the period of the measurements (May–July), are used in the model then the resulting fluxes are 0.46 ± 0.20 PW southwards for P21 and 0.16 ± 0.3 PW northwards for P6 which is a radical difference for the south section.

Table 2. Characteristics of some of the inverse models. Model 1 is the standard model. The climatological mean Ekman flux is included in the first layer in all models. The salt transport due to Ekman flux is only included in model 4. The reference level is the isotherms for the central Pacific at 3300 dbars or 2200 dbars elsewhere. Only in model 9 a uniform reference level is applied.

Model	Reference level	Net Mass flux (Sv)	Topog. constr.	Vert. Veloc.	Mass Balance in layers	Salt Balance in layers
1	3300 dbar 1.2˚C 1.5˚C	0	Yes	No	all	2-15
2	3300 dbar 1.2˚C 1.5˚C	0	Yes	Yes	all	2-15
3	2200 dbar 1.2˚C 1.5˚C	0	Yes	No	all	2-15
4	3300 dbar 1.2˚C 1.5˚C	0	Yes	No	all	1-15
5	3300 dbar 1.2˚C 1.5˚C	0	Yes	No	all	–
6	3300 dbar 1.2˚C 1.5˚C	10	Yes	No	all	2-15
7	3300 dbar 1.2˚C 1.5˚C	20	Yes	No	all	2-15
8	3300 dbar 1.2˚C 1.5˚C	0	No	No	all	2-15
9	2200 dbar	0	Yes	No	all	2-15

Acknowledgement

The first author is supported by HCM (EC) contract ERB4050PL931072.

References

Banks, H., H. Bullister, S. Bacon, and H. Bryden, 1995: The Deep Western Boundary Current at 17˚S in the Pacific Ocean. International WOCE Newsletter, 19, 3–5.

Hellerman, S., and M. Rosenstein, 1983: Normal monthly wind stress over the world ocean with error estimates. J. Phys. Oceanogr., 13, 1093–1104.

Wunsch, C., 1978. The North Atlantic General Circulation west of 50˚W determined by inverse methods. Rev. Geophys. Space Phys., 16(4), 583–620.

Wunsch C., D. Hu, and B. Grant, 1983: Mass, heat, salt and nutrient fluxes in the South Pacific Ocean. J. Phys. Oceanogr., 13, 725–753.

Preliminary Estimates of the North Atlantic Wind Stress Fields from Visually Observed Wave Data

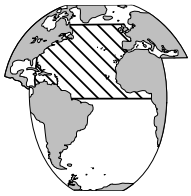

Sergey Gulev, P. Shirshov Institute of Oceanology, RAS, Moscow, Russia; and
Lutz Hasse, Institut für Meereskunde, Düsternbrooker Weg 20, D-24105 Kiel, Germany,
rocc@sovam.com

Wind stress on the sea surface is a key parameter of the ocean-atmosphere interaction. Ocean general circulation models and coupled models use wind stress to force ocean circulation. Experimental studies focused to compute meridional fluxes on WOCE sections use wind stress estimates to account for the Ekman component of meridional fluxes. During the last two decades a number of wind stress climatologies were produced. These climatologies use for the computations of the wind stress the so-called traditional bulk formulations, based on the dependence of drag coefficient on wind speed and stability (Large and Pond, 1981; Smith, 1988). During the last 30 years a number of experimental, laboratory and theoretical results (*e.g.* Hasselmann *et al*., 1973; Smith *et al*., 1992 (S92); Janssen, 1989) developed the physics of the influence of the sea state on wind stress on the sea surface. These results demonstrate that the roughness of sea surface, and therefore the drag coefficient appear to be a function of wave age. In this context it is interesting to apply these results to the wind stress climatologies, based on voluntary observing data in order to produce the climatology of wind stress, based on its dependence on the sea state, and to figure out whether this dependence (if it exists) is important for climatological forcing fields.

Data

We used the collection of compressed marine reports (CMR) and long marine reports (LMR) for the period 1946–1993, available from COADS Releases 1 and 1a (Woodruff *et al*., 1993). CMR and LMR contain in coded form in addition to basic meteorological variables height, period, and direction of wind waves and swell, taken visually by voluntary observing ships. This data set is the

only source at present of separate sea and swell estimates. For example, satellite signatures provide data about significant wave height which results from both sea and swell. Wave parameters, observed visually, should not be worse than Beaufort estimates of wind speed, which still contribute about 70–80% of the total number of marine wind observations. Sailors, estimating Beaufort force, make use of the sea state, and the latter is always under their considerable attention. It is difficult to estimate the accuracy of night observations, but again, it should not be worse than in the case of wind speed which is underestimated in night time by 10–20% for moderate and strong winds (Kent et al., 1993). Visible presence of reports with wave observations appears in COADS in 1963 and for later decades their contribution is close to 60%. Decoded wave variables after quality control were used for computations of the wind stress and its components over the North Atlantic for individual months from 1964 to 1993. Climatology of individual wave variables is presented in Gulev (1994).

Methods

To estimate sea state-dependent wind stress we first obtained estimates of the wave age (Smith, 1991), as $a = C_p / V_{ef}$, where C_p is the deep water wave phase speed at spectral peak, and V_{ef} is component of wind in wave direction. In general, if $a < 1$, waves are assumed to be sea, and if $a > 1$, waves are considered as swell. An alternative estimate of wave age $a_* = C_p / u_*$, where u_* is the friction velocity, from a theoretical viewpoint appears to be more credible (Janssen, 1989). At the same time wind speed is a much more easily available parameter, than u_*. The deep water wave phase speed was computed from wave period p_w, as $C_p = (g/2\pi)p_w$. We assumed, that the visual estimate of wave period and height is taken at "spectral peak". The effective wind is evaluated from the actual wind vector, as $V_{ef} = V_{10}\cos\theta$, where θ is the angle between wave and wind direction, V_{10} is wind speed at 10 m anemometer reference level. Following da Silva *et al.* (1994) we assumed measured winds in COADS CMR to be taken at 20 m, and adjusted wind speeds to the 10 m level according to the Smith (1988) formulation. Estimated winds in the COADS CMR collection were assumed to be taken at 10 m reference height. According to the recommendations of Dobson *et al.* (1994) we eliminated those reports, which give $|\theta| > 30°$, when sea was not in wind direction and those reports, which give $a > 1.2$. Selected reports with wave observations were accepted for the calculations of wave age and for the evaluation of the wind stress. S92 introduced a "neutral drag coefficient anomaly" which represents the departure of neutral drag C_{va}, caused from its dependence on wave age. Following S92 and Dobson *et al.* (1994), this anomaly can be computed from wave age, as

$$10^3 \delta C_n = 1.85 - 2.24\, a. \qquad (1)$$

Equation (1) gives zero departure at a wave age of 0.83. For every individual report we applied anomaly (1) to the neutral drag coefficient of Smith (1988), and computed a revised drag coefficient, which has been taken for the computations of the wind stress and its components:

$$\tau = \rho_a C_v V^2,\ \tau_x = \rho_a C_v V V_x,\ \tau_y = \rho_a C_v V V_y. \qquad (2)$$

Individual estimates of wave age and sea-state-based wind stress, computed from different parameterizations were averaged into 5-degree boxes for 30-year period from 1964 to 1993.

Results

The annual mean wave age indicates the area with youngest waves in the central North Atlantic mid latitudes where a is smaller than 0.74. Another local minimum with ages ranging from 0.74–0.76 is in the Norwegian Sea. Tropical local maximum in the trade wind zone is characterized by ages from 0.76–0.79. Highest annual values in the subtropical North Atlantic and in the equatorial area vary from 0.78–0.82, but never reach the 0.83 value. Considering the annual cycle, youngest waves are observed in winter and are characterized by values of 0.67–0.71 in mid latitudes. Summer values are higher than 0.82 practically everywhere, except for some areas in the mid latitudes and the tropics. Highest wave age, ranging from 0.88–0.90 appears during summer months in equatorial areas.

To compare different estimates of stress with and without considering wave age we computed ratios between

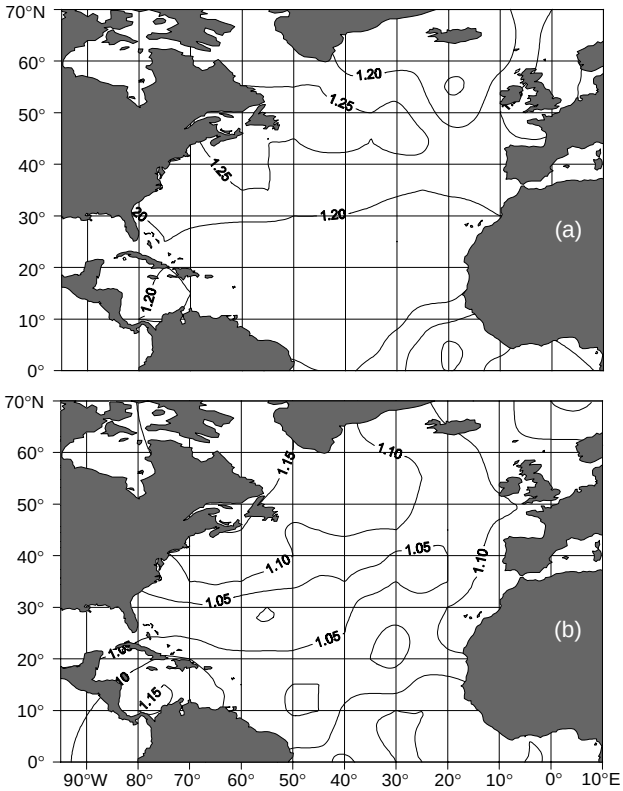

Figure 1. Ratios between S92 and traditional estimates of wind stress for January (a) and July (b).

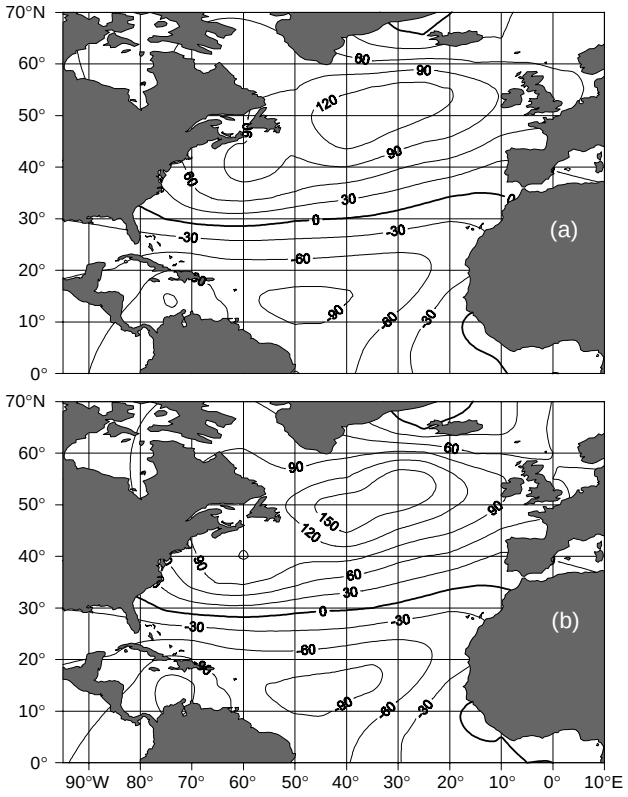

Figure 2. Annual mean east and north component of wind stress (10 N/m), computed traditionally (a) and from wave age (S92) (b).

them for individual months. Charts of these ratios are shown in Fig. 1. In winter Smith's (1992) estimate (2) is 10–25% higher than traditional. A maximum of the ratio between two estimates is located in the mid-latitude North-West Atlantic. In July, when waves become significantly more developed, the ratio ranges from 0.95–1.13. In some very limited regions in the subtropics and the equatorial area the ratio between Smith (1991) and traditional estimates is smaller than 1, indicating higher values of stress taken traditionally. If we compare east and north components of wind stress, there will be major differences for the east component. Fig. 2 compares east components of wind stress taken traditionally with those computed with Smith's (1992) method and indicates from to larger positive values in mid latitudes and from 20×10^{-3} to 30×10^{-3} N/m^2 stronger negative τ_x in the tropics, when computed with wave age based approach.

Impact of the sea state on wind stress can have profound implication for the evaluation of wind-driven circulation in ocean models. We applied the obtained wind stress to the calculation of Ekman volume transport and Ekman meridional heat transport to see whether any differences appear in these important climatological parameters, when computed with wave dependent stress. Meridional Ekman volume and heat fluxes were computed as:

$$EV_\gamma = -\tau_x/f\rho, \quad EH_\gamma = -c_p(T_w - \theta)\tau_x/f, \qquad (3)$$

where f is the Coriolis parameter, ρ is the density of sea water, c_p is the specific heat of sea water, θ is the annual vertical mean potential temperature, which has been taken from Levitus (1987). We computed Ekman volume transports and Ekman heat transports from (3) and then integrated these values over the North Atlantic latitudinal belts. If we compare traditional estimates with those obtained by Levitus, there is a general agreement, although the absolute value of his winter negative transport in mid latitudes is smaller, and the tropical maximum in winter and spring is more pronounced. Seasonal Ekman volume transport, computed with revised wind stress, gives from 10–15% higher tropical values and 20% stronger negative mid-latitude values in winter. Nearly the same relation between the two estimates of wind stress is obtained for the meridional Ekman heat transport. If we consider mean climatological curves of the meridional Ekman volume and heat transports, taken with traditional and wave-based wind stress for the period 1964–1993 (Fig. 3), tropical maximum indicates 10–15% higher values of the Ekman transport when computed on the basis of wave age. Concerning this comparison, we note that Böning *et al.* (1991), made experiments with an eddy resolution circulation model, forced by Isemer and Hasse (1987) wind stress and Hellerman and Rosenstein (1983) wind stress. He obtained significant differences in the intensity of subtropical gyre of the North Atlantic in two experiments,

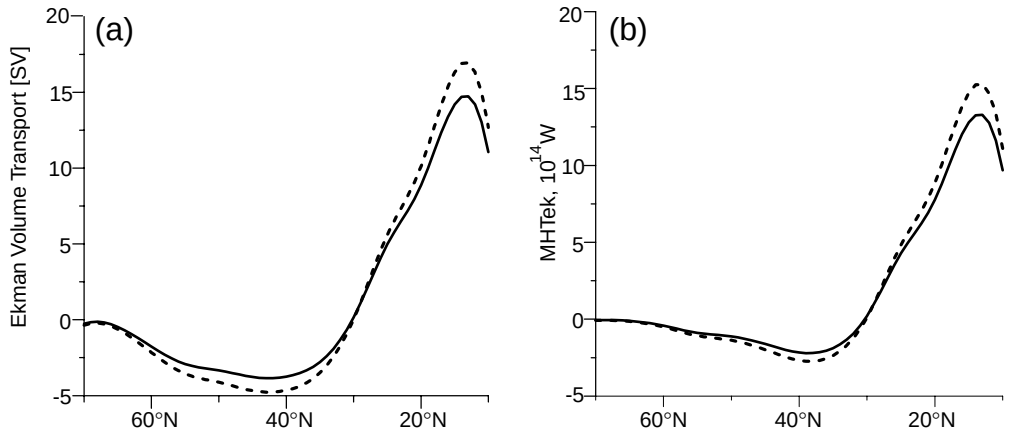

Figure 3. Annual zonal mean meridional Ekman volume transport (Sv) (a), and meridional Ekman heat transport (10°W) (b), computed traditionally (solid lines), and with wind stress, estimated by S92 method (dashed lines).

forced by different stresses.

Our wave age and wind stress calculations give evidence of the climatological significance of the impact of sea state on the wind stress. Of extreme importance still is to attend to such estimates with non-random errors, caused from parameterizations of drag coefficient dependence on wave age. Another important problem is the validation of wave height and especially wave period fields obtained from voluntary reports. In this context it is important to make a comprehensive comparison of visual observations of waves with the few instrumental measurements at a number of locations of the North Atlantic OWS for periods from several months to several years (Bacon and Carter, 1991) and with earlier products based on wave data from voluntary observing fleet (Hogben *et al.*, 1986). We plan also to validate our wave variables against NODC wave buoys, satellite signatures (Cotton and Carter, 1994) and model runs together with scientists from KNMI (de Bilt) and SOC (Southampton). One possible line of future investigation is connected with the evaluation of other important wave-based climatological parameters such as albedo of the sea surface and some other radiation characteristics.

Acknowledgements

This study has been done at IfM (Kiel) and was supported by Deutsche Forschungsgemeinschaft, SFB 133. Individual COADS data were made available by courtesy of Steve Worley of NCAR (Boulder). During this work we had extremely helpful discussions with Fred Dobson and Stuart Smith of BIO (Dartmouth).

References

Bacon, S., and D.J.T. Carter, 1991: Wave climate changes in the North Atlantic and North Sea. Int. J. Climatol., 11, 545-588.

Böning, C., R. Doesher, and H.-J. Isemer, 1991: Monthly mean wind stress and Sverdrup transports in the North Atlantic: A comparison of the Hellerman-Rosenstein and Isemer-Hasse Climatologies. J. Phys. Oceanogr., 21, 221–235.

Cotton, P.D., and D.J.T.Carter, 1994: Cross calibration of TOPEX, ERS-1, and GEOSAT wave heights. J. Geophys. Res., 99, C12, 25025–25033.

da Silva, A.M., C.C. Young, and S. Levitus, 1994: Atlas of surface marine data 1994. Volume 2, NOAA, Washington, DC, 419pp.

Dobson, F.W., S.D. Smith, and R.J. Anderson, 1994: Measuring the relationship between wind stress and sea state in the open ocean in the presence of swell. Atmosphere-Ocean, 32, 61–81.

Gulev, S.K., 1994: North Atlantic wind waves climatology from COADS. Tech. Rep. Institut für Meereskunde, Kiel, 43pp with 73 fig.

Hasselmann, K., *et al.*, 1973: Measurements of wind-wave growth and swell decay during the Joint North Sea Wave Project (JONSWAP). Deutsch. Hydrograph. Zeit., Suppl. A8, 12, 22pp.

Hellerman, S., and M. Rosenstein, 1983: Normal monthly wind stress over the World Ocean with error estimates. J. Phys. Oceanogr., 13, 1093–1104.

Hogben, N., N.M.C. Dacunha, and G.F. Oliver 1986: Global wave statistics. Unwin Brothers, London.

Isemer, H.-J. and L. Hasse, 1987: The Bunker climate atlas of the North Atlantic Ocean. Vol. 2: Air-sea interactions. Springer-Verlag, 252pp.

Janssen, P.A.E.M., 1989: Wave-induced stress and drag of air flow over sea waves. J. Phys. Oceanogr., 19, 745–754.

Kent, E.C., P.K. Taylor, B.S. Truscott, and J.S. Hopkins, 1993: The accuracy of voluntary observing ships' meteorological observations-results of the VSOP-NA. J. Atmos. Oceanic Techn., 10, 591–608.

Large, W.G., and S. Pond, 1981: Open ocean momentum flux measurements in moderate to strong winds. J. Phys. Oceanogr., 11, 324–336.

Levitus, S., 1987: Meridional Ekman heat flux for the World Ocean and individual Ocean basins. J. Phys. Oceanogr., 17, 484–492.

Smith, S.D., 1988: Coefficients for sea surface wind stress, heat flux, and wind profiles as a function of wind speed and temperature. J. Geophys. Res., 93, 15467–15472.

Smith, S.D., 1991: Some early results of the humidity exchange over the sea main experiment. Deep convection and deep water formation in the oceans. Elsevier Science Publishers, Amsterdam, 377–382.

Smith, S.D., R. Anderson, W.A. Oost, C. Kraan, N. Maat, J. DeCosmo, K. Katsaros, K.L. Davidson, K. Bumke, L. Hasse, H.M. Chardwick, 1992: Sea surface wind stress and drag coefficients: the HEXOS results. Bound.-Layer Met., 60, 109–142.

Woodruff, S.D., S.J. Lubker, K. Wolter, S.J. Worley, and J.D. Elms, 1993: Comprehensive ocean-atmosphere data set (COADS) Release 1a: 1980–92. Earth System Monitor, 4, No. 1, 1–8.

Russian Cruise: Tracer Measurement Opportunity

The P. Shirshov Institute of Oceanology in Moscow is organizing a cruise for late spring 1997 in the North Atlantic.

The cruise plan will include CTD data plus nutrients and oxygen concentrations along the AR7, AR5 and AR20N lines.

There is an opportunity for a group/s to collect small volume tracers such as CFC and ^{18}O.

Anyone interested please contact the Chief Scientist:

Dr Alexey Sokov
P. Shirshov Institute of Oceanology
Krasikova 23
117218 Moscow
Russia
e-mail: rocc@sovam.com

The Impact of Seasonal Forcing on the Variability of the Meridional Heat Flux at 30°S Using a Sigma-Coordinate Primitive Equation Model

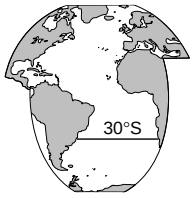

B. Barnier, P. Marchesiello and A. Pimenta de Miranda, Equipe de Modélisation des Ecoulements Océaniques et des Marées, Laboratoire des Ecoulements Géophysiques et Industriels, CNRS URA 1509, BP 53, 38041 Grenoble, France, Bernard.Barnier@img.fr

The South Atlantic Ocean is the only ocean basin wherein the meridional heat flux is towards the equator in subtropical regions. Rintoul (1991) has estimated this flux to be 0.25 PW ($1\,PW = 10^{15}$ W) across 32°S, in relation with a path toward the north of cold and fresh Antarctic Intermediate Water (AAIW) to compensate for a southward flow of Deep Water (DW) mainly from the North Atlantic. Gordon *et al.* (1992) suggested a different path of water masses for the closing of the thermohaline circulation associated with the formation of NADW, and proposed that the return flow has a larger proportion of warm thermocline waters (TW) coming in part from the Agulhas Current, a solution consistent with larger values for the meridional heat transport.

In the context of the participation of France to WOCE, the modelling group in Grenoble is carrying on a long-term modelling program (MOCA, Modélisation de la Circulation Atlantique) to simulate the ocean circulation and its variability in the South Atlantic. The results presented here focus on the seasonal variability of the meridional heat transport at 30°S.

Modelling strategy

Modelling the South Atlantic is a difficult challenge. The South Atlantic Ocean is widely open to the Indian and the North Atlantic, and has a large inflow from the Pacific through the Drake Passage. The basin is also characterised by important topographic features. Consequently, several aspects of the modelling approach are unique.

The model domain is limited to the South Atlantic basin shown in Fig. 1. Exchanges with the other oceans are accounted for with active open boundaries at the Drake Passage, between Brazil and Angola, and between South Africa and Antarctica. The primitive equation model uses a topography-following (sigma) coordinate, and the present work is one of the very first application of this type of coordinate to basin scale ocean modelling. Finally, recent and self-consistent estimates of seasonal fluxes, derived from analyses performed at ECMWF are used to force the model (Barnier *et al*., 1995).

Model configuration and experiments

The numerical code is the Sigma-coordinate Primitive Equation Model (SPEM) developed by Haidvogel *et al.* (1991). In the results presented here, the model horizontal grid is coarse and isotropic (1.375°) and 20 levels are used in the vertical. Robust open-boundary conditions have been developed for the application to a wide-open basin like the South Atlantic. An inflow of 130 Sv ($1\,Sv = 10^6\ m^3\ s^{-1}$) is imposed at Drake Passage. The bathymetry is smoothed but retains the large scale features (Fig. 1). The validation of the model configuration with regard to numerical errors is presented in Barnier e*t al*. (1996).

Simulations are started from an ocean at rest and initial temperature and salinity fields (T,S) which are derived from the climatology of Levitus (1982). The model is integrated for 20 years, first in a quasi-diagnostic mode then in a fully prognostic mode. In the following, the definition of the various water masses follows the proposition of Rintoul (1991).

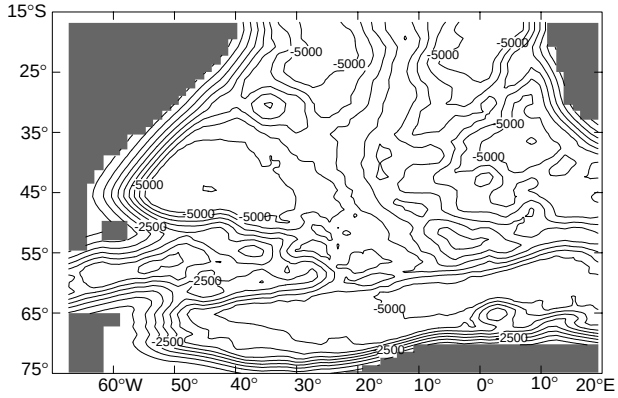

Figure 1. Configuration of the SPEM model in the South Atlantic, with the smoothed bottom topography. Open boundary conditions are applied at the artificial limits of the basin. Contour interval: 500 m.

Variability of the meridional heat transport at 30°S

The circulation produced by the model (Fig. 2) is in good agreement with the one drawn by hydrographic observations (Peterson and Stramma, 1991). It exhibits fine strucures in the Confluence Region and in the ACC. The detail of the model circulation is described in Marchesiello *et al.* (1996). It is shown that fine structures found in the mean flow, which are not found in other coarse resolution model studies, are a direct benefit of the sigma coordinate.

The annual average strength of the overturning cell, measured as the southward flow of DW, is 16 Sv (Fig. 3a, page 23). The model solution suggests that the return flow of the cell is predominantly composed of AAIW (9 Sv) rather than TW (5.3 Sv). The northward heat transport across 30°S (Fig. 3b) is within the low estimates (0.29 PW).

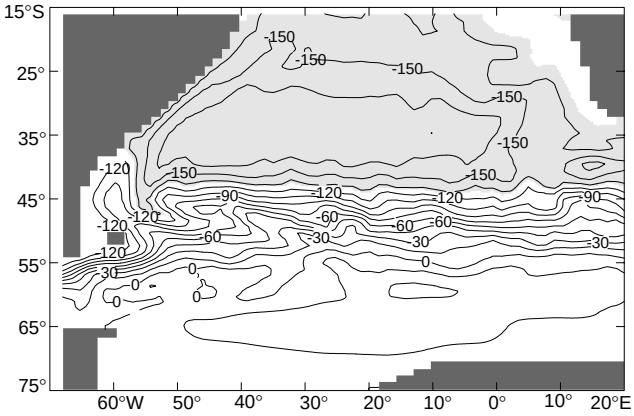

Figure 2. Application of the SPEM model in the South Atlantic. The annual mean barotropic streamfunction (in Sverdrups). The Subtropical gyre is the grey area. Contour interval: 15 m.

AAIW has a low salinity and the fresh water flux to the north is 0.27 Sv. The contribution of Bottom Water (BW) to the meridional heat flux is fairly small due to their cold temperature.

The model solution indicates large seasonal variations in the meridional mass and heat transports at 30°S (Fig. 4). The heat flux is maximum during the austral winter and reaches a large value of 0.62 PW in June, and is minimum in summer (0.2 PW in December). Our analysis indicates

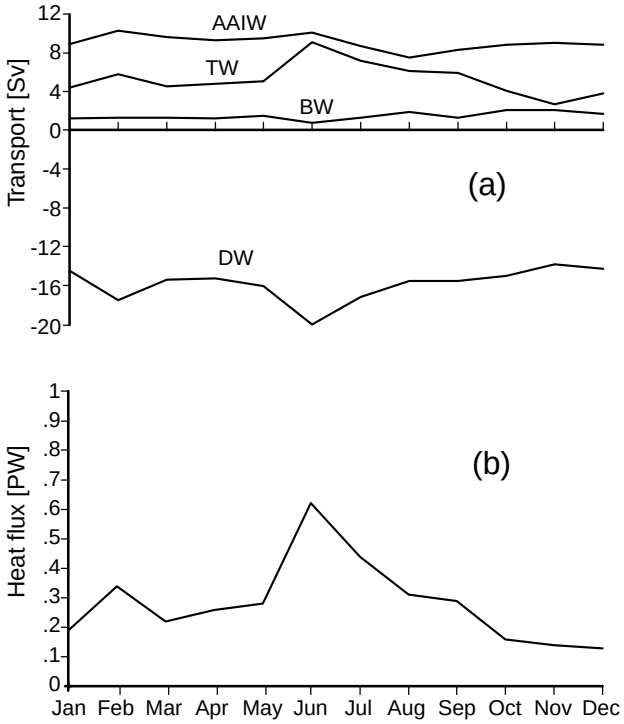

Figure 4. Seasonal variation of meridional transports across 30°S. (a) Northward transport (in Sv) of the various water masses. Strong winds intensify the transport of thermocline water in winter. (b) Northward heat transport (in PW). The heat flux is maximum in winter as a result of the large flow of warm thermocline water towards the equator.

that these variations result from the action of the seasonal wind forcing on the circulation of the subtropical gyre in the South Atlantic. The wind forces an equatorward flow of warm (above 9°C) and salty thermocline water (TW) which is large in winter (10 Sv) and reduced by half in summer (Fig. 4b). The northward flow of AAIW, which also varies during the year by an amount of 2 Sv, still presents large values in summer when the flow of TW is weak.

Conclusion

The model gives new estimates for the fluxes of heat and water masses in the South Atlantic. At 30°S, the model solution shows a large seasonal cycle of the transport of various quantities, and makes allowance, according to the season, for the two major circulation paths discussed in the introduction. Thus a more complex scheme is proposed for the meridional circulation in which the seasonal wind forcing in the Subtropical Atlantic has a significant role in preconditioning the waters of the return flow of the overturning cell.

Acknowledgements

The authors are supported by the Centre National de la Recherche Scientifique and Ministère de l'Education et de la Recherche. This research is funded by the Institut National des Sciences de l'Univers and IFREMER through the Programme National d'Etude de la Dynamique du Climat. Support for computations is provided by the Institut du Developpement et des Ressources en Informatique Scientifique. We are grateful to A. Beckmann, D. Haidvogel, K. Hedstrom, and J. Wilkin for frequent discussions around the SPEM model.

References

Barnier, B., L. Siefridt, and P. Marchesiello, 1995: Thermal forcing for a global ocean circulation model using a three-year climatology of ECMWF analyses. J. Mar. Systems, 6, 363–380.

Barnier, B., P. Marchesiello, A. Pimenta de Miranda, M. Coulibaly, and J.M. Molines, 1996: A sigma-coordinate primitive equation model for studying the circulation in the South Atlantic. Part I: model configuration with error estimates. Submitted to Deep-Sea Res.

Marchesiello P., B. Barnier, and A. Pimenta de Miranda, 1996: A sigma-coordinate primitive equation model for studying the circulation in the South Atlantic. Part II: The upper branch of the overturning cell. Submitted to Deep-Sea Res.

Gordon, A.L., R.F. Weiss, W.M. Smethie, and M.J. Warner, 1992: Thermocline and intermediate water communication between the South Atlantic and Indian Oceans. J. Geophys. Res., 97, 7223–7240.

Haidvogel, D.B., J.L. Wilkin and R. Young, 1991: A semi-spectral primitive equation ocean circulation model using vertical sigma and orthogonal curvilinear horizontal coordinates. J. Comp. Phys., 94, 151–185.

Levitus, S., 1982: Climatological atlas of the world ocean. NOAA Prof. Paper N013, US Government Printing Office, Washington, DC, 173 pp.

Peterson R.G. and L. Stramma, 1991: Upper-level circulation in the South Atlantic Ocean. Progr. Oceanogr., 26, 1–73.

Rintoul, S.R., 1991: South Atlantic interbasin exchange. J. Geophys. Res., 96, 2675–2692.

Preliminary Results from a Low Resolution Model of the South Atlantic Ocean

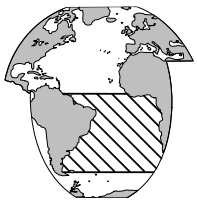

Sören Stutzer and Wolfgang Krauß, Institut für Meereskunde, Universität Kiel, 24105 Kiel, Germany, stutzer@ifm.uni-kiel.de

One aim of the South Atlantic modelling efforts at IfM Kiel is to find a modelled mean state of the circulation and tracer distribution. When comparing model results with observed data (*cf.* hydrographic sections, calculations of mass and heat transports) one finds more or less pronounced deviations. By restoring to an independent data set (drift data in this case) into the numerical model the attempt is made to diminish these discrepancies. This paper gives some insight into the effects on the three-dimensional circulation and temperature/salinity distributions of the assimilation of a velocity field into a single layer. Experiments with a more realistic approach (*i.e.* less divergent observational data base and a much more longer relaxation timescale, see below) are now being performed.

The numerical experiments are based on the GFDL primitive equation ocean model developed by Bryan (1969) and make use of the numerical formulation described by Pacanowski *et al.* (MOM I, 1991). The model grid has a resolution of 1.0° x 1.2° in meridional and zonal direction respectively. The vertical coordinate is resolved in 30 unequally spaced levels ranging from 35 m at the top to 250 m in the bottom layer. The bottom topography is realistic in the limits given by the numerical grid. No active open boundary conditions are applied. Velocity, temperature, salinity and streamfunction are prescribed and fixed at the lateral open model boundaries instead. Parallel running buffer zones are used to damp outgoing waves and possible reflections. A 25 year spin-up experiment from a motionless state and an initial tracer distribution derived from Levitus (1982) and Olbers *et al.* (1992) was performed using climatological wind forcing. The preliminary results are extracted from a model run extending over a further 15 years, now implying a restoring to the horizontal velocity field as described below. The restoring was applied to the momentum equations of the third model layer which is centred at about 90 m depth. This means that the modelled velocity is relaxed to the observed velocity at every timestep. This method is a rather rudimental version of data assimilation because neither the data nor the relaxation method depend on time in contrast for example to similar and common nudging-techniques. The strength of the relaxation is controlled by the parameter τ, which is a timescale, and of course by the model-data difference:

$$U_t = \mathrm{PHYSICS} + \frac{1}{\tau} \times \left(U_{obs} - U_{mod} \right).$$

The use of a very short timescale τ = 6h, thus allowing a predominant relaxation term compared to the physical terms and the natural forcing, leads to results shown here. The reason to choose this particular timescale is that we wanted to test the numerical stability of the model and to examine the response of the model to a strong and divergent forcing which is at least partly inconsistent with the model physics.

Trajectories (daily averages) of 245 buoys which were deployed in the South Atlantic Ocean and southwest Indian Ocean between 1990 and 1995 are depicted in Fig. 1. For a detailed analysis see Schäfer and Krauß (1995). Eulerian velocities were obtained simply by regarding the displacements of the drifters in a given time interval. The velocity data were averaged within a 3° x 3.6° box which was centred at a model gridpoint. This box was shifted stepwise by 1° in latitude and 1.2° in longitude, thus covering the entire South Atlantic Ocean as far as data were available. Choosing a Lagrangian timescale of 2 days and rejecting only those boxes that contain data from less than 3 independent observations means that an optimum data coverage is favoured over a reliable mean. A velocity field within the model domain as shown in Fig. 2 was finally obtained. Now in almost all parts of the South Atlantic north of the Antarctic Circumpolar Current and south of the equator velocity observations are available. Clearly visible are the regimes of the Agulhas- and Agulhas Return Currents, the Antarctic Circumpolar Current and the South Equatorial/ North Brazil Current. Notice also the divergences and convergences as artificially produced by the

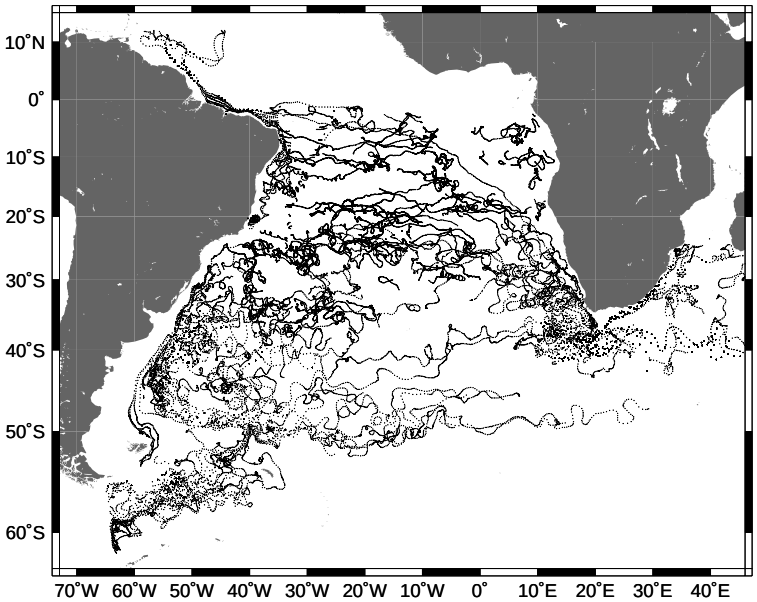

Figure 1. Buoy trajectories 1990–1995; daily mean positions.

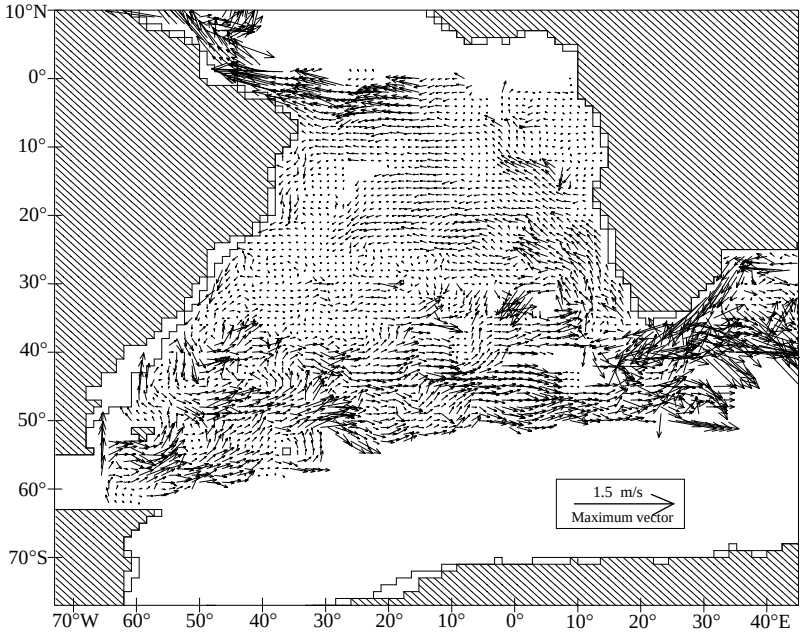

Figure 2. Model domain and velocity field which is derived from the drift data by a linear interpolation and averaging method and used for restoring experiments.

imperfect computation of the averages.

A few model results are shown in Figs. 3 and 4. The effect of the restoring on the velocity field below the disturbed model layer is illustrated in a comparison of Figs. 3a and 3b. The restoring affects the velocity in the subsurface ocean by stimulating higher velocities on a smaller scale (Fig. 3b), features that are not generated by the model physics alone (see Fig. 3a). The density distribution (not shown) indicates that the velocity relaxation induces a stronger ageostrophic motion than is present in the undisturbed case.

Zonal sections of temperature in the upper ocean at 20°S are depicted in Fig. 4. When comparing the sections from a model realization with restoring (4b) and one without (4a) one recognizes the sharpening of the vertical temperature gradient in the upper 500 m as the most prominent consequence of the velocity relaxation on temperature. This behaviour is more distinct in the eastern part of the South Atlantic than west of the Mid Atlantic Ridge. Smaller differences occur in the deep ocean below 2000 m.

Future numerical experiments will make use of an improved drift data set obtained by a statistically more reliable averaging method that takes into account the distance of a single data point from the box centre and also rejects mean values computed with less than 50 statistically

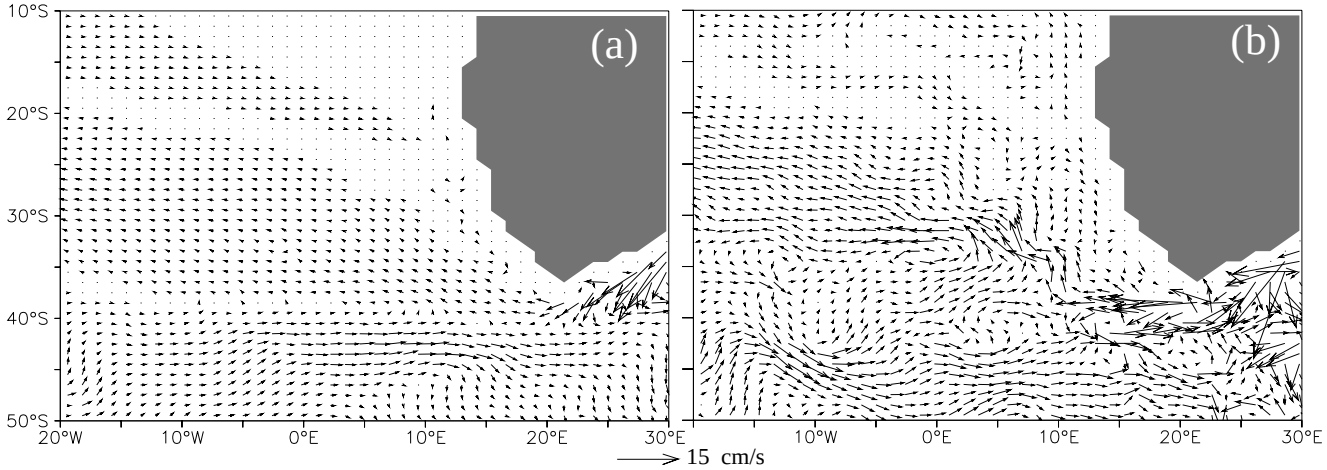

Figure 3. Velocity fields at model layer 10 (centred about 570 m) west and south of South Africa; five year averages. (a) reference run without restoring; (b) restoring run.

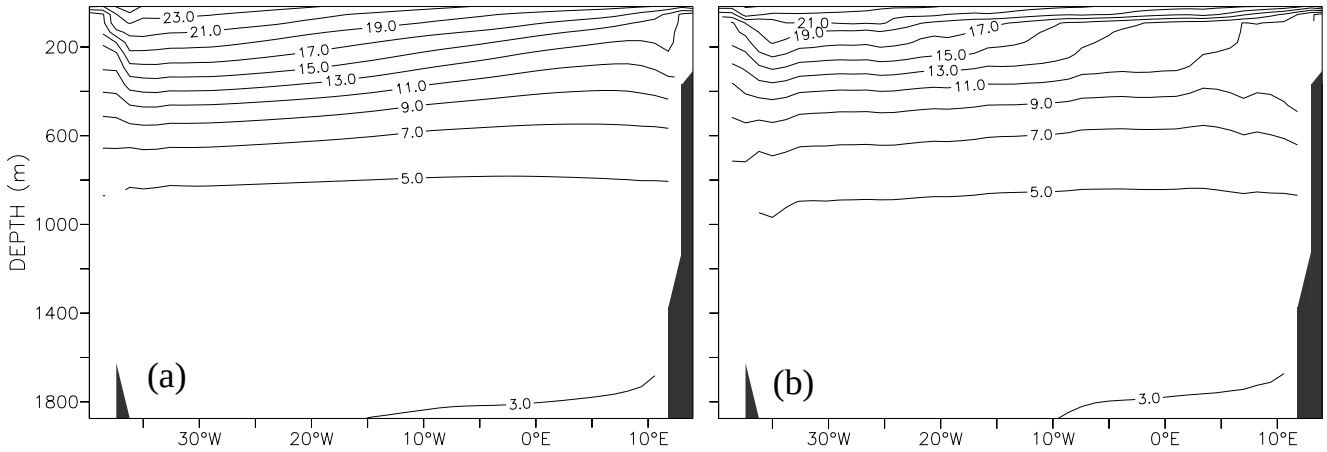

Figure 4. Zonal sections of temperature along 20°S, depth range 0–2000 m, five year averages: (a) reference run without restoring; (b) restoring run.

independent data. Accumulated means suggest that this is the minimum number of data points needed to obtain fairly robust averages. The result is as shown in Fig. 5. The divergence of the velocity field is diminished to a lower level at the cost of a scarcer data coverage of the model domain.

References

Bryan, K., 1969: A numerical method for the study of the circulation of the World Ocean. J. Comput. Phys., 4, 347–376.

Levitus, S., 1982: Climatological Atlas of the World Ocean. NOAA Prof. Paper No. 13, Geophysical Fluid Dynamics Laboratory, Princeton University, N.J., 173pp.

Olbers, D., V. Gouretski, G. Seiss and J. Schröter, 1992: Hydrographic Atlas of the Southern Ocean. Alfred Wegener Institut, Bremerhaven, Germany

Pacanowski, R.C., K.W. Dixon and A. Rosati, 1991: The GFDL modular ocean model users guide Version 1.0, GFDL Ocean Group Tech. Rep. No. 2, 46pp.

Schäfer, H., and W. Kraub, 1995: Eddy statistics in the South Atlantic as derived from drifters drogued at 100 m. J. Mar. Res., 53, 403–431.

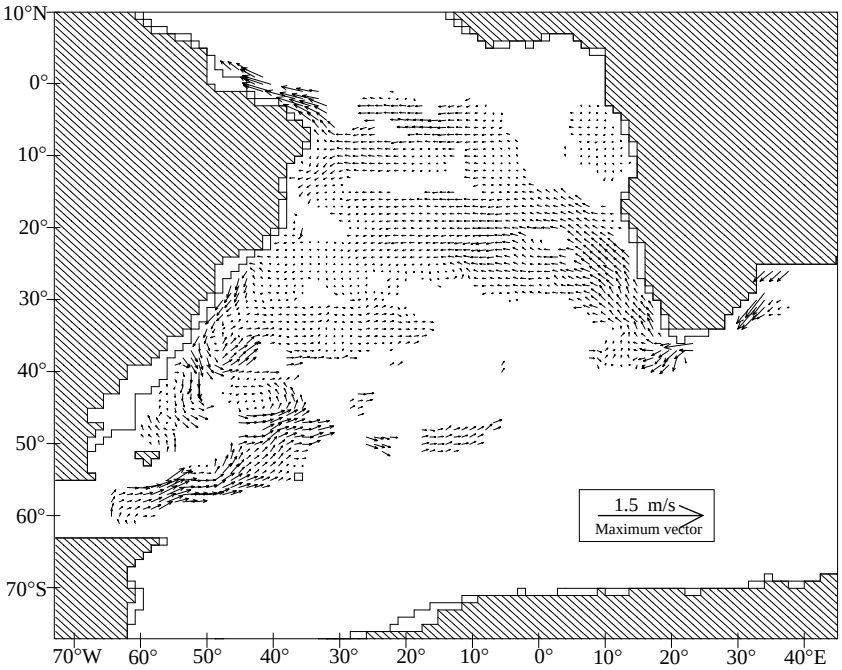

Figure 5. Velocity field as derived from the drift data using an improved averaging and interpolation method.

Electronic Copies of Newsletter Issues 23 and 24

For readers anxious to minimise paper in their office an electronic version of the Newsletter is available. It is an exact electronic image of the printed copy, is in PDF format and requires Acrobat Reader to view it. Viewing CANNOT be done on the WWW, the reader must import the PDF file and then utilise an on site reader.

The electronic images of the last two issues are stored in compressed form as news23.pdf.gz and news24.pdf.gz at the ftp site socnet.soc.soton.ac.uk in the directory pub/woceipo. Before capturing these files issue the binary instruction and note that compressed files have a size 3-4 Mbytes and that they uncompress to 15-20 Mbytes (mostly due to colour plates).

Acrobat Reader is freeware and can be obtained at numerous sites. Use http://www.adobe.com/acrobat/3beta on the WWW.

Further information can be found on the WOCE IPO Home Page.

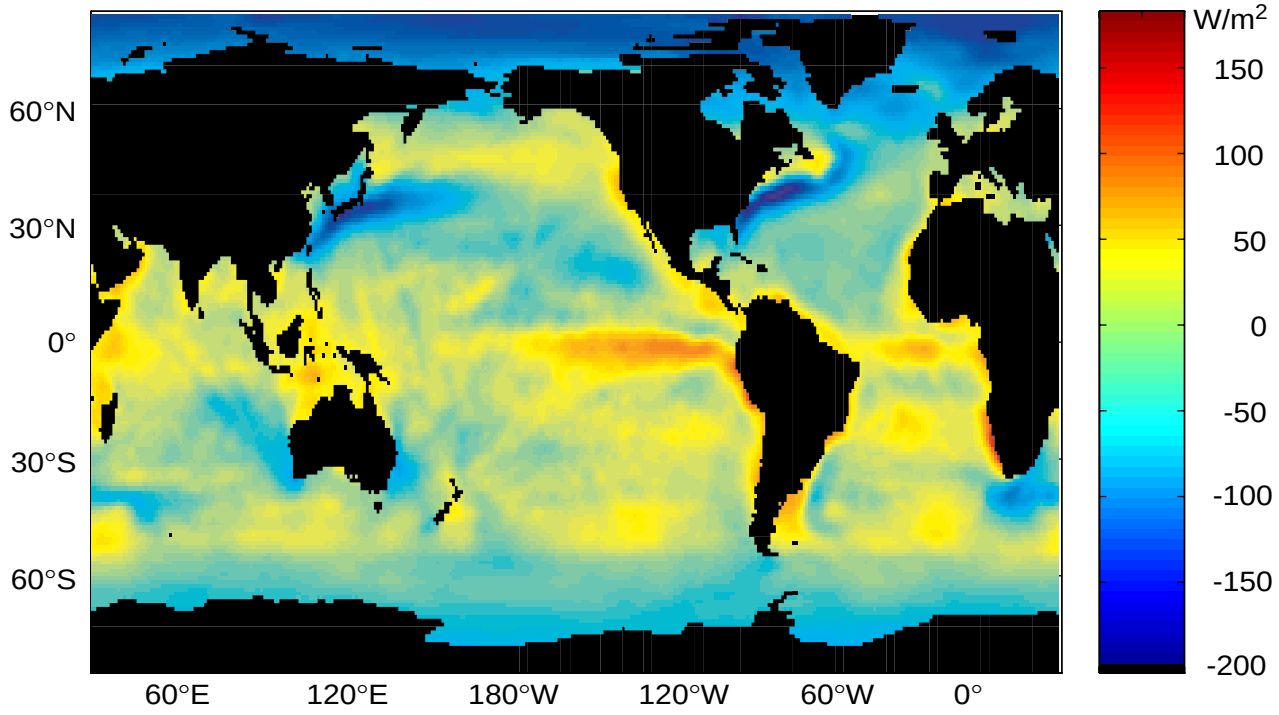

Josey, et al., page 3 *Figure 1. Climatological annual mean net air-sea heat flux after corrections have been made to the latent and shortwave flux terms (positive flux values represent heat gain by the ocean).*

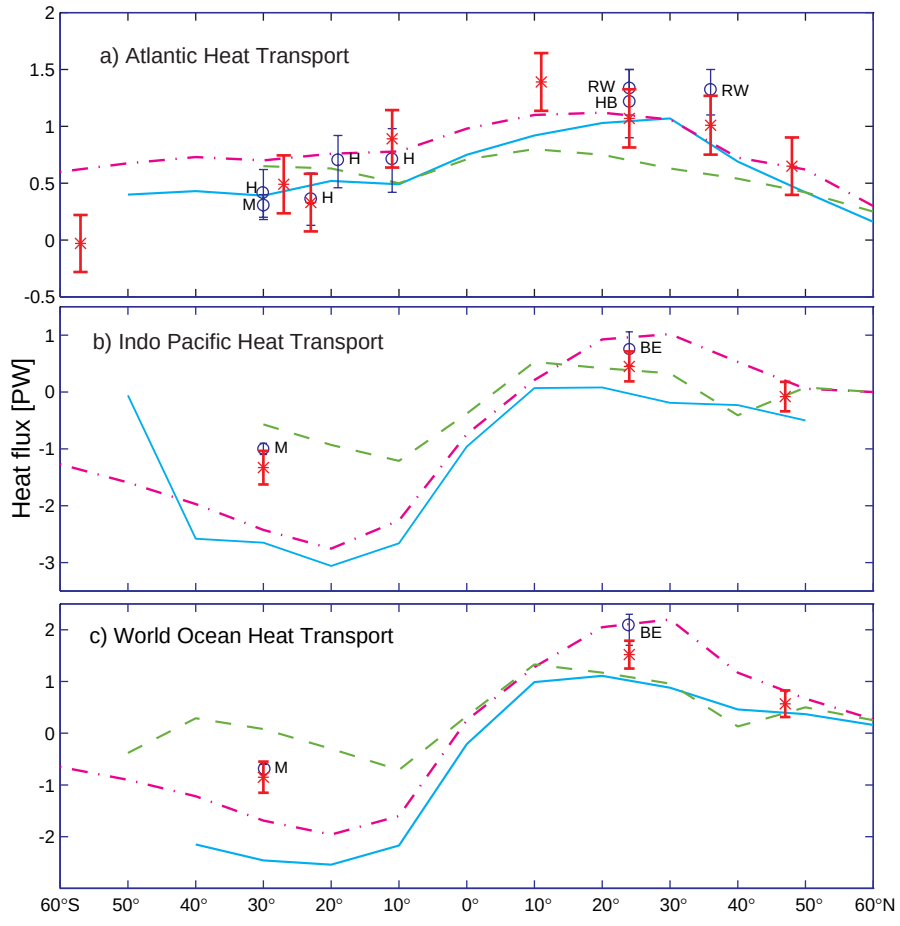

Macdonald and Wunsch, page 5 *Figure 1. Comparison of best-estimate model meridional heat flux estimates (red asterisks with thick error bars) with previously published values (curves and blue open circles with thin error bars), which were based on mass-conserving transoceanic observations and accompanied by uncertainty estimates. Figures a, b and c represent the Atlantic, Indo-Pacific and World Ocean, respectively. Solid blue curve from Talley (1984); dotted pink curve from Hastenrath (1982); green dashed curve from Semtner and Chervin (1992). The reference initials represent the following: BE (Bryden et al., 1991), HB (Hall and Bryden, 1982), H (Holfort, 1994), M (Macdonald, 1993), and RW (Rintoul and Wunsch, 1991). All values are in PW.*

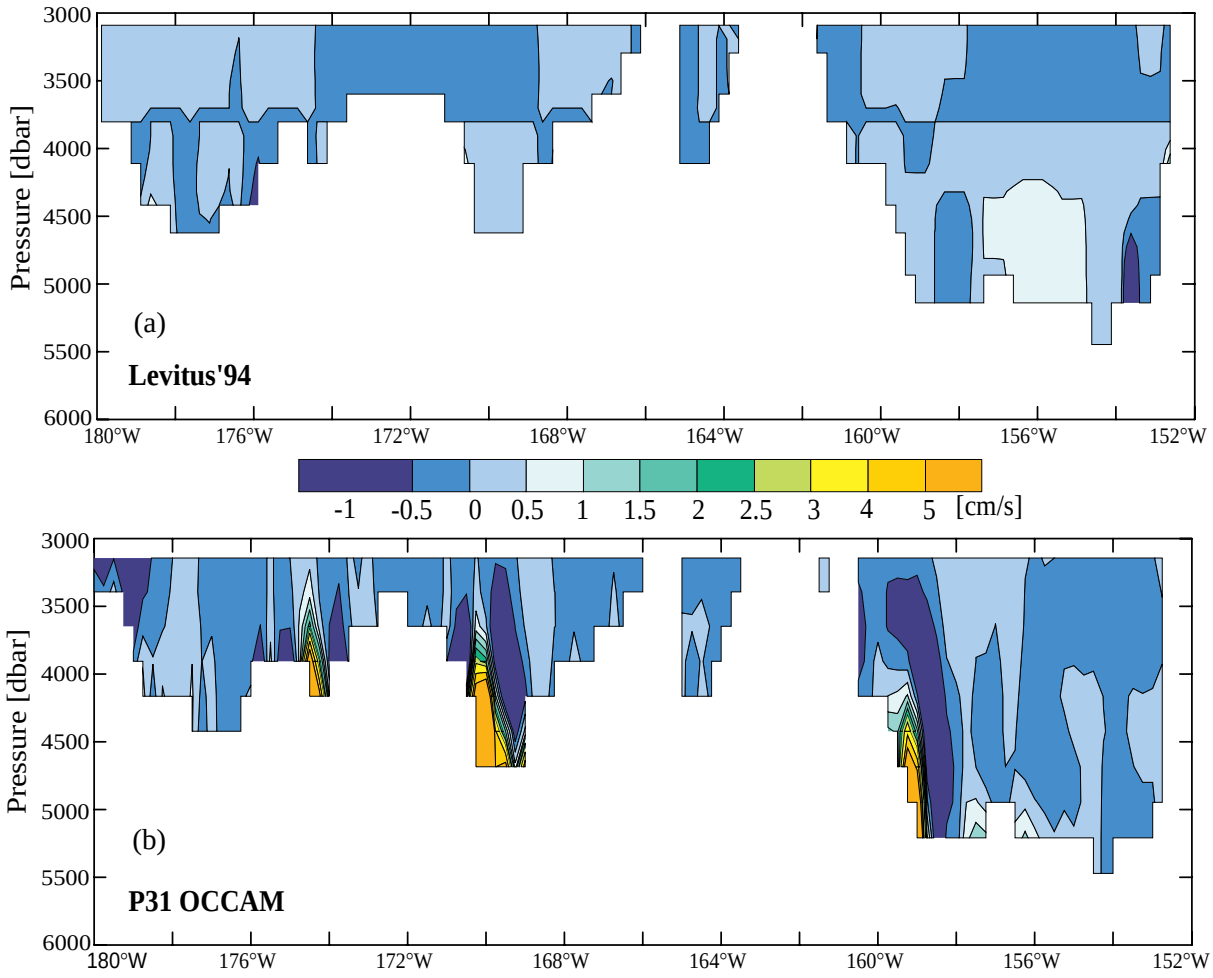

Saunders and Coward, page 9 *Figure 4. North components of currents on 10°S. (a) from Levitus'94 (using a reference level of 3800 m); (b) from OCCAM 5–7 year output.*

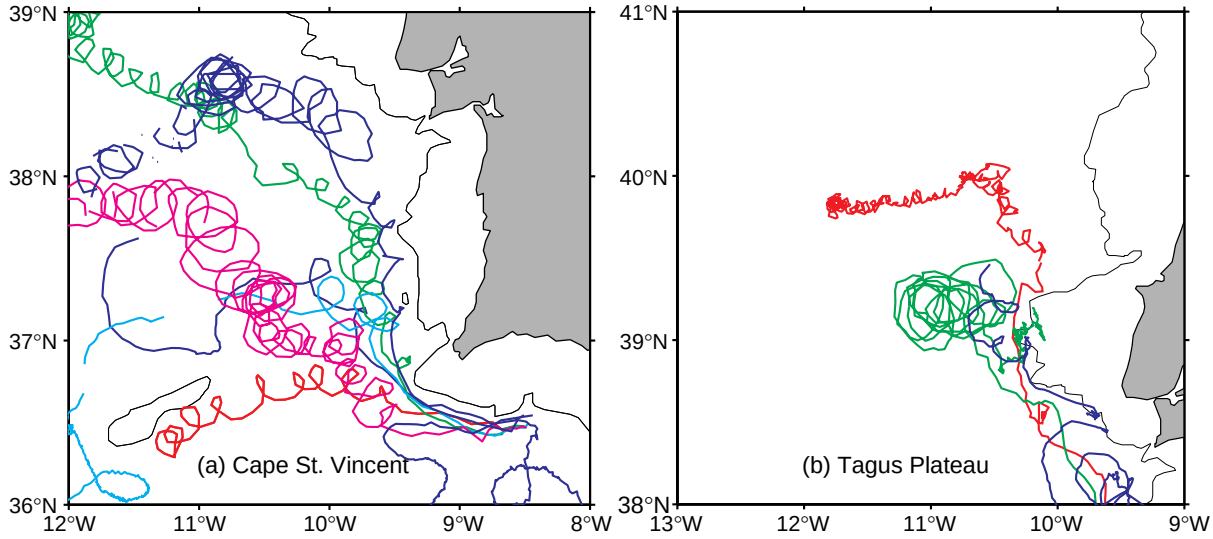

Bower, et al., page 29 *Figure 3. (a) Tracks of six RAFOS floats that revealed six meddy formation events at Cape St. Vincent, at the southwestern corner of the Iberian Peninsula (see Fig. 1 for location); (b) tracks of three floats caught in meddy formation near the Tagus Plateau. The 1000 m isobath is also shown.*

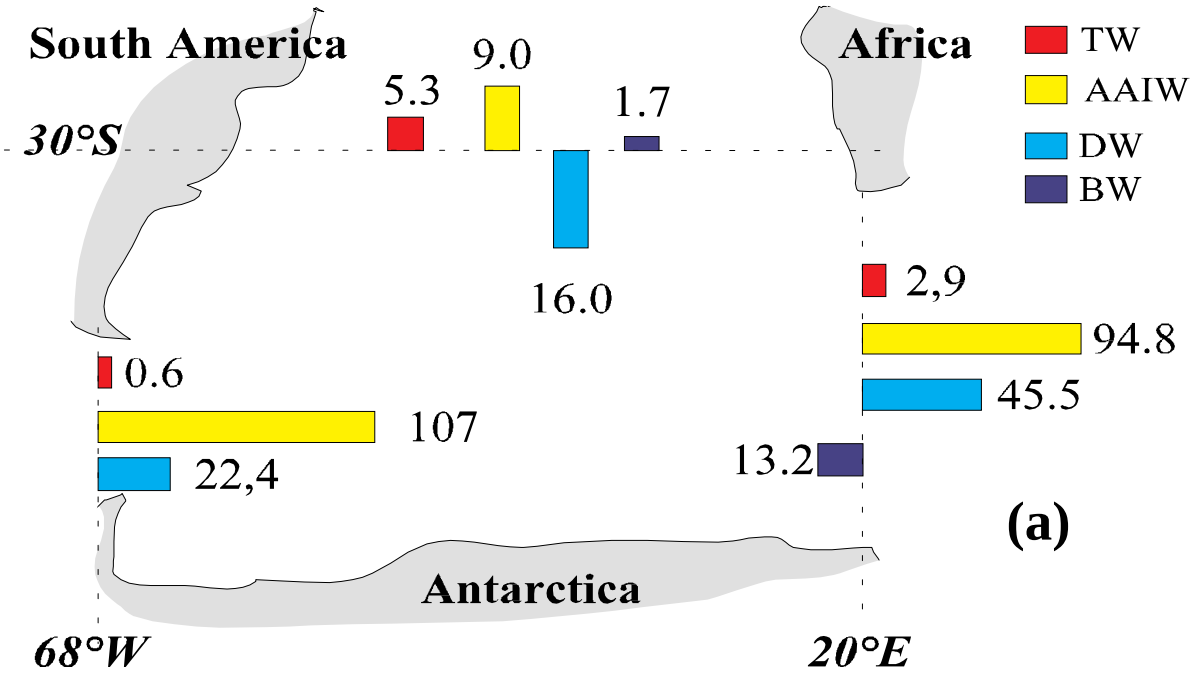

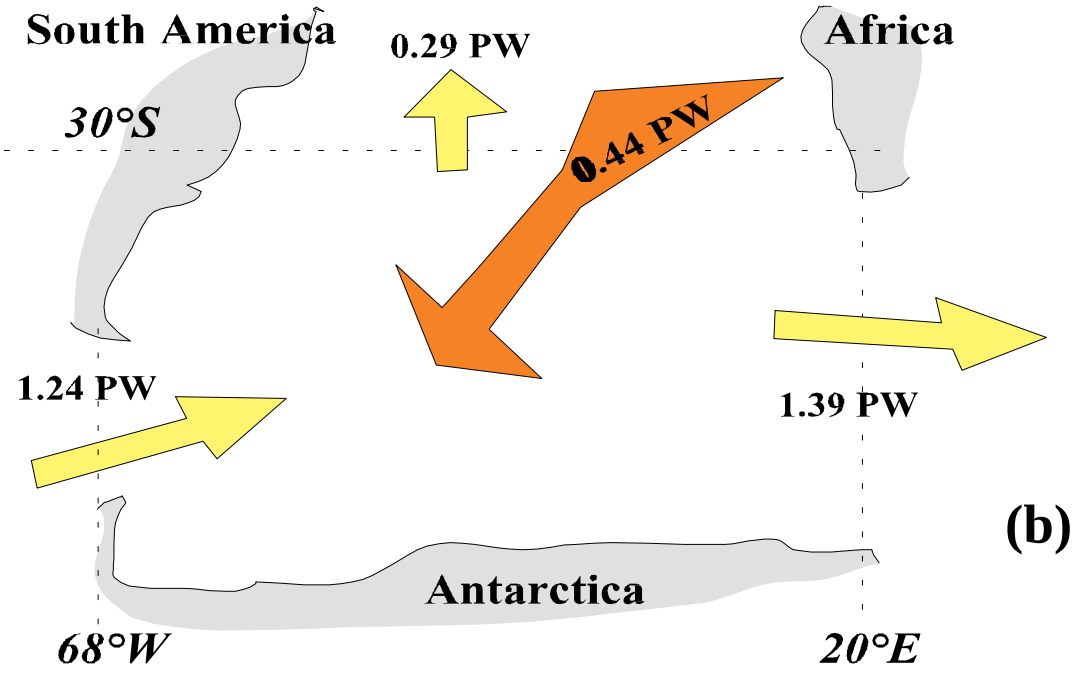

Barnier, et al., page 17 *Figure 3. Annual mean transports across the limits of the South Atlantic. (a) Transport of the various water masses (in Sv). (b) Heat transport (in PW). The surface heat flux is indicated by the orange arrow.*

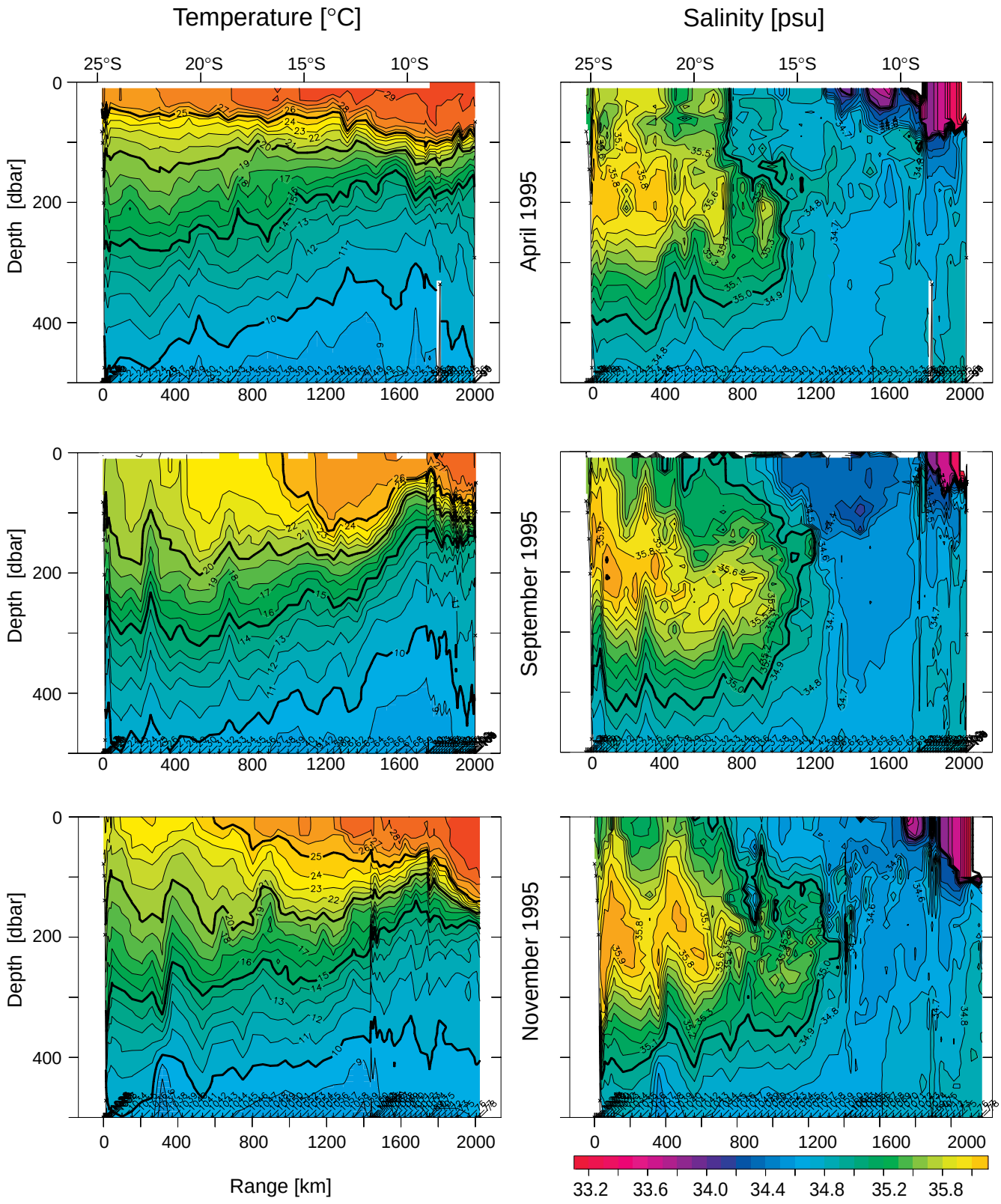

Wijffels, et al., page 26 *Figure 3. Upper ocean temperature (left panels) for the three occupations, and upper ocean salinity (right panels), projected onto a line of constant longitude.*

The WOCE Indonesian Throughflow Repeat Hydrography Sections: I10 and IR6

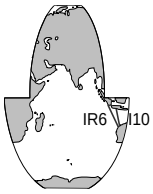

Susan E. Wijffels, CSIRO, Hobart; Nan Bray, SIO; Susan Hautala, University of Washington; Gary Meyers, CSIRO, Hobart; and Werner M.L. Morawitz, SIO, susan.wijffels@ml.csiro.au

The region between Northwest Australia and Indonesia (here referred to as the North Australian Bight) is characterized by a complex set of zonal currents that vary in strength and location both seasonally and interannually. The currents also vary with depth. Fig. 1 shows the near-surface system. The current variability has been shown by the WOCE/TOGA XBT line IX1 from W. Australia to Indonesia, which has been monitored roughly fortnightly since 1983 (Meyers, *et al.*, 1994). Based on these data the seasonal cycle of the flows across IX1 are well known in the upper ocean (0-400 db).

To summarise these results: along the Java shelf break and slope, the flow is highly variable, reversing every 3 months. We call this the South Java Current (SJC) regardless of its direction. Variability in the SJC is driven by semiannually varying winds in the central and western equatorial Indian Ocean that modulate the flow off Sumatra and Java through the propagation of equatorial and coastal Kelvin waves (*e.g.* Wyrtki, 1973; Clarke and Liu, 1994). The SJC has a deep as well as near-surface expression, and little is known about the seasonal variations of the deep SJC. The shallow SJC (above the thermocline) carries water that is fresher than the throughflow, and originates from runoff in the Java Sea or along the west coast of Sumatra. The deep SJC, extending to at least 1000 m, carries relatively saline North Indian Central Water into the throughflow region.

The Eastern Gyral Current (EGC) and South Equatorial Current (SEC) are part of the southern Indian Ocean circulation. Both vary seasonally in strength, especially the SEC as it incorporates the seasonally-varying throughflow transport. The EGC is a shallow eastward shear found in the upper 150 m of the water column. Along the coast of Australia, warm waters flow southward in the Leeuwin Current, primarily in winter.

The Indonesian Throughflow (ITF) varies in strength with the Australasian monsoon. WOCE cruises were timed to capture the extremes in ITF transport in April at the end of the northwest monsoon when winds blow towards the Pacific giving low throughflow transport and in the September maximum associated with the southeast monsoon. November marks a transition between the monsoons, and coincides with one of two semiannual maxima in eastward transport of the SJC, the other being in May.

Because of the extensive IX1 data, we occupied WOCE I10 (November, US RV Knorr) and IR6 (April and September, Australia RV Franklin) along the IX1 line. Despite initial optimism, none of the cruises received clearance to work in the Indonesian EEZ (lying between about 9.5°S and Java). Observations there are limited to XBT and XCTD sections taken from merchant ships within 9 days of each hydrographic section. The XCTD data are still being processed.

Because we expected clearance for the I10 cruise, at the request of the Indonesian military, the northern end of the section was moved from Sunda Strait to central Java, shifting the entire line off IX1 east to near 110°E (Fig. 2). When clearance was denied, I10 was completed by occupying stations northwestward back toward the IX1 line. This near-zonal line had also been occupied during IR6 in September (Fig. 2). XBT data have been used to extend the sections from the southern limit of the EEZ to Sunda Strait at the western tip of Java. T/S relationships from the 1989 French JADE stations between Christmas Island and Sunda Strait (Fieux *et al.*, 1994) are used to estimate salinity for the XBT temperatures. These data, along with the research ship CTD casts, give three nearly-synoptic (0–800 db), eddy-resolving (<40 km) sections from NW Australia to Sunda Strait.

In addition, each of the three cruises sampled for nutrients/oxygen and made underway ADCP measurements. On I10, there were lowered ADCP on each station and samples were taken for analysis of tritium, helium-3,

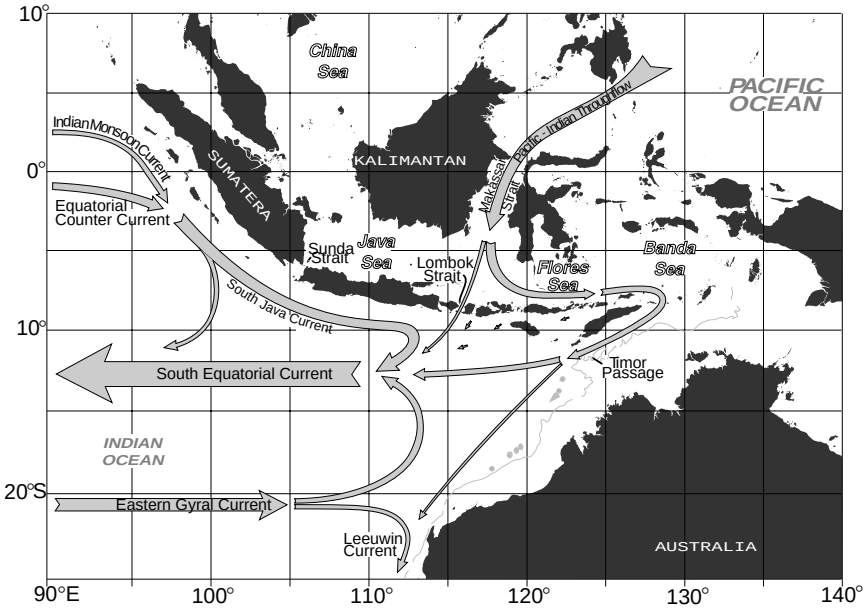

Figure 1. Schematic of the near-surface current systems of the throughflow region.

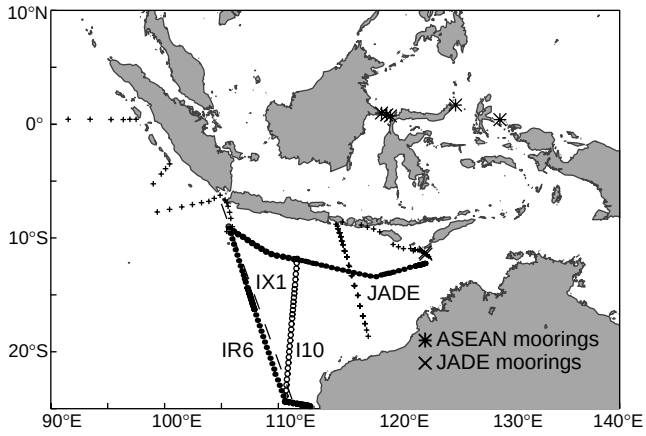

Figure 2. CTD and XBT section locations.

CFCs, carbon dioxide, alkalinity, carbon-14 and radium-228. Underway measurements of sea surface temperature (SST) and salinity, meteorological variables and pCO_2 were also recorded.

Thermal structure

For a simple comparison between cruises, the hydrographic data are contoured, ignoring the difference in longitude between the I10 and IR6 cruises (Fig. 3, page 24). Some variations seen in the November cruise (I10) may be attributable to its different cruise track. This projection collapses the structure of the Leeuwin Current onto one point. For brevity we focus only on the larger scale flows.

The potential temperatures sections from the three cruises have common features: the shoaling and thinning of the thermocline (15°–20°C) from south to north; and northward increasing SST (Fig. 3, left panels). Apart from these features, the thermal structure varies remarkably between cruises. In April there is a strong seasonal thermocline in the southern part of the section, as expected for the end of summer. The northern half of the section (15°–6°S) contains a bowl in the thermocline centred at 10°S. This structure reverses with depth, so that the deep isotherms form a ridge along 10°S. In September, winter cooling gives deeper colder mixed layers (~100 m) south of 12°S, compared to April; also in contrast to April, there is a sharp thermocline ridge at 10°S that penetrates to depth. The deepest part of the bowl in the thermocline is shifted south to 13°S. The November survey retains the 10°S thermocline ridge, though it is weaker, while the thermocline south of Java has deepened by more than 50 m. A new seasonal thermocline has also formed between September and November, and the isothermal bowl centred at 13°S in September has become stratified and colder.

South of 15°S, thermocline changes are less obvious but substantial: isotherms between 20°–15°C shoaled by 50–100 m in April compared to the austral spring; the upward tilt of isotherms in the upper 250 m at the southern end of the section is also not apparent in April. In terms of the major currents, the latter feature is associated with the EGC, while the SEC and SJC lie on either side of the thermocline ridge at 10°S. The changes in thermal structure imply large changes in transport: the SEC is absent in April, strong in September and weakening in November; the shallow SJC is strongest eastward in November, weaker in September and possibly westward in April, although the deep SJC is strongly eastward in all three sections. The EGC appears absent in April, while present in the other two cruises. Transports will be discussed quantitatively below.

Salinity structure

Three primary water types influence the thermocline: salty South Indian Central Water (SICW) found south of a water mass front located at roughly 15°S; fresh Banda Sea Water (BSW), almost vertically homogeneous in salinity north of 15°S; and salty North Indian Water (NIW) in the deep SJC along the coast of Java (salinities north of 9.5°S are based on the JADE T/S and may not represent the true seasonal variations). Based on the flow field determined by Meyers *et al.* (1994), we expect the EGC to advect the saltiest SICW into the North Australian Bight and that the SEC must recirculate this water to the Indian Ocean again: hence the region produces a 'mixed water' of SICW and BSW. This is evident along the sections (Fig. 3, right panels) which are characterised by strong small-scale salinity structures around and to the south of the main water mass front located at 15°S.

The upper 100 m salinity structure is quite different to that in the main thermocline: the surface salinity front is further south and is more variable in position. This may reflect the effect of several mechanisms: Ekman transport, the influence of BSW or the shallow SJC, and the strength of the EGC, which is confined to the upper 150 m or so.

The lowest salinities in the three sections are along the coast of Java in the shallow SJC. These salinities are based on the JADE August 1989 survey when the SJC was flowing to the east across the line. Hence these low salinities could have either come from the west coast of Sumatra or the Java Sea via Sunda Strait: rainfall and runoff freshen the waters of the Java Sea to values around 32 producing a source of very fresh water. The variation in salinity in the SJC will become clearer when the XCTD casts are examined. In April, the freshcap south of Sunda extends to 13°S. The underway ADCP data show strong southward flow in the freshcap, suggesting direct advection from the fresh SJC. In September, moderately low salinities (34.2–34.4) are found in the top 100 m of the SEC in the isothermal bowl. By November, this near surface bowl structure has also become saltier.

Between the three cruises the position and strength of the main BSW/SICW salinity front varies noticeably, as do the areas of the section occupied by BSW, SICW and mixed water. If pure SICW is marked by salinities greater than 35.7 and BSW is fresher than 34.7, then mixed water occupies the range in between. In April SICW is found only south of 20°S, BSW is in a small area between 13°S and 11°S, while mixed water occupies the bulk of the section. In September, salinities north of 14°S have dropped

dramatically (by more than 0.1) in the thermocline (100–300 m) and the BSW has increased its sectional area substantially, while to the south the SICW also occupies a larger area of the section and has increased its maximum salinity. In November, the SICW has penetrated further north and become saltier still, while the BSW has retreated in both area and strength.

If the extreme core properties occur during strongest advection, the above suggests that the advection of SICW into the region is strongest in November, and is weakest in April, while the SEC carrying BSW is strongest in September and weakest in April. Interestingly, in April, when the SICW/BSW contrast is weakest (and thus advection is weakest), the salinity gradient between the BSW and SICW has concentrated into two very sharp fronts. During the spring cruises, the fronts are much broader.

Transports

The meridionally-integrated transport along the three WOCE sections relative to and above 800 m is shown in Fig. 4. 800 m is chosen as the maximum depth of the XBTs used to complete the sections through the Indonesian EEZ. The variation of current strength between the cruises is consonant with the deductions from salinity field changes. In April the flow is weak except in the SJC – recall that the BSW and SICW extrema are weakest during this cruise. The strongest flow into the section from the South Indian Ocean occurs in September and November south of 20°S where the SICW signature is strongest. The SEC is strongest in September and still flowing in November, consonant with the variation of the BSW properties. Note that in September, the peak of the transport curve is near 13.5°S, in the centre of the fresh isothermal surface-layer bowl indicating that a good measure of the fresh, warm geostrophic near-surface SEC is recirculating eastwards back into the North Australian Bight.

In all three WOCE cruises the SJC transports roughly 10 Sv eastward, largely due to the timing of the cruises during or near its semiannual maxima in eastward transport

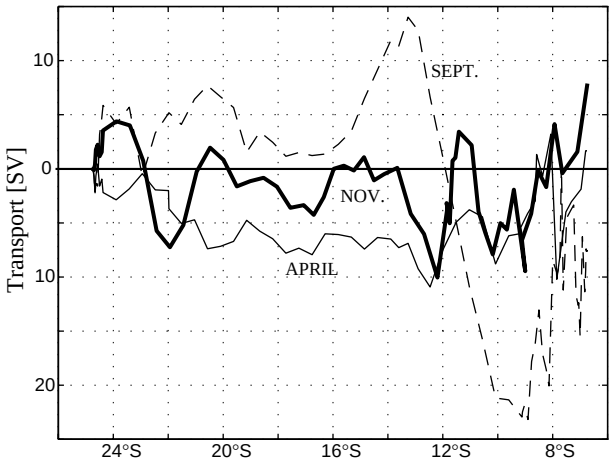

Figure 4. Composite of 0/800 transports, integrated from the southern end of the section.

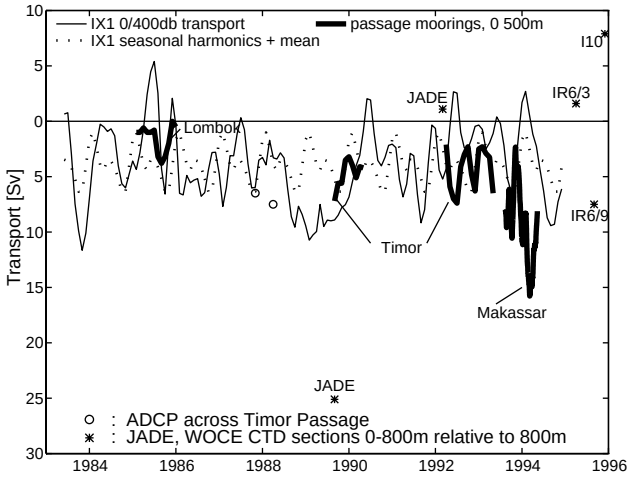

Figure 5. Composite of upper ocean transports from the Indonesian throughflow region. Timor mooring curves (top 1250 m) are adapted from Molcard et al., (1994; 1996). The Lombok mooring curve is adapted from Murray and Arief (1988). The Makassar mooring curve (top 500 m) is from Cresswell, pers. communication. JADE CTD transports are from Fieux et al. (1996), Timor Passage ADCP transports are from Cresswell et al. (1993).

and are thus unlikely to reflect the annual mean situation. The IX1 XBT provide a time-series of temperature structure and hence inferred transport out of the North Australian Bight. In Fig. 5, transport relative to 400 m, using average Levitus T/S to get density, is plotted with other recent estimates of throughflow transport, including the 0/800 db net transports from I10 and IR6. Note that neither the latter three nor the XBT estimate are corrected for Ekman transport. Also plotted in Fig. 5 is the average seasonal cycle of net transport through IX1, showing the maximum westward transport in August/September and a pronounced semiannual variation due to the SJC. The WOCE sections are consistent with both the seasonal and interannual variations in IX1 transports, although the IX1 transports seldom change sign. The amplitude of fluctuations in transport from CTD sections (JADE as well as WOCE) is in general somewhat larger than the ±5 Sv in the IX1 transports. It is worth noting that the JADE section in August of 1989 coincided not only with a seasonal maximum, but also with an interannual one. Also, it appears that there is about a 3-month phase lag between Timor Passage and the IX1 line, with Timor leading. One aim of our future analysis will be to test the concept of 'calibrating' the transport time series based on the IX1 XBT data to better account for the flow below 800 db and the variation in salinity.

Conclusions

The WOCE sections show the strong seasonality of currents in the throughflow region and of the ITF. The 8 Sv of net eastward transport in November confirms the occasional ITF reversals in the IX1 transports. We note that

reversals of the ITF do not necessarily imply flow into the Pacific, as the mass involved may be stored in the upper ocean of the North Australian Bight and internal Indonesian seas, by changing the thermocline depth, as suggested by Meyers et al., (1994). The average upper ocean net transport, identified as the ITF, from the JADE and WOCE CTD sections is -3.8 ±11.7 Sv. This agrees with the average of -3.9 ±3.5 Sv from the long-term XBT data. The smaller standard deviation in the XBT data is partly due to differences in the way the transports are estimated: the XBT data are filtered to represent scales larger than two months and 100 km, and represent 0 to 400 m transport relative to 400 m, as opposed to 0 to 800 m relative to 800 m for the CTD sections. Climatological Ekman transport across these sections is also varying seasonally from -1.5 to -5 Sv, with an annual average of about -3 Sv. Thus, the net ITF including Ekman transport is about -7 Sv. This estimate will be revised as we look in more detail at the deeper transports.

Property distributions indicate a significant recirculation of water masses within the North Australian Bight, and conversion of water mass type through lateral mixing, including mixing between SICW and BSW as well between fresh SJC surface waters and BSW. Future work will examine the deep property distributions and flow fields, and linking changes in large-scale currents (SJC, SEC, EGC) to possible forcing mechanisms. For example, the northern boundary of the subtropical water mass appears to retreat to the south as the shallow SEC intensifies during the Southeast monsoon (September). We hypothesize that, in combination with cooling of the upper ocean at the southern end during austral winter, this increase of the meridional salinity gradient acts to spin up the EGC as observed.

Acknowledgements

The authors wish to acknowledge the contributions to the data collection effort by other I10 PIs: John Toole, Teresa Chereskin, Rana Fine, Bob Key and Bill Jenkins. We are especially indebted to the skilled technicians from both CSIRO and the ODF at Scripps for work at sea, and in preliminary data processing. Rick Bailey runs the CSIRO XBT network. Much of the XBT data processing is done by Ann Thresher and Peter Jackson. We gratefully acknowledge the untiring support received from the US WOCE Office (Piers Chapman and Sasha Walters), the US and Australian Embassies in Jakarta in trying to obtain clearance for I10. All went beyond the call of duty in trying to get clearance for the cruises. We thank our Indonesian colleagues who both worked for clearance and participated in the cruises: Dr Mulia Purba of Bogor University and his students, Yuli Naulita and I. Nyoman, M. Naith, and Mr Ahmad Najid, Mr Muhamad Ilyas and Mr Basri Ghani from BPPT.

References

Clarke, A.J., and X. Liu, 1994: Interannual sea level in the northern and eastern Indian Ocean. J. Phys. Oceanogr., 24, 1224–1235.

Cresswell, G., A. Frische, J. Peterson, and D. Quadfasel, 1993: Circulation in the Timor Sea. J. Geophys. Res., 98, 14,379–14,389.

Fieux, M., C. Andrie, P. Delecluse, A.G. Ilahude, A. Kartavtseff, F. Mantisi, R. Molcard, and J.C. Swallow, 1994: Measurements within the Pacific-Indian Oceans throughflow region, Deep Sea Research, Part I, 41, 1091–1130.

Fieux, M., R. Molcard, and A.G. Ilahude, 1996: Geostrophic transport of the Pacific-Indian Oceans throughflow. J. Geophys. Res., 101, 12,421–12,432.

Meyers, G., R.J. Bailey, and A.P. Worby, 1994: Volume transport of Indonesian throughflow. Deep-Sea Res., Part I, 42, 1163-1174.

Molcard, R., M. Fieux, J.C. Swallow, A.G. Ilahude, and J. Banjarnahor, 1994: Low-frequency variability of the currents in Indonesian channels. Deep-Sea Res., Part I, 41, 1642–1661.

Molcard, R., M. Fieux, and A.G. Ilahude, 1996: The Indo-Pacific throughflow in the Timor Passage. J. Geophys. Res., 101, 12,411–12,420.

Murray, S.P., and D. Arief, 1988: Throughflow into the Indian Ocean through the Lombok Strait, January 1985–January 1986. Nature, 333, 444–447.

Wyrtki, K., 1973: An equatorial jet in the Indian Ocean. Science, 181, 262–264.

Update on "A Mediterranean Undercurrent Seeding Experiment" (AMUSE)

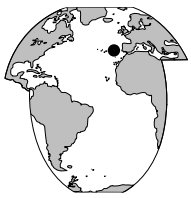

Amy S. Bower, Woods Hole Oceanographic Institution; Laurence Armi, Scripps Institution of Oceanography; and Isabel Ambar, Instituto de Oceanografia, University of Lisbon, abower@whoi.edu

Traditionally, the well-known Mediterranean salt tongue in the North Atlantic was interpreted to be the result of advection and/or diffusion of Mediterranean Water (MW) from its source near the Strait of Gibraltar. This view has been challenged by the discovery of meddies, coherent vortices containing cores of warm and salty MW. In the past two decades, many meddies have been found in the eastern North Atlantic, and their basic structure has been relatively well-documented (*e.g.,* Armi *et al.,* 1989; Richardson *et al.,* 1989*).* It is also now recognized that meddies are not just curiosities in the eddy zoo, but that they play a significant role in distributing heat, salt and other tracers in the North Atlantic (*e.g.,* Arhan *et al*., 1994).

In spite of our increasing awareness of the importance of meddies, some fundamental questions about where, how often and by what mechanism they form have remained unanswered, largely due to the lack of observations of meddy formation.

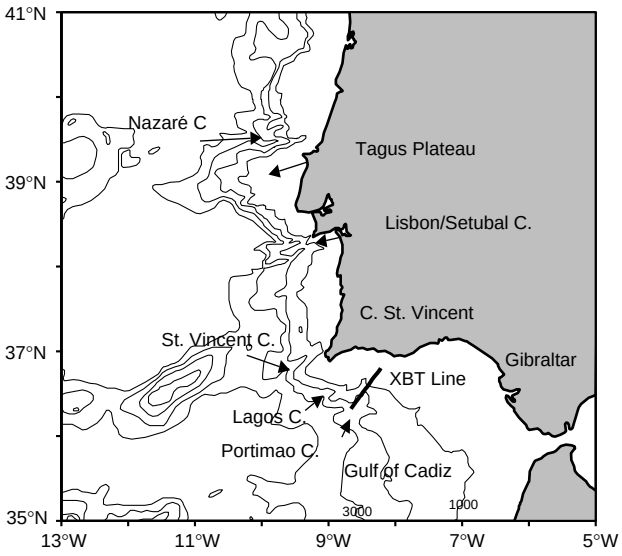

Figure 1. Chart of the southwestern corner of the Iberian Peninsula and adjacent waters. Coastline and isobaths at 1000 m intervals are plotted. RAFOS floats were launched between the 1000 and 2000 m isobaths along the XBT line.

The measurements

A major field programme, called "A Mediterranean Undercurrent Seeding Experiment" (AMUSE), has been carried out to identify the most important meddy formation sites, to directly estimate the rate of meddy formation and the time required for meddies to form, and to observe the spreading pathways of MW into the North Atlantic via meddies and other processes. 49 RAFOS floats were deployed sequentially in the Mediterranean Undercurrent south of Portugal (Fig. 1) between May 1993 and March 1994, and tracked acoustically for up to 11 months. The deployment site was chosen to be upstream of all potential formation sites that had been proposed in the literature, and downstream of where the Mediterranean outflow current is sinking from the sill depth in the Strait of Gibraltar (~300 m) to its depth of neutral buoyancy (~1000 m) near 8°W, along the northern rim of the Gulf of Cadiz. The floats, which collected temperature, pressure and acoustic tracking data three times daily were launched in pairs and triplets near the level of the lower core of the undercurrent (1000–1200 dbars) on a series of 25 cruises spaced nominally one week apart. The float deployments were accompanied by high-resolution (3 km) XBT sections across the undercurrent.

Results

A total of 44 float trajectories were obtained, representing over 20 float-years of data, Fig. 2. The average length of these tracks is 180 days. The concentration of trajectories along the continental slope south of Portugal indicates that the majority of floats were initially advected westward from the launch site toward Cape St. Vincent. A significant fraction turned the corner at the cape and continued drifting northward along the western continental slope of Portugal. Many of these floats apparently peeled away from the slope at various locations such that most had left the boundary before reaching 40°N. In addition to the preferred pathway along the slope, another grouping of trajectories extends northwestward from Cape St. Vincent, suggesting that this is also a dominant pathway by which MW spreads into deeper water. Note also that a few floats initially drifted away from the launch site toward the south, and circulated in the Gulf of Cadiz.

Meddy formation

Fourteen floats exhibited the rapid and/or persistent anticyclonic looping characteristic of meddies. Ten of these were caught in nine separate meddy formation events, six near Cape St. Vincent, Fig. 3a (page 22), and three near the Tagus Plateau along the western Portuguese slope, Fig. 3b. One possible formation event was detected near Lisbon and Setubal Canyons. Two floats were trapped in new meddies for only a few looping periods, while others traced out the path of a meddy for many months (up to 328 days). Looping periods of the floats were 3–7 days, at radii 3–15 km. Floats caught in newly-formed meddies at Cape St. Vincent observed temperatures warmer than 12°C while they were looping, consistent with the temperature of the lower core in the undercurrent near the cape. Slightly cooler temperatures were observed in the meddies formed near the Tagus Plateau, reflecting the dilution of the undercurrent water properties by mixing along the continental slope of Portugal. In all cases, meddy formation seemed to be tied to specific locations along the slope where the coastline

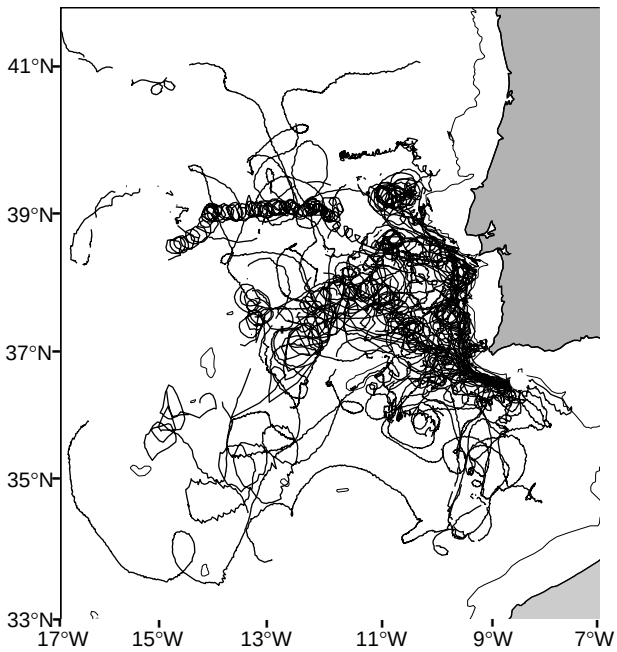

Figure 2. Spaghetti diagram of 44 RAFOS float trajectories obtained during AMUSE. The 1000 m isobath is also shown.

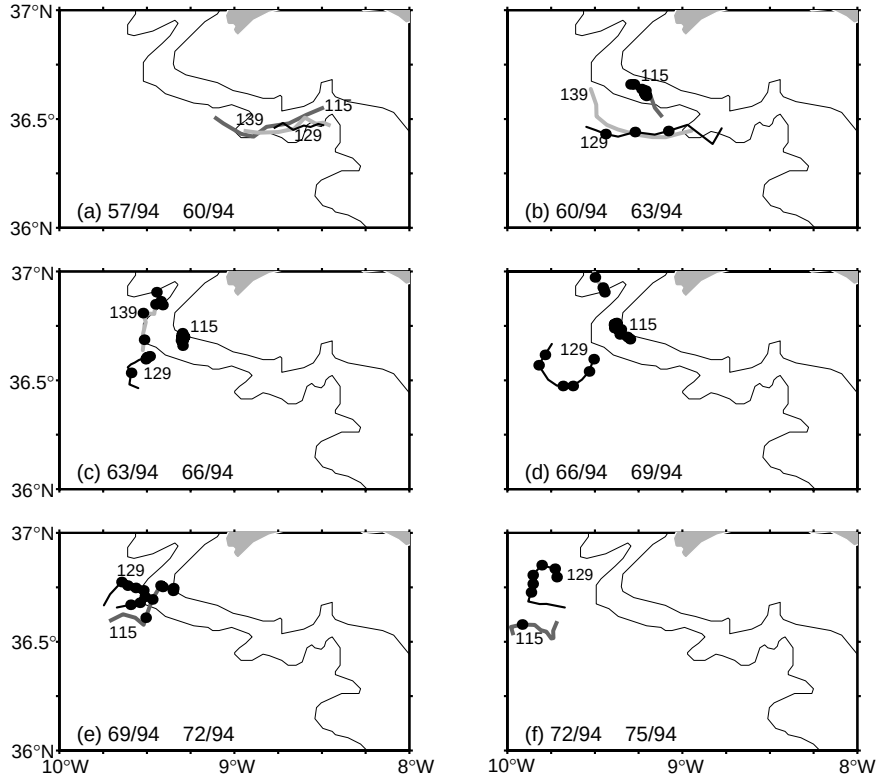

Figure 4. Time sequence of three-day track segments for am115, am139 and am129 starting on yearday 57/94 (26 February 1994). Dots indicate where the floats observed temperature ≥12°C. The 1000 and 2000 m isobaths are also plotted. Dates are indicated in yearday/year.

turns sharply to the right (facing downstream), strong evidence that topography plays a critical role in meddy formation. Most of the newly formed meddies drifted away from the formation sites within a few days, suggesting a formation time scale on the order of 3–7 days.

Fig. 4 illustrates one formation event at Cape St. Vincent in more detail with a time sequence of 3-day track segments for three floats launched in the undercurrent at about 1100–1150 dbars on 26 February 1994 (yearday 57/94). Am115 was deployed farthest inshore, and am139 and am129 4.0 and 5.3 km farther offshore, respectively. All three floats initially drifted west-southwestward and observed temperatures less than 12°C for the first several days of their missions, Fig. 4a. As am115 crossed the entrance to Lagos Canyon, Fig. 4b, it curved northwestward and onshore. Its temperature increased to over 12°C after it crossed the 2000 m isobath. It stalled near the 1000 m isobath on about yearday 63/94, and its pressure record fluctuated somewhat during that time (not shown), suggesting that the float may have come in contact with the sea floor.

Meanwhile, am139 and am129 were advected more toward the west-southwest, and am129 started to occasionally observe temperatures greater than 12°C on yearday 61/94. At about 9.3°W, am139 veered anti-cyclonically toward the north and crossed the entrance to St. Vincent's Canyon between yeardays 63–66/94, Fig. 4c. Its temperature increased to greater than 12°C while it was in the vicinity of the canyon. Am129 started looping anticyclonically on yearday 63/94. Its temperature continued to fluctuate above and below 12°C until yearday 74/94, when the float started its third loop and temperature stabilized above 12°C, Fig. 4f. When am129 was making its second loop, am115 was swept off the slope in a series of cyclonic cusps, its temperature dropping below 12°C once it left the slope, Fig. 4e,f. Am129 continued to loop in the meddy until the end of its mission six months later.

Summary

The RAFOS float data collected during AMUSE have revealed some of the basic characteristics of meddy formation that will help to focus future studies of this process, both observational and theoretical. In particular, it is apparent that meddy formation takes place at corners in the topography. It is not obvious whether it is the corner itself, or the adjacent canyon (St. Vincent's Canyon, Nazaré Canyon), that triggers meddy formation. More detailed observations, concentrated in the formation regions identified by the floats, are needed to fully resolve the detailed dynamics of meddy formation.

This work is being sponsored by the US National Science Foundation and the Luso-American Foundation for the Development.

References

Arhan, M., A. Colin de Verdière, and L. Memery, 1994: The eastern boundary of the Subtropical North Atlantic. J. Phys. Oceanogr., 24, 1295–1316.

Armi, L., D. Hebert, N. Oakey, J.F. Price, P.L. Richardson, H.T. Rossby and B. Ruddick, 1989: Two years in the life of a Mediterranean Salt Lens. J. Phys. Oceanogr., 19, 354–370.

Richardson, P.L., D. Walsh, L. Armi, M. Schroeder and J.F. Price, 1989: Tracking three Meddies with SOFAR floats. J. Phys. Oceanogr., 19, 371–383.

Ocean Weather Ship Station M (66°N, 2°E): The Longest Homogeneous Time Series from the Deep Ocean

Svein Østerhus, Nordic WOCE Project Office, Bergen; Tor Gammelsrød, Bergen; and Reidun Hogstad, Geophysical Institute, Bergen, Norway, svein@regn.gfi.uib.no

Having performed daily oceanographic measurements in the deep Norwegian Sea since 1 October 1948, Ocean Weather Ship Station (OWS) Mike, at 66°N, 02°E, is the longest homogeneous time series from the deep ocean. Station M is operating above the eastern margin of the Norwegian Sea deep basin where a branch of the Atlantic Current enters the area, Fig. 1. The location proved to be strategic both for studying the Atlantic inflow and the Norwegian Sea Deep Water. The OWS M is operated by the Norwegian Meteorological Institute (DNMI) and the hydrographic programme is carried out by the Geophysical Institute of the University of Bergen.

History

With the expansion of civil aviation and growing understanding of the impact of aerological observations on weather forecasts after World War II, ICAO (International Civil Aviation Organization) demanded a greater network of aerological stations, primarily in the North Atlantic.

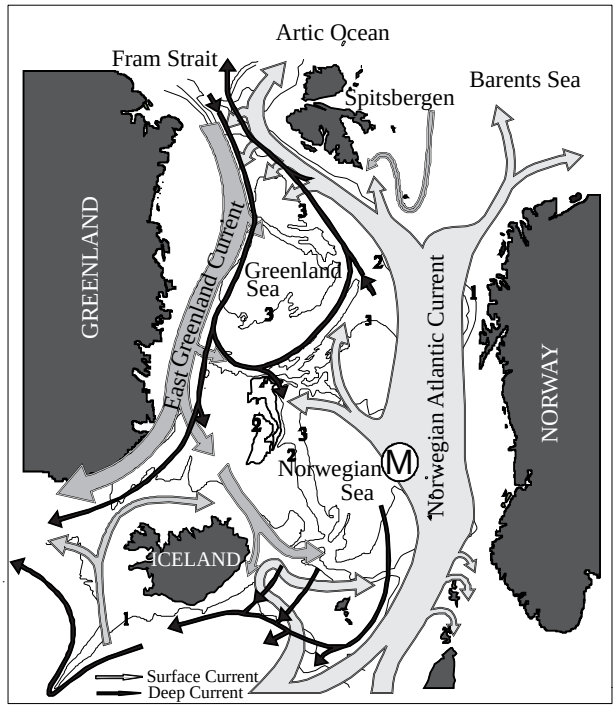

Figure 1. The main current system (schematic) in the Nordic Seas with the position of the weather ship station MIKE. The open hatched arrows indicate the surface current patterns, and the black arrows indicate the deep/ bottom current.

In 1946 a plan for a network of 13 ocean weather stations in the North Atlantic was set forth under the auspices of ICAO. The stations were to supply meteorological services, search and rescue services, and navigational aids to aircraft. The USA, Canada and 8 European countries would be responsible for operating the stations, which were referred to by letters from A to M. Norway was to operate station M (Mike) at 66°N, 02°E, with financial backing from Sweden and Great Britain.

ICAO attempted to organize an international oceanographical research programme for the weather ships, but failed due to lack of interest, shortage of money and difficulties in procuring the necessary scientific equipment. In Norway, a country which held great traditions in oceanographical research, a small group of three scientists, led by the oceanographer Håkon Mosby, took upon themselves to implement an extensive research programme on station M (Hogstad and Østerhus, 1996).

Håkon Mosby implemented a routine programme of physical oceanography, including serial observations of temperature, salinity, and (since 1953) oxygen weekly at standard depths to 2000 metres, and serial observations of temperature and salinity at standard depths down to 1000 metres 3 or 4 times a week. This programme has been running continuously since 1 October 1948 only hampered by occasional extreme weather. The method of obtaining temperature and salinity observations (Nansen bottles with reversing thermometers) has not changed significantly either so the time series are indeed homogeneous.

Some results

Altogether more than 9200 hydrographic stations (Nansen cast) have been performed, including more then 180000 thermometer readings and 90000 salinity samples. In addition to standard observation of hydrography and meteorology several other samples are taken (Gammelsrød *et al.*, 1992). The hydrographic data can be obtained from the Norwegian Oceanographic Data Centre.

Figs. 2 and 3 show that the Atlantic water has become cooler and fresher since 1991. For depths below 200 m the temperature and salinity are down to the levels observed during the late 70s, when the so-called "Great Salinity Anomaly" passed through (Dickson *et al.*, 1988). Independent observations (Hansen and Kristiansen, 1994) indicate that the inflow of Atlantic Water to the Nordic Seas has been reduced. The long term trends are a cooling and freshening of the upper layer consistent with accumulation of Arctic Surface Water in the Nordic Seas (Blindheim *et al.*, 1996).

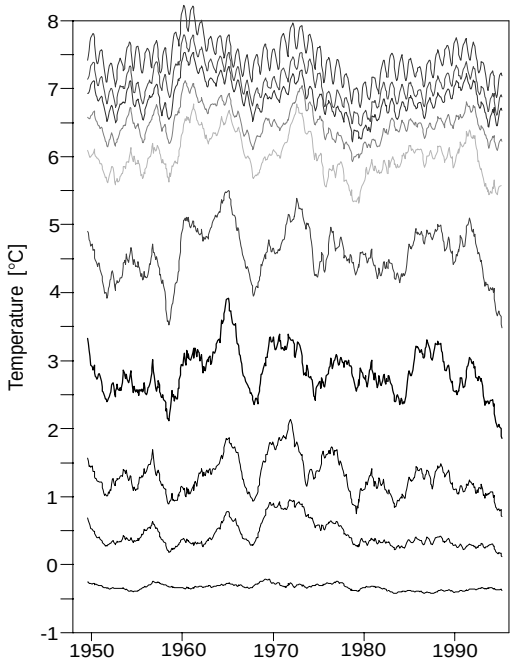

Figure 2. Time series of temperature in the Atlantic Water (50, 75, 100, 150, 200, 300, 400, 500, 600, 800 m).

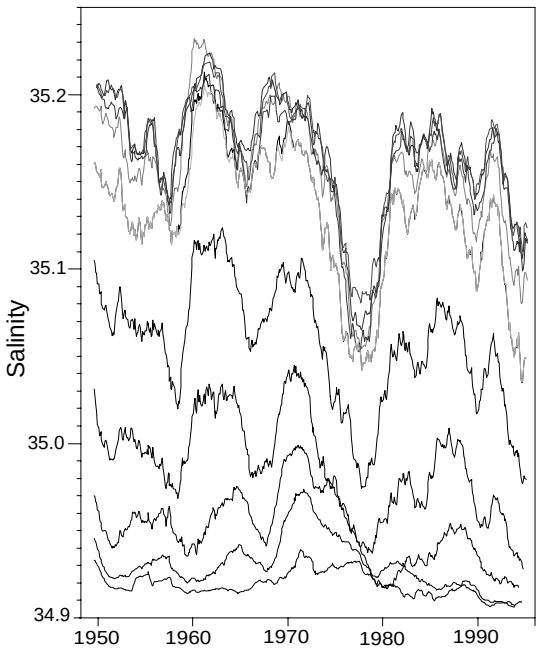

Figure 3. Time series of salinity in the Atlantic Water (50, 75, 100, 150, 200, 300, 400, 500, 600, 800 m).

Smoothed monthly mean temperatures for the 3 deepest standard depths (1200 m, 1500 m, 2000 m) are shown in Fig. 4 for the period 1948–1995. Notice that a recent warming has occurred, starting at 2000 m in 1985, then gradually penetrating upwards through 1500 m in 1987 and reaching the 1200 m level in 1990. The temperature increase is about 0.07°C, and nearly constant with depth.

The low temperature of the Norwegian Sea Deep Water (NSDW) is maintained by the contribution of the Greenland Sea Deep Water (GSDW). The bottom water in the Greenland Sea is renewed locally by surface cooling of relative fresh water, resulting in the coldest bottom water found in the deep ocean. NSDW is formed by mixing GSDW and the deep water from the Arctic Ocean. The recent warming of the NSDW has its forerunner in an even more marked warming of the GSDW, see Fig. 5, consonant with the idea that the deep water formation in the Greenland Sea has ceased. The Greenland Sea and the Norwegian Sea basins are separated by the Mohn Ridge (Fig. 1), and the exchange of water masses between the two deep basins takes place through a channel which has a sill depth of 2200 m and is situated just north of Jan Mayen. Since the warming of GSDW appears to have continued unchecked to date, (Fig. 5) the cessation of warming observed in the NSDW since 1990 is certainly unexpected, (Fig. 4), suggesting that as GSDW production has (virtually) ceased, the transport through the Jan Mayen Channel may have reduced or even reversed, see Fig. 6, cutting off the deep Norwegian Sea from the influence of the GSDW and its changes, see Østerhus *et al.*, 1996.

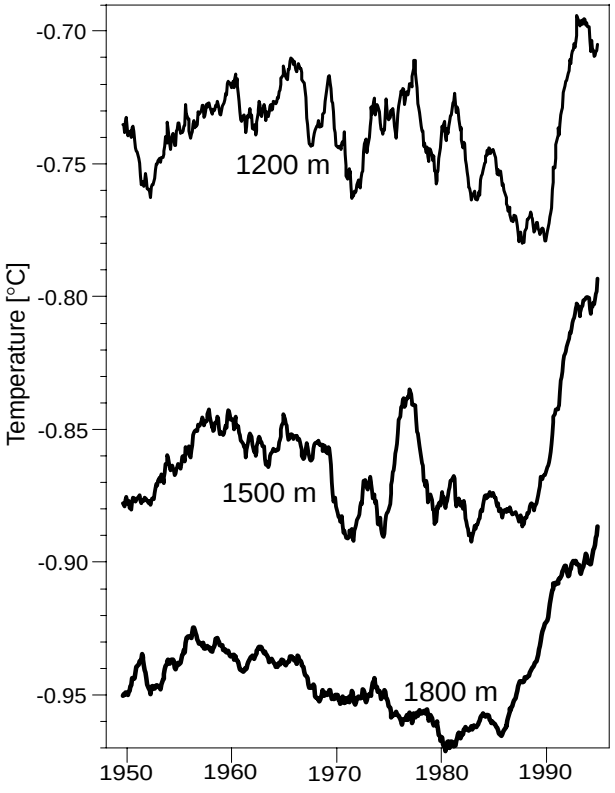

Figure 4. Time series of smoothed monthly mean temperature at depth of 1200 m, 1500 m, 2000 m from the weather ship station Mike.

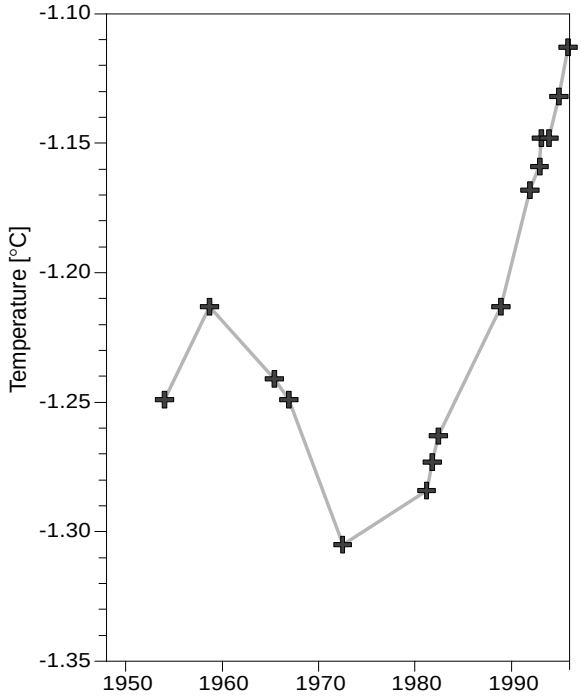

Figure 5. Time series of the mean temperature below 2000 m in the central Greenland Sea.

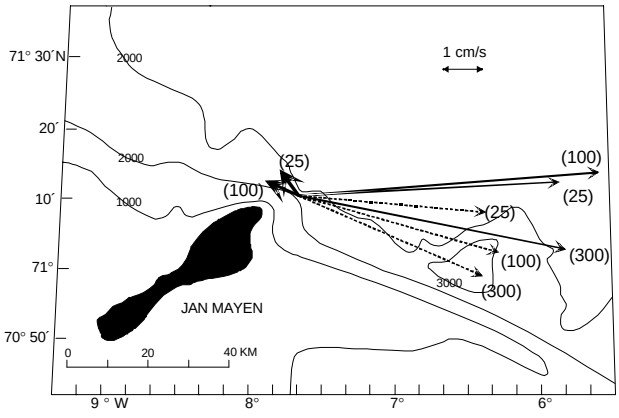

Figure 6. Results from the current measurements in the Jan Mayen Channel from April to November 1991 (thin dotted arrows), September 1983 to July 1984 (thin arrows) and from November 1992 to July 1993 (thick arrows). The numbers in parentheses indicate height of current meter above the bottom. The stability factor (defined as the absolute value of the average current vector divided by the average speed) was 0.91 in 83/84 and 0.18 in 92/93. The mean temperature was -1.01°C in 83/84, increasing to -0.94°C in 92/93.

Planned activity

The OSW M will continue its operation at least to the year 2000. A CD containing quality-controlled hydrographic data (as station data and time series) is planned for the 50 year anniversary in 1998. The history of OWS M is being written. It is proposed that the ship presently operating the station, Polarfront, should be equipped with an Acoustic Doppler Current Profiler (ADCP). Twenty-four ADCPs and XBTs sections a year across the Norwegian Atlantic Current will be invaluable for monitoring the influx of Atlantic water to the Arctic. Plans for extending the hydrographic, biological and geochemical programmes exist. The future of M depends on us as researchers being able to convince the funders that these data are really necessary for climate research.

References

Blindheim, J., V. Borovkov, B. Hansen, S-A. Malmberg, B. Turrell, and S. Østerhus, 1996: Recent upper layer cooling and freshening in the Norwegian Sea. ICES C.M. 1996/C:7.

Dickson, R.R., J. Meincke, S-A. Malmberg, and A.J. Lee., 1988: The "Great Salinity Anomaly" in the Northern North Atlantic 1968–1982. Prog. Oceanog. Vol. 20, pp 103–151.

Gammelsrød, T., S. Østerhus, and Ø. Godøy, 1992: Decadal variations of ocean climate in the Norwegian Sea observed at Ocean Station "Mike" (65°N 2°E). ICES Mar. Symp., 195:68–75,1992.

Hansen B., and R. Kristiansen, 1994: Long-term changes in the Atlantic water flowing past the Faroe Islands. ICES C.M. 1994/S:4.

Hogstad, R.D., and S. Østerhus, 1996: Verskipstasjon M 1948–1998. A preliminary internal report.

Østerhus, S., B. Turrell, B. Hansen, J. Blindheim, A.J. Bennekom, 1996: Changes in the Norwegian Sea Deep Water. ICES C.M. 1996/O:11.

WOCE Newsletter No. 26:
Call for Articles

The International WOCE Newsletter provides an opportunity for members of the WOCE community to present recent scientific results and progress on their research.

As the new WOCE phase of Analysis, Interpretation, Modelling and Synthesis (AIMS) is starting, No. 26 of the International WOCE Newsletter will be dedicated to global circulation or ocean-atmospheric coupled models that can be used to assess the oceans' impact on our climate.

Articles on this topic are invited for submission before the end of January 1997. The length should NOT exceed a total of 3 pages including figures. For further details please contact:

woceipo@soc.soton.ac.uk

Arabian Sea Eddies Simulated by an Ocean Model with Thermodynamics

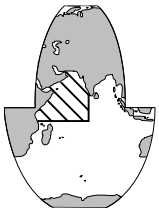

P.K. Pal and M.M. Ali, Meteorology and Oceanography Group, Space Applications Centre, Ahmedabad 380 053, India, mmali@sac.ernet.in

A reduced gravity, primitive equation thermodynamic model originally developed by Gent and Cane (1989) for the equatorial Pacific basin has been applied to the Arabian Sea basin. Arabian Sea eddies have been simulated using ECMWF analysed winds of 1986. The model could simulate the circulation patterns of the Somali eddies. Variations in mixed layer depth and sea surface elevation could also be obtained by this model.

Introduction

Formation of eddies in the Arabian Sea is a regular phenomenon during the monsoon season, which occurs due to a particular wind pattern along the Somali coast creating a wind stress curl. Observations reveal a two gyre system (Swallow and Fieux, 1982) along the western coast depending upon the monsoon activity (Dubey *et al.*, 1990). These eddies were simulated by many investigators with a shallow water model, where thermodynamics is not considered (*e.g.* Luther and O'Brien, 1985 and 1989). Their model is driven by the wind stress only. Observations (*e.g.* Bruce and Beatty, 1985; Ali and Sharma, 1994) show that these eddies have typical geometric and thermodynamic structure. In the northern hemisphere anticyclonic eddies have an elevation with a warm core at the centre. Geometric shape of such gyres is modelled by an approximate paraboloid (Pal and Ali, 1992). Using this model the rotational velocity of the Somali eddy has been estimated from the simulated altimeter data. This type of model is only an approximation of the shape. Actual shape, currents and other characteristics have to be studied by an appropriate three-dimensional ocean circulation model with thermodynamics.

In this paper a reduced gravity, primitive equation thermodynamic model originally developed by Gent and Cane (1989) for the equatorial Pacific basin has been converted for Arabian Sea basin. By running this modified model Arabian Sea eddies have been simulated using ECMWF analysed winds and sea surface temperatures (SST). The characteristics of these eddies have been analysed.

The model

The reduced gravity model is described in detail by Gent and Cane (1989). The model domain is limited in both the horizontal and vertical. The primitive equation model uses the reduced gravity assumption so that the deep ocean is at rest below the active upper ocean. The model consists of a surface mixed layer and an active layer below, which is divided into a number of numerical layers by means of sigma coordinates. The model equations in a generalised vertical coordinates are

$$\frac{\partial h\mathbf{u}}{\partial t} + \nabla\cdot(\mathbf{u}h\mathbf{u}) + \frac{\partial w\mathbf{u}}{\partial s} + f\times h\mathbf{u} + h(\nabla P - b\nabla z) = t + \frac{\partial}{\partial s}\left(\frac{\nu}{d}\frac{\partial \mathbf{u}}{\partial s}\right)$$

$$\frac{\partial hT}{\partial t} + \nabla\cdot(\mathbf{u}hT) + \frac{\partial wT}{\partial s} = Q + \frac{\partial}{\partial s}\left(\frac{\kappa}{h}\frac{\partial T}{\partial s}\right)$$

$$\frac{\partial h}{\partial t} + \nabla\cdot(h\mathbf{u}) + \frac{\partial w}{\partial s} = 0$$

where $h = \frac{\partial z}{\partial s}$ and $b = \alpha g(T - T_B)$.

Here, P represents the dynamically active part of the pressure and is zero at the model base, consistent with the reduced gravity approximation. T_B is constant deep ocean temperature, a is coefficient of thermal expansion, g is gravity, **u** is the current vector, *w* is the vertical velocity, T is temperature, t is wind stress, *f* is coriolis parameter, Q is heat flux at the surface, v is vertical eddy diffusivity and k is the conductivity.

Gent (1991) studied the heat budget in the domain 140°E–180°E, 10°S–10°N in the western Tropical Pacific. In the present study the model domain has been changed to 40°E–77.5°E, 10°S–20°N. While changing the model domain over to the Arabian Sea, particular care has been taken for proper boundary conditions. In this area wind forcing is very strong during the monsoon season. Analysed monthly average winds and SST from ECMWF for July 1986 have been used to drive the model. The resolution is uniform in longitude (0.5°) and is stretched in latitude as described in Gent and Cane (1989). The boundary conditions are: no normal flow at horizontal boundaries and no vertical flow at the top and bottom.

The upper layer of the model is taken to represent the well mixed layer at the ocean surface. The vertical coordinate over the remaining layers has taken to be like a sigma coordinate which divides the total depth in six more layers. As the winds are very strong during July along the Somali coast, Richardson number dependent vertical mixing (Gent, 1991) has been included in the model. In the regions of weak currents Richardson mixing is not used. The horizontal smoothing in the model is done by Shapiro filter to control the nonlinear computational instability. The heat flux parametrization is that of Seager *et al.* (1988).

Results and discussions

The model is integrated from rest with constant average wind forcing of January 1986 for six years. After reaching the January equilibrium the model is further integrated for 12 more years with annual cycle of monthly average winds

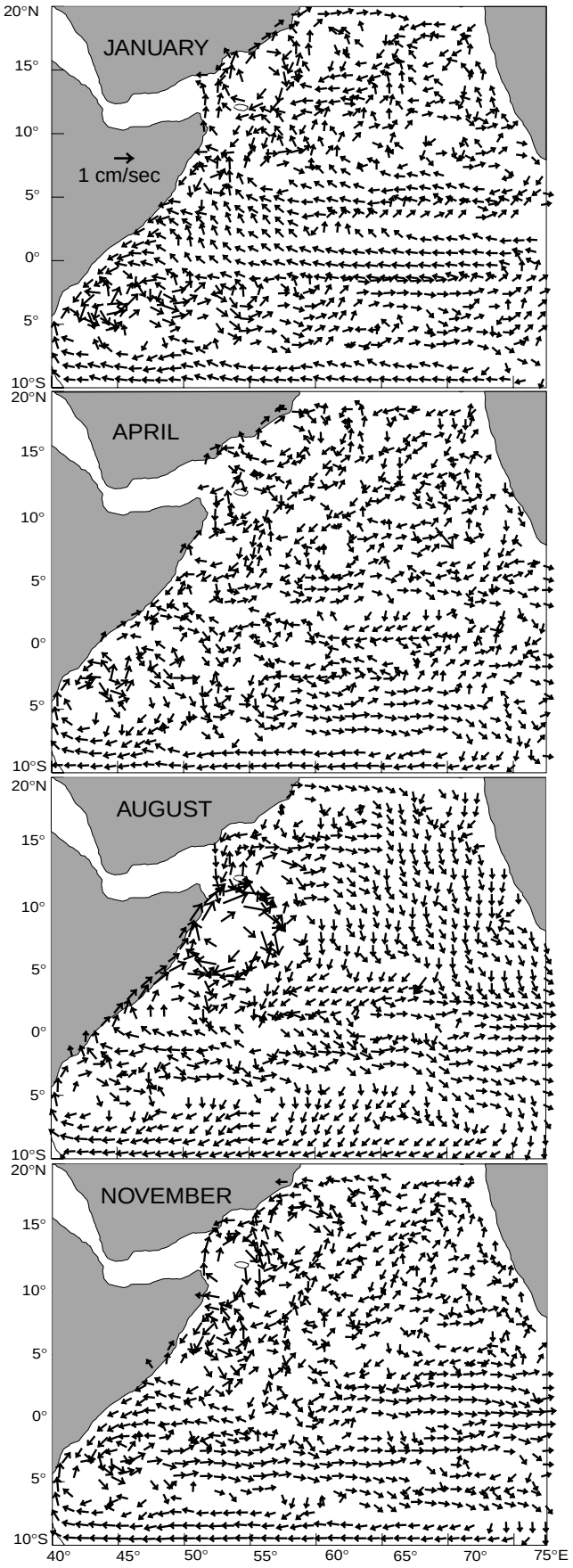

Figure 1. Surface current vectors for 1986.

and SST. In the last two years of run the change in model total energy integrated over the domain is less than 0.5% of the total which shows that the model has reached an equilibrium. The model has successfully simulated the Somali eddy structure. The corresponding features of the eddies in MLD and sea level could also be simulated.

Monthly upper layer velocity patterns for four typical months of 1986 are shown in Fig. 1. The winter Somali current flowing southward along the western boundary is well developed in January. The South Equatorial Current is also prominent. Two large eddies have also developed north of Socotra. The southern eddy is stronger than the northern. Luther and O'Brien (1989) have simulated three eddies. By March, this southern eddy has weakened and in April it has dissipated while the northern eddy continued till May and dissipated by June. Northward flow along the Somali coast has started by April with two anticyclonic circulations south of Socotra. Though the northward Somali current continued till November it is very strong in June and July. The other weak anticyclonic circulation present in April south of Socotra dissipated in June. Again in July a weak anticyclonic circulation has started which has been well developed by August and continued till October and started dissipating in November. Above this major eddy another anticyclonic eddy has been found which has been weakened by November. By December, a pattern similar to January has started developing.

The model has also simulated the sea surface height patterns very well over the eddy. Surface height structure of the Somali eddy was not shown in the earlier model results. In August where an anticyclonic eddy was well developed south of Socotra, sea surface elevation is very clearly seen (Fig. 2) with an elevation of about 40 cm compared to its periphery. Ali and Sharma (1994) observed a relative elevation of about 50 cm from the ERS-1 altimeter observations of September 1991 near the Somali region. The simulated surface elevation matches with this order of observed elevation. The weak anticyclonic eddy observed in the circulation patterns is also reflected in the sea surface

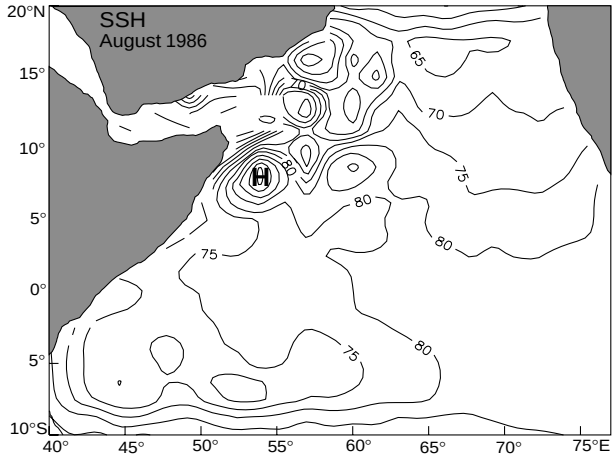

Figure 2. Sea surface height patterns for August 1986.

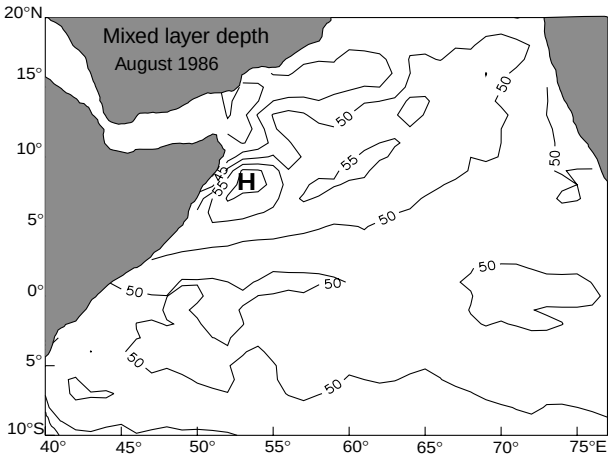

Figure 3. Mixed layer depth for August 1986.

elevation patterns with a gradient of about 15 cm only. Thus the gradients in the current magnitudes could be reflected in the sea surface elevations.

Similarly the model could also reflect the gradients in the MLD over the eddy region. In August (Fig. 3) mixed layer is 15 m deeper than the periphery at the centre of the stronger eddy while it is only 5 m at the centre of the weaker eddy. Earlier model simulations of the Somali eddy have not given the mixed layer structure. However, the SST patterns are not very satisfactory may be because (i) heat flux parameterisation in model at present is very crude and (ii) a constant annual cycle cloud cover has been given as the input. Efforts are being made to change the flux parameterisation besides incorporating the actual cloud cover. Observed surface winds derived from ERS-1 scatterometer will also be used to drive the model.

Acknowledgements

Peter Gent, B. Kauffman and E. Brady of NCAR have provided the original version of the Pacific Ocean model. We acknowledge their help.

References

Ali, M.M., and R. Sharma, 1994: Detection of Arabian Sea eddy using ERS-1 Altimeter data. Proceedings Second ERS-1 symposium - Space at the service of our environment, Hamburg, Germany, 11–14 October 1993, ESA SP-361, pp 557–563.

Bruce, J.G. and W.H. Beatty, III, 1985: Some observations of the coalescing of Somali eddies and a description of the Socotra eddy. Oceanologica Acta, Vol. 8, pp 207–220.

Dubey, S.K., M.E. Luther, and J.J. O'Brien, 1990: Relationships between interannual variability in the Arabian Sea and Indian summer monsoon rainfall. Meteorology and Atmospheric Physics, 44, 153–165.

Gent, P.R., 1991: The heat budget of the TOGA-COARE domain in an ocean model. J. Geophys. Res., Vol. 91, pp 3323–3340.

Gent, P.R., and M.A. Cane, 1989: A reduced gravity, primitive equation model of the upper equatorial ocean. J. Comput. Phys., Vol. 81, pp 444–480.

Luther, M.E., and J.J. O'Brien,, 1989: Modelling the variability in the Somali current. In: Mesoscale/synoptic coherent structures in geophysical turbulence, Eds. J.C.J. Nihoul and B.M. Jamart, Elsevier Science Publishers, Amsterdam, pp373–386.

Luther, M.E., and J.J. O'Brien, 1985: A model of the seasonal circulation in the Arabian Sea forced by observed winds. Progr. in Oceanogr., Vol. 14, pp 353–437.

Pal, P.K., and M.M. Ali, 1992: Estimation of the azimuthal velocity and the elevation of an eddy from simulated altimeter data. Int. J. Rem. Sens., Vol. 13, pp 2215–222.

Seager, R., S.E. Zebiak, and M.A. Cane, 1988: A model of the tropical Pacific sea surface temperature climatology. J. Geophys. Res., Vol. 93, pp 1265–1280.

Swallow, J.C. and M. Fieux, 1982: Historical evidence for two gyres in the Somali current. J. Mar. Res., supplement to 40, 747–755.

Significant Improvement in Ocean Tide Models

P.L. Woodworth, Proudman Oceanographic Laboratory, UK; C.K. Shum, Center for Space Research, University of Texas at Austin, USA; C. Le Provost, University of Grenoble, France; and R.D. Ray, Goddard Space Flight Center, USA, plw@unixa.nerc-bidston.ac.uk

In May 1995, the TOPEX/POSEIDON Science Working Team (T/P SWT) conducted an assessment of a large number of new global ocean tide models. These models had become available largely as a result of the superb accuracy and coverage of T/P data and of progress in numerical modelling. The primary reason for the study was to provide the SWT with a recommendation on which models to use for future altimetric analyses. However, as ocean tides play a major role in many areas of geophysics, it was felt that such as assessment would also be useful to the wider community.

The assessment report was not finalised until late-1995 as there were several outstanding problems which needed more research. That report has since been submitted for publication (Shum *et al*., 1996), and this short note presents some of the main conclusions.

Before the T/P era, two main global ocean tide models had been used by researchers, those of Schwiderski and Cartwright and Ray. These two older models were also included in the study so as to provide a comparison to the 10 new ones listed in Table 1. The Schwiderski model dates from 1980 and was constructed by means of a hydrodynamic interpolation scheme for the assimilation of the tidal constants dataset derived from the global collection of tide gauge data. That model, although now known to contain decimetric and larger errors, played a central role in

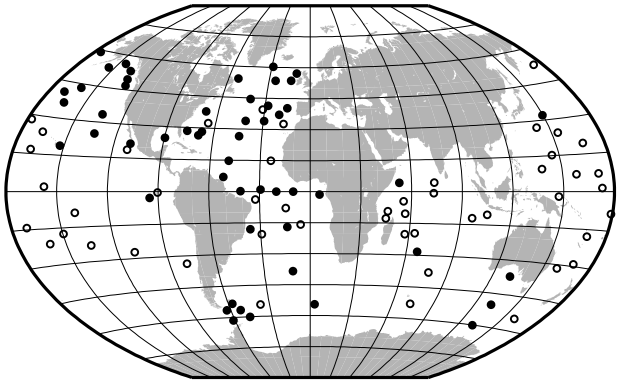

Figure 1. Locations of selected ocean tide observations at 49 island tide gauges (circles) and 53 bottom pressure stations (dots).

oceanographic and geophysical research for more than a decade. Geosat in the late-1980's provided the first copious altimetric dataset for extended global tide studies and enabled the derivation of models of comparable or better accuracy than Schwiderski (*e.g.* Cartwright-Ray). However, it was not until 1995, when almost three years of T/P data had become available, that really significant improvements in this field started to emerge.

The new models were computed in different ways. Some (*e.g.* SR95.0, DW95.0, GSFC94A, RSC94) are purely empirical solutions derived from T/P data, somewhat analogous to Cartwright-Ray although analysis details are different in each case. Two of the models (GSFC94A and RSC94) parameterised tidal solutions in terms of Proudman Functions in order to provide spatial smoothing and dynamical constraints. Some of them applied an early version of the Grenoble pure hydrodynamic tide model (FES94.1) to T/P data, and computed new models in terms of tidal corrections to that reference model. In this way, optimal solutions were obtained which were consistent with the medium and large scale tidal information provided by the T/P data, while preserving the short wavelength features of the tide from the finite element Grenoble model. Four models (Kantha, FES95.1, ORI and TPXO.2) could be said to differ from the others in being the results of different forms of sophisticated data assimilation into numerical models wherein hydrodynamic constraints effectively act as a filter on the data.

Preliminary evaluations and comparisons of all the new models showed that they were very similar, with barely a centimetre or two difference between them in most parts of the world. It was clear that choosing between them was going to be difficult. So, a set of seven evaluation tests was constructed. However, as space is limited in this note, we shall mention only the two most important. These two tests were:

1. A comparison of tidal parameters derived from the models to those obtained from pelagic and island tide gauge data, and
2. A study of how well each model reduces altimetric crossover residuals.

Pelagic and island tide gauge analysis

In the course of the T/P project, tide gauge data have been employed extensively in order to provide in-situ tests of altimeter information. In the case of ocean tide studies, sets of deep ocean tidal constants were assembled from pelagic and island sites for comparison to the models. Fig. 1 shows the locations of 49 island and 53 bottom pressure recorder (pelagic) stations. At these 102 sites, we have compared the previously determined harmonic constants to those from the 10 new models, and Table 2 shows the rms differences between data and models for each constituent. In the case of the main M2 constituent, most of the newer models can be seen to have residual rms values of less than 2 cm, which is a significant improvement on the Schwiderski and Cartwright-Ray models. Best results were obtained from the Schrama-Ray SR95.0 model, closely followed by CSR3.0, AG95.1 and FES95.1.

Table 2 also shows the overall rss (square root of the sum of the squares of the 8 rms values) for each model. Once again, SR95.0 ranks first, followed by CSR3.0, FES95.1 and AG95.1.

Table 1. Ocean Tide Models

AG95.1	KMS Andersen-Grenoble
CSR3.0	UT/CSR Eanes
DW95.0/.1	CU Desai-Wahr
FES95.1/.2	Grenoble Le Provost *et al.*
Kantha.1/.2	CU Kantha
ORI	U. Tokyo Ocean Research Institute Matsumoto *et al.*
SR95.0/.1	Delft/GSFC Schrama-Ray
GSFC94A	GSFC Sanchez-Pavlis
RSC94	GSFC Ray-Sanchez-Cartwright
TPXO.2	OSU Egbert *et al.*

The "/" after model acronyms indicates later revisions of some of the models which were used in this study.

Altimeter crossover analysis

Another tool for assessing the model accuracies can be derived from examination of variance reduction in those T/P altimeter crossover measurements which were not used in the construction of the models. Table 3 shows T/P crossover residual rms using different models for T/P cycles 82-95 *i.e.* from 140 days (14 cycles) of data from the later part of the mission which had not contributed to model development. (Full details of this analysis are included in our paper).

Table 3 shows crossover statistics for the global ocean, deep ocean (>800 m) and shallow ocean (<800 m) separately, with tide models listed according to the lowest crossover residual rms in the deep ocean. The number of valid data points are also shown in Table 3 for each model; CSR3.0 has the most valid crossover points in this test indicating that this model is probably valid in more areas than other models.

Table 3 also contains statistics for a number of revised versions of the models *i.e.* of further developments since the May 1995 meeting. It is evident that the revised models

Table 2. Tidal RMS Comparisons to 102 Tide Gauge Stations (cm)

Model	Q1	O1	P1	K1	N2	M2	S2	K2	RSS
Schwid.	0.35	1.22	0.61	1.43	1.22	3.86	1.66	0.59	4.84
Cartw.-Ray	0.46	1.23	0.63	1.89	0.98	3.20	2.21	0.67	4.59
AG95.1	0.29	1.04	0.45	1.22	0.83	1.64	1.06	0.48	2.75
DW95.0	0.34	0.98	0.42	1.28	0.70	1.85	1.09	0.56	2.88
CSR3.0	0.30	0.95	0.40	1.12	0.67	1.64	1.03	0.52	2.62
FES95.1	0.29	1.04	0.45	1.22	0.83	1.65	1.00	0.48	2.74
Kantha.1			2.80						
ORI	0.42	1.02	0.62	1.34	0.87	1.93	1.42	0.90	3.27
SR95.0	0.29	0.96	0.45	1.04	0.70	1.55	0.99	0.48	2.53
GSFC94A	0.35	1.06	0.54	1.41	0.87	2.18	1.21	0.63	3.30
RSC94	0.37	0.99	0.39	1.26	0.78	1.89	1.18	0.49	2.94
TPXO.2	0.29	0.98	0.44	1.31	0.75	2.16	1.23	0.55	3.16

Note that Schwiderski's model (Schwid.) is not independent of comparison data, but all others are. Also all bottom pressure (pelagic) data have been corrected for the S2 air tide. Root-summed-Squares (RSS) of the 8 rms values are shown for each model.

Table 3. T/P Crossover Residual Statistics Using Different Tide Models

Tide Models	Global Ocean RMS (cm)	Global Ocean Points	Deep Ocean RMS (cm)	Deep Ocean Points	Shallow Ocean RMS (cm)	Shallow Ocean Points
CSR3.0	5.82	53058	5.74	50001	10.05	3057
SR95.1	5.91	50267	5.83	47708	10.16	2557
DW95.1	5.98	52769	5.87	49998	11.78	2771
RSC94	6.06	52281	5.98	49759	10.78	2522
DW95.0	6.18	52967	6.02	49998	13.69	2969
FES95.2	6.12	52630	6.02	49943	11.51	2687
TPX0.2	6.17	52832	6.07	49971	10.72	2861
Kantha.2	6.28	52582	6.21	49863	11.30	2719
AG95.1	6.58	52645	6.49	49941	11.80	2704
FES95.1	6.59	52506	6.49	49855	11.93	2651
ORI	6.65	52802	6.52	49946	13.05	2856
Kantha.1	6.61	52998	6.53	50001	11.22	2997
GSFC94	7.07	52348	6.95	49946	13.11	2569

FES95.2 is a revised model of FES95.1. (It was called FES95.2.1 in some workshop reports.) DW95.1 is a revised model of DW95.0. Kantha.2 is a revised model of Kantha.1.

are generally performing better than their earlier versions. The improvement in crossover residual variance with the present generation of models over that with the historic models has been very dramatic. Typical crossover variances now are approximately half of those obtained using Schwiderski or Cartwright-Ray.

Conclusions on T/P tide model selection

One of the primary objectives of this study was to select two of the best models for future reprocessing of T/P data. Clearly, we could not work in future with 10 models, even if many of them were almost as good as each other. After considerable discussion concerning the relevance of the seven tests, the final selection criteria were based simply on the highest combined rankings for the two tests described above, with the condition that models must not be incompatible with the other tests. CSR3.0 scored best overall followed by SR95.0, RSC94 and DW95.0.

One of the original specifications for the selection was that one of the two models should be a pure hydrodynamic model and that the other should be based primarily on T/P data. However, in practice that choice was not possible as the nearest candidate pure hydrodynamic model (FES94.1) was nowhere near accurate enough. Moreover, many of the models are the result of assimilation schemes combining both data and dynamical insight provided either by an *a priori* model (*e.g.* FES94.1) or data smoothing (Proudman Functions). Consequently, after discussion, the choice was made to select CSR3.0, as primarily a T/P derived model but with hydrodynamic model information content, and FES95.2, as primarily a hydrodynamic model but with T/P information content. These two models, therefore, can in some sense be said to approach an optimum model from different directions.

It is important to stress that the choice of these two models does not mean that they are necessarily "better" than the others and no model removes the tidal contributions completely. Much interesting work remains to be performed to improve models even further. For example, detailed analysis of altimetry shows many short-wavelength tidal features which are not yet included in the global models. There is also the need to extend the "global" models, which are essentially deep-ocean models, so that they are useful to studies of shallow seas.

We should also add that over the past 2–3 years a number of new regional tide models have been developed by several authors independently of the T/P project. For example, detailed models are now available for the Arctic Ocean, Southern Ocean including the Weddell Sea, Mediterranean Sea etc. Tidal studies have a very long history but it seems that the field has never been more active.

Applications of tide models

The most obvious application of better tide models is to the work of oceanographers studying altimeter data in order to "correct" sea surface heights. However, there are many uses of tide models within geophysics including studies of satellite and lunar orbits, length of day, ocean and solid earth tidal dissipation, tidal loading at geodetic (GPS, VLBI and SLR) stations etc. In order to celebrate the achievements of the new models, and to demonstrate their many applications, a meeting entitled "Tidal Science '96" will be held at the Royal Society in London on 21–22 October 1996 prior to the next meeting of the T/P SWT in Southampton.

Reference

C.K. Shum, P.L. Woodworth, O.B. Andersen, G. Egbert, O. Francis, C. King, S. Klosko, C. Le Provost, X. Li, J. Molines, M. Parke, R. Ray, M. Schlax, D. Stammer, C. Tierney, P. Vincent, and C. Wunsch, 1996: Accuracy assessment of recent ocean tide models. Submitted to J. Geophys. Res.

New Depth Equation for Sparton XBT-7 Expendable Bathythermographs, Preliminary Results

P. Rual, ORSTOM, Surtropac Group, Noumea, New Caledonia; A. Dessier and J.P. Rebert, ORSTOM, Brest, France; A. Sy, BSH, Hamburg, Germany; and K. Hanawa, Tohoku University, Sendai, Japan, rual@noumea.orstom.nc

Sparton XBT-7s, manufactured after July 1992, were provided by the manufacturer to ORSTOM (Noumea and Brest), to BSH (Hamburg) and to Tohoku University (Sendai), to be compared with simultaneous CTD profiles. In December 1992, 18 probes were tested in the western-equatorial Pacific at 156°E and in June 1995, 23 additional probes were tested in the western north Pacific, along 34°N across the Kuroshio. In early 1993, 11 probes were tested in the tropical Atlantic along 7°N and, in June, another 11 probes were tested in the north-western Atlantic around 45°N. The XBT profiles were recorded on digital ARGOS-XBT/ST, Sippican MK12 or MURAYAMA Z60-II onboard units.

The CTD profilers (Neil-Brown MK III, or Seabird SBE 9 and SBE 11-plus) were calibrated before and after the cruises, and the calibration results were applied to the CTD data before analysis. Therefore CTD data errors are at least an order of magnitude smaller than XBT data errors and, for this study, will be considered as negligible.

New depth-time equation

For the XBT-7, the depth-time equation provided by Sparton is identical to the Sippican/TSK equation for T-4, T-6 and T-7 probe types:

$$z_m = 6.472\,t - 0.00216\,t^2 \qquad [1]$$

where z_m is the depth and *t* is the elapsed time, in seconds, starting when the probe hits the surface.

Following the temperature-error-free method described in full in UNESCO (1994) or in Hanawa et al. (1995), the new depth-time equation for the 63 Sparton XBT-7 probes studied here, at a confidence level of 95%, becomes:

$$Z = (6.705 \pm 0.024)t - (2.28 \pm 0.36)10^{-3}\,t^2 \qquad [2]$$

The quadratic coefficient is strongly correlated (0.87) to the linear coefficient, therefore the depth variability of the individual profile is much less than if they were independent.

Observed variability and manufacturer's specifications

Fig. 1a shows the distributions of the 1754 detected depth-errors (using the manufacturer's equation 1), as a function of their CTD depth. The data are generally outside the manufacturer's specifications (15 m or 12% whichever is the greatest), except close to the surface where the mean depth-error is within 15 m down to a depth of 200 m. The mean depth-error ranges from zero at 100 metres to -25 m at 750 m. Only the very slow fall rates, outside minus two standard deviations, are entirely within the specifications down to the maximum depth.

When the new equation 2 is used instead of the original manufacturer's equation 1 (Fig. 1b), the mean depth-error is greatly reduced and is now within 12 m of the CTD depth. However, even the 2-standard deviation confidence interval is not entirely within the specifications.

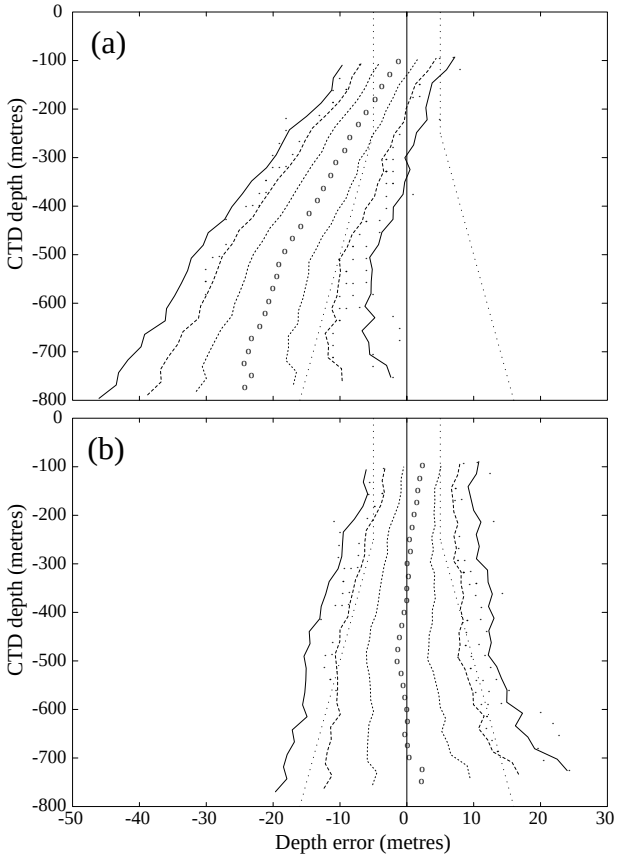

Figure 1. Sparton XBT-7 data set: depth-errors and their statistics as a function of depth. (a) Using the manufacturer's depth-time equation 1. Mean depth-error (open circles) and the 1, 2, 3 standard deviations curves (respectively dotted, dash-dotted and full curves). The individual depth-errors above 2 standard deviations are also added (dots). The manufacturer's specifications (15 m or 12% of the depth, whichever is the greater) are indicated as dotted lines. (b) Same figure, but using the preliminary Sparton XBT-7 equation 2.

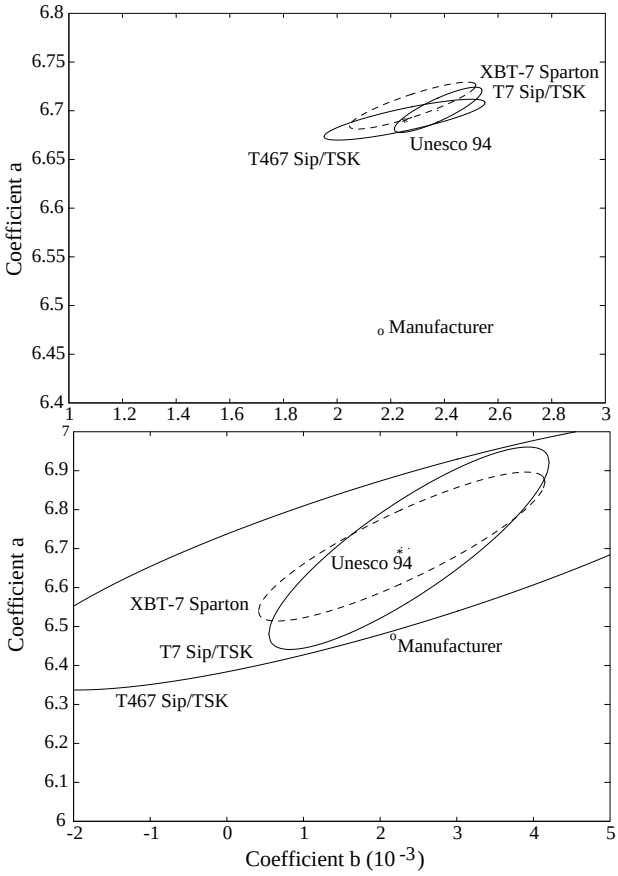

Figure 2. Comparison between the Sparton XBT-7 and the Sippican/TSK probes. (a) Two-standard deviation ellipses of the mean AB points (mean depth-time equations) for the Sparton XBT-7 (dashed ellipse), Sippican/TSK T-7 (upper full ellipse) and Sippican/TSK T-4, T-6, T-7 (lower full ellipse); the star indicates the AB point of equation 3 and the small circle the AsBs point of the manufacturer's equation 1. (b) Same figure, but for the individual profiles (individual ab points).

Comparison with the new equation for Sippican/TSK T-4, T-6 and T-7 Probes

UNESCO (1994), and Hanawa et al. (1995), give the following new reference equation for the Sippican/TSK T-4, T-6 and T-7 probes:

$$Z = (6.691 \pm 0.021)t - (2.25 \pm 0.30)10^{-3}\, t^2 \qquad [3]$$

The statistical ellipses (Fig. 2a) of the mean time coefficients of the two equations do intersect, meaning that these two equations are not statistically different at a confidence level of 95%. If, in addition, we consider the Sippican/TSK T-7 equation given also in the same publications, the corresponding statistical ellipse (Fig. 2a) does intersect the Sparton XBT-7 ellipse and the AB point of equation 3 belongs also to these 2 ellipses. Thus, considering these preliminary results, the mean Sparton XBT-7 fall-rate can not be distinguished from the fall rate of the Sippican/TSK T-7 probe. If one considers now the individual profile, the statistical ellipse of the Sparton XBT-7 probe (Fig. 2b) is almost identical to the corresponding ellipse of the Sippican/TSK T-7 probe, and completely embedded in the ellipse of the Sippican/TSK T-4, T-6 and T-7 group of probes.

Discussion and recommendations

A preliminary fall rate equation for the Sparton XBT-7 was determined by a temperature-error-free method applied to an XBT/CTD comparison data set which was collected, under controlled conditions, in tropical waters as well as in the cold waters of the north-west Atlantic and Pacific Oceans. The variability of the probes' characteristics was found comparable to the variability of similar Sippican/TSK probes. A negligible error (about 0.2%), less than 1.2 m at 800 m, is induced when replacing that preliminary equation by the new reference equation proposed for the Sippican/TSK T-4, T-6 and T-7 probes by Hanawa *et al.* (1995), and adopted from 8 November 1995 by the World Meteorological Organisation. Therefore, unless contradicted by further experiments, equation 3 can be used for the Sparton XBT-7 as well as for Sippican/TSK probes, and the same linear correction (+3.36%, see UNESCO, 1994) might be applied to previous data, irrespective of the above-mentioned probe types. However, it should be noted that several other experiments gave different results, but they were not taken into consideration here as their CTD depth accuracy was not considered adequate.

Acknowledgements

We are indebted to all those involved in the field acquisition and in the processing of the data, specially to the officers and crew of the research vessels, to the engineers who carefully calibrated the CTD profilers and to the cruise leaders who kindly provided us with the temperature profiles.

References

Hanawa, K., P. Rual, R. Bailey, A. Sy, and M. Szabados, 1995. A new depth-time equation for Sippican or TSK T-7, T-6 and T-4 expandable bathythermographs (XBT). (accepted by Deep-Sea Res.). UNESCO, 1994. Calculation of new depth equations for expendable bathythermographs using a temperature-error-free method (application to Sippican/TSK T-7, T-6 and T-4 XBTs). UNESCO Technical Papers in Marine Sciences, 67, 46pp.

First Announcement

WOCE Southern Ocean Workshop
8–12 July 1997
Antarctic Cooperative Research Centre
Hobart, Tasmania, Australia

The World Ocean Circulation Experiment (WOCE) announces a workshop on the large-scale physical oceanography of the Southern Ocean to be held 8–12 July 1997 in Hobart, Australia. The purpose of the workshop is to facilitate progress toward the scientific and technical goals of WOCE for the Southern Ocean. It will bring together scientists who are working on various aspects of *in situ* and satellite data sets and models and encourage their interaction. The Southern Ocean workshop will be the third in a series of WOCE ocean basin workshops, following the Pacific workshop held in August 1996 in California and a South Atlantic workshop to be held in June 1997 in France.

The primary objective of the workshop is to initiate close collaboration between individual scientists working on scientific questions relevant to Southern Ocean WOCE. A second objective is to ensure that the Southern Ocean WOCE data set and model results are assembled prior to the workshop, for use by Southern Ocean WOCE investigators during and after the workshop. The meeting is intended to motivate work towards joint publications, including a special volume based on results discussed at the workshop.

The workshop will be structured around working groups which will address the major scientific questions WOCE set out to answer in the Southern Ocean. A number of invited overview talks will help focus attention on the important issues related to Southern Ocean WOCE. The workshop agenda and list of working groups will be announced in a "Final announcement" later this year.

Facilities at the workshop will include a number of networked work stations with internet access. The Southern Ocean WOCE data sets will be assembled by the relevant DACs and made available at the workshop, along with software for display and processing. We anticipate that results from a number of models will also be available.

The workshop follows the IAMAS/IAPSO conference which is to be held in Melbourne, Australia from 1–9 July 1997. (Deadline for abstracts is 2 December 1996.) An international symposium on "Antarctica and Global Change: Interactions and Impacts" sponsored by the International Glaciological Society (IGS), the Australian Meteorological and Oceanographic Society (AMOS) and the Scientific Committee for Antarctic Research - Global Change in Antarctica (SCAR-GLOCHANT) will be held from 13–18 July in Hobart and may also be of interest. (For more information on the IGS meeting see http://www.antcrc.utas.edu.au/antcrc.html.) (Deadline for abstracts for this meeting is 31 January 1997.)

Please indicate your interest in receiving the final announcement and attending the workshop by 15 November 1996. The following information is needed:

Name:
Address:
Telephone:
Fax:
e-mail:
Main topics of interest:

E-mail your response to: wocesow@antcrc.utas.edu.au
Or fax to: 61-3-6232 5123
Or mail to: Dr S. Rintoul
CSIRO Oceanography
GPO Box 1538
Hobart, Tasmania 7001
Australia

Organizing Committee:

Steve Rintoul, Antarctic CRC/CSIRO Division of Oceanography
Nathan Bindoff, Antarctic CRC
Kevin Speer, IFREMER
Dudley Chelton, Oregon State University
Eberhard Fahrbach, Alfred Wegener Institut, Bremerhaven
David Webb, Southampton Oceanography Centre
Brian King, Southampton Oceanography Centre
Mark Warner, University of Washington
Eric Lindstrom, US WOCE Office

WOCE South Atlantic Workshop to be held in Brest (France), 16–20 June 1997

The World Ocean Circulation Experiment announces a workshop on the large scale circulation and dynamics of the Southern and Equatorial Atlantic Ocean, to be held in Brest (France), 16–20 June 1997. The goals of the workshop are to summarize scientific results obtained so far, to identify significant outstanding problems where progress has to be made to reach the goals of WOCE, to encourage and facilitate collaboration among the scientists involved, and to prepare data synthesis and joint publications.

Topics will include the large-scale circulation, boundary and interior mixing, cross-equatorial transports and processes, ventilation and water mass formation, heat and freshwater transport and surface fluxes and the connection with the Southern Ocean. Special sessions will be devoted to results from the Deep Basin Experiment in the Brazil Basin. Particular emphasis will be given to data-model comparisons and the related numerical and inverse modelling and assimilation.

The workshop will consist in a mix of overview and shorter papers, poster and computer presentations, and working group sessions centred on specific scientific or scientific/technical issues.

As with companion WOCE workshops it is expected that a special issue of an appropriate journal, will be published after the meeting; its scope, content and timetable will be decided nearer the workshop date.

The scientific programme and working group topics are still under discussion and will obviously depend on participants interests and contributions. It is anticipated that all topics relevant to the circulation and dynamics of the Southern and Equatorial Atlantic Ocean will be covered. In order to foster scientific exchanges most efficiently, contributed poster presentations will be encouraged. Contributions from observations, modelling, data assimilation or data-models comparison are solicited.

The first announcement was released in July 1996. To facilitate planning and organization of the workshop and to organize the working groups, it is requested that those who have not yet expressed their interest in the workshop, and wish to receive the final announcement, do so before 15 December 1996, indicating the particular area of interest. Registration deadline will be 1 March 1997.

Please notify Y. Desaubies (yves.desaubies@ifremer.fr, Fax: 33 02 98 22 44 96).

Scientific Organizing Committee:

B. Barnier,
Y. Desaubies (Chair),
S.L. Garzoli,
N. Hogg,
J.R. Lutjeharms,
H. Mercier,
W. Roether,
P. Saunders,
G. Siedler.

Scripps Institution of Oceanography
WOCE Hydrographic Programme Office

The WOCE Hydrographic Programme Office – now being moved to the Scripps Institution of Oceanography, at the University of California, San Diego – is interested in hiring an experienced data technician/manager with a great deal of practical knowledge to maintain frequent communication with data providers, streamline data transfers, carry out data assembly functions, keep data catalogues and change histories up to date, maintain the data services of the WHPO and oversee routine correspondence, reports, and publications.

Qualified candidates will be either (a) scientific programmers, programmer analysts, or staff research associates with at least several years experience working with oceanographic data (staff position), or (b) specialists with background in oceanography and solid computer skills (academic position).

Closing date is 15 November 1996. Prospective candidates should send a letter of application, curriculum vitae, statement of interests, and the names and addresses of at least three references to: James Swift, c/o Meilani N. Rivera, Physical Oceanography Research Division, Scripps Institution of Oceanography, University of California, San Diego, 500 Gilman Drive, Dept. 0230, La Jolla, CA 92093-0230, USA, e-mail: mnrivera@ucsd.edu, Tel: 1-619-534-6362.

A more detailed description of the position is located at:

http://cyberia.ucsd.edu/~kkuney/WHPO_job.html

The University of California is an equal opportunity/affirmative action employer.

XXII General Assembly of EGS, Vienna, Austria, 21–25 April 1997

Special Session OA8: Intercomparison and validation of the ocean-atmosphere flux fields

This special session will review the status of our knowledge of the reliability and accuracy of fluxes of momentum, thermal energy and mass across the air sea interface, available from data collected on voluntary observing ships, in field experiments, by remote sensing from space or from reanalyses of numerical weather prediction models. Our focus is on parameterizations schemes and data processing techniques used for climate research and model simulations. Special attention will be paid to the decades of the 1980s and 1990s, which provide and overlap between different data sources and therefore an exceptional opportunity to establish links between different methods and data types by performing cross-validations and intercomparisons. We hope to discuss a strategy for the creation of unbiased climatologies of sea-air exchange parameters, that will be acceptable both to researchers involved in creating the climatologies and to the users.

For this session we invite participation by scientists occupied in the different domains related to sea-air flux estimation: sea-air flux climatology from voluntary observing ships, satellite remote sensing, sea-air flux parameterization, model intercomparison, operational flux products and numerical model reanalyses. We invite participation by specialists in data assimilation, who are dealing with different sources of sea-air flux estimates. Topical studies related to the energy budgets of the enclosed and semi-enclosed seas and sea-air interaction field experiments (TOGA/COARE, SOFIA/ASTEX, SEMAPHORE) are especially welcome. Contributions focused on the interannual and decadal variability of the forcing fields will be also of a great interest.

Convener: Dr Sergey Gulev, P. Shirshov Institute of Oceanology, Russian Academy of Sciences, Krasikova 23, 117218 Moscow, Russia; Tel: +7-095-1247985, Fax: +7-095-1245983, E-mail: ROCC@SOVAM.COM.

Co-Conveners: Prof. Kristina Katsaros, Dept. d'Oceanographie Spatiale, IFREMER, B.P. 70, 29280 Plouzane, France; Tel: +33-98224316, Fax: +33-98224533, E-mail: KATSAROS@IFREMER.FR; Tel: +33-2-98224316, Fax: +33-2-98224533; Dr Peter Taylor, James Rennell Division (254/27), Southampton Oceanography Centre, Southampton, SO14 3ZH, United Kingdom; Tel: +44-1703-596408, Fax: +44-1703-596400, E-mail: PETER.K.TAYLOR@SOC.SOTON.AC.UK.

Deadline for abstracts: 15 December 1996.

Forms can be obtained from either Convener, or EGS Office on request or via WWW.

EGS Office,
Max-Planck Str., 1
37191 Katlenburg-lindau
Germany
tel +49-5556-1440
fax +49-5556-4709
Email EGS@LINAX1.MPAE.GWDG.DE
http://www.mpae.gwdg.de/EGS/EGS.htlm

Note on Copyright

Permission to use any scientific material (text as well as figures) published in the International WOCE Newsletter should be obtained from the authors.

WOCE is a component of the World Climate Research Programme (WCRP), which was established by WMO and ICSU, and is carried out in association with IOC and SCOR. The scientific planning and development of WOCE is under the guidance of the Scientific Steering Group for WOCE, assisted by the WOCE International Project Office.

The WOCE Newsletter is edited at the WOCE IPO at the Southampton Oceanography Centre, Empress Dock, Southampton SO14 3ZH (Tel: 44-1703-596789, Fax: 44-1703-596204, e-mail: woceipo@soc.soton.ac.uk).

We hope that colleagues will see this Newsletter as a means of reporting work in progress related to the Goals of WOCE as described in the Scientific Plan. The SSG will use it also to report progress of working groups, experiment design and models.

The editor will be pleased to send copies of the Newsletter to institutes and research scientists with an interest in WOCE or related research.

Printed by the Design and Print Centre of the University of Southampton